STUDIES OF THE GEOCHEMICAL SIMILARITY OF PLUTONIUM AND SAMARIUM AND THEIR IMPLICATIONS FOR THE ABUNDANCE OF ^{244}PU IN THE EARLY SOLAR SYSTEM

Thesis by

John Hume Jones

In Partial Fulfillment of the Requirements

for the Degree of

Doctor of Philosophy

California Institute of Technology

Pasadena, California

1981

(Submitted April 17, 1981)

ACKNOWLEDGEMENTS

No project is accomplished in a vacuum. I have benefitted from the guidance and support of Don Burnett. Tim Benjamin initiated me into high temperature geochemistry and contributed much through his supportive and thoughtful commentary. Just as importantly, I have had the continuous moral support of my parents, my family and my friends, which means a great deal to me. This research has been sponsored by NASA grant NSG 7202 and NSF grant EAR76-84402.

ABSTRACT

^{Pu}D and ^{Sm}D have been measured for diopsidic pyroxene and whitlockite in the system Di-An-Ab ($\pm$ $Ca_3(PO_4)_2$). ^{Pu}D was determined by fission track radiography and ^{Sm}D was determined on the same samples by beta radiography. The analytical difficulties encountered in using photographic emulsions to determine beta fluences have been studied in detail. These studies have resulted in a technique which should be generally applicable to the radiography of low energy beta emitters (Appendix I).

^{Pu}D and ^{Sm}D for clinopyroxene are 0.17 and 0.31, respectively, at about 1250°C and $^{Sm}D/^{Pu}D$ = 1.9. The addition of 1.4% P_2O_5 to the DiAnAb system lowers ^{Sm}D and ^{Pu}D by factors of 1.5 and 2.0, respectively; this P_2O_5 addition raises the $^{Sm}D/^{Pu}D$ ratio to 2.6. ^{Pu}D and ^{Sm}D for whitlockite are 3.8 and 6.4, respectively.

The problem of approach to interfacial equilibrium is discussed in detail, and D values of crystals grown using various thermal histories are compared. Whitlockite D values appear to be independent of thermal history, implying a close approach to equilibrium at the crystal-liquid interface. Differences are seen between pyroxene D values for different thermal histories, and these variations are compared to the results of a simple kinetic disequilibrium model. The result of this comparison suggests that interfacial equilibrium was closely approached and that variations in pyroxene D values are mainly due to the temperature dependence of partitioning. This appears to be true for both Sm and Pu, even though the partitioning of other elements (e.g. Al) may be influenced by kinetic disequilibrium.

The magnitudes of ^{Sm}D and ^{Pu}D and (≤ 0.3) for clinopyroxene imply that Pu and the light REE's are difficult to fractionate during ordinary igneous processes. $^{244}Pu/^{238}U$ ratio measurements of meteorites are reviewed in light of the results of this study and a $^{244}Pu/^{238}U$ ratio of 0.005 ± 0.002 for the early solar system is favored. This is supportive of the $^{244}Pu/^{238}U$ ratio calculated by Marti et al.(1977) and suggests that the Podosek (1970a) value of 0.015 is invalid.

TABLE OF CONTENTS

I. INTRODUCTION

In low-energy (asymmetric) nuclear fission approximately 10% of all fission fragments decay to isotopes of xenon (Hyde, 1962). Because of this, Rowe and Kuroda (1966) suggested that the excess of heavy xenon isotopes in some meteorites was due to the contribution of fission products from ^{244}Pu ($t_{1/2}$ = 82 m.y.). Subsequently, Cantelaube et al. (1967) found fossil fission tracks and Wasserburg et al. (1969a) found large concentrations of fission-type xenon in the whitlockite ($Ca_3(PO_4)_2$) of the St. Severin (LL6) chondrite. The fission tracks were too numerous and the fission Xe concentration was too high to be ascribed to the spontaneous fission of ^{238}U. Additionally, the relative abundances of heavy xenon isotopes were not in the proportions known for either the spontaneous fission of ^{238}U or the neutron-induced fission of ^{235}U--indeed, no mixture of these two types of fission-xenon would result in a Xe whose isotopic proportions would match that found in the St. Severin phosphate. These data suggested that an unknown fissioning isotope was present in some meteorites or that such an isotope had once existed but subsequently decayed. The confirmation that this unknown nuclide was ^{244}Pu came from Alexander et al. (1971) who found that the isotopic proportions of xenon in synthetic ^{244}Pu were identical to the fission-xenon in the St. Severin phosphate. This confirmation legitimized earlier calculations on the time dependence of r-process nucleosynthesis in the galaxy which assumed the existence of ^{244}Pu (Hohenberg, 1969; Wasserburg et al., 1969b) and opened up the possibility of a ^{244}Pu chronology which could be used to assign relative formation times of meteorites.

Unfortunately, however, these interesting aspects of ^{244}Pu have proven difficult to exploit. Both the question of the initial ^{244}Pu abundance in

the solar system and the meteorite ^{244}Pu chronometer have been plagued by the lack of a stable plutonium isotope. The chemical difference between isotopes of the same element is small for heavy elements such as plutonium. Thus, for an initially isotopically homogeneous solar system, the concentration of a radioactive isotope (R) in a rock could be affected by geologic processes, but the ratio (R/S) of a radioactive isotope to a stable isotope of the same element will only be changed by nuclear processes such as radioactive decay. Because Pu has no such stable isotope, meteoritic ^{244}Pu abundances are not sufficient to determine either meteorite ages or the average solar system concentration of plutonium.

Because of this difficulty, various chemical analogues of Pu have been proposed. Hohenberg (1969) and Wasserburg et al. (1969b) compared moderately detailed nucleosynthetic models to the St. Severin whitlockite $^{244}Pu/^{238}U$ ratio (0.035) and assumed that Pu and U would not chemically fractionate. This assumption was based on the constancy of the Th/U ratio of terrestrial rocks and meteorites which implied that Th and U do not fractionate in typical non-aqueous geological processes (Wasserburg et al., 1964).

Doubt was placed upon this assumption by two experiments. First, Podosek (1970a) found correlations between xenon isotopes in neutron-irradiated samples of the St. Severin chondrite which suggested that the whole-rock $^{244}Pu/^{238}U$ ratio (0.015) was different from that measured by Wasserburg et al. (1969a) for the whitlockite of the same meteorite (0.035)--implying Pu-U fractionation. Secondly, Crozaz (1974) showed that the Th/U ratio of the St. Severin whitlockite was 11 and that the Th/U ratio of St. Severin apatite ($Ca_5(PO_4)_3Cl$) was 2. These data indicated that Th and U could be internally fractionated from the

chondritic Th/U ratio of 3.8, thus invalidating the original assumption of no Pu-U fractionation.

The experiments of Benjamin (1979) showed in some detail that U is not a good substitute for a stable Pu isotope. The partition coefficients (D's) of Pu and U were not found to be equal for any mineral studied. Since the crystal/liquid partition coefficient of an element M is defined to be:

$$M_{D}\ \text{crystal} = \frac{\text{concentration of M in crystal}}{\text{concentration of M in liquid}},$$

if ^{U}D is not equal to ^{Pu}D then Pu and U can chemically fractionate.

Lugmair and Marti (1977) and Wasserburg et al. (1977) suggested a solution to this dilemma by presenting data from Angra dos Reis (Ador) which implied that Pu and Nd do not fractionate and that neodynium was a reasonable pseudo-isotope of Pu. Additionally, Marti et al. (1977) found the $^{244}Pu/Nd$ ratio of several meteorites to be constant at about $1.5X10^{-4}$ (by weight). Pyroxene and whitlockite from Angra dos Reis, melilite from a coarse-grained inclusion in Allende, and a whole-rock analysis of Juvinas all gave approximately the same Pu/Nd ratio. This constancy of Pu/Nd in such a wide variety of materials led Marti et al. (1977) to calculate a $^{244}Pu/^{238}U$ ratio for the solar system using the Pu/Nd they had measured and the solar system (i.e. chondrite) Nd/U ratio. Their calculated $^{244}Pu/^{238}U$ ratio was .004, a factor of four smaller than that measured by Podosek (1970a) in St. Severin.

Jones and Burnett (1979) investigated the U distribution in St. Severin and concluded that 50-70% of the U was sited on grain boundaries and that if the Pu were similarly sited, as Podosek's data implied, then Podosek's method should give the correct $^{244}Pu/^{238}U$ ratio. Jones and

Burnett did observe that the Podosek experiment required accurate knowledge of the thermal neutron fluence and that the KI neutron monitor used by Podosek could be less reliable than a U standard. But since this type of monitor gave acceptable results for Alexander et al. (1972), (see Appendix III), they concluded that 0.015 should be accepted as a valid $^{244}Pu/^{238}U$ ratio for St. Severin. As a result, the discrepancy between St. Severin and the Pu/Nd data still stood.

This thesis was undertaken as an effort to further test the chemical coherence of Pu and the light rare earths. Partition coefficients of Pu and Sm between silicate liquid and diopsidic pyroxene and whitlockite have been measured at known temperatures, pressures and oxygen fugacities. This study provides a data base which can be used to help evaluate the hypothesis of Marti et al. (1977).

II. EXPERIMENTAL PROCEDURE

A. Sample Generation

Four starting compositions were used in this study: Pul4 ($Diopside_{50}$ $Anorthite_{25}$ $Albite_{25}$, weight proportions), Pul5 (Pul4+ 25 wt.% $Ca_3(PO_4)_2$), Pul6 ($Di_{60}An_{20}Ab_{20}$) and Pu 17 (Pul6 + 3 wt.% $Ca_3(PO_4)_2$). All starting compositions were prepared by melting mixtures of reagent grade oxides and carbonates (in Pt tubes) after an initial sintering and decarbonation step (Benjamin, 1979; Appendix I). The Pul4 and Pul6 compositions were quenched to glass in liquid nitrogen, ground to a fine powder in a Spex ball mill, spiked with aqueous solutions to concentrations of ~50ppm ^{151}Sm and ~8ppm ^{239}Pu, remelted at ~1400°C (above the liquidus) for ~12 hours, requenched to glass and reground. Splits of Pul4 and Pu 16 were then diluted with the proper amounts of $Ca_3(PO_4)_2$ to make Pul5 and Pul7. These compositions were then melted in the presence of Ni metal (to remove any H_2O), quenched and reground in the same manner as Pul4 and Pul6. Microprobe analyses of glasses indicate a starting composition homogeneity of better than 5%. The one exception to this is the P_2O_5 content of Pul7 which shows a variation of 7%. Based upon the reproducibility of microprobe analyses (Champion et al., 1975), any variation above the 2% level is considered to be real. Representative microprobe analyses and liquidus temperatures of starting compositions are given in Table 1. Diopside is the liquidus phase of all compositions except Pul5, whose liquidus phase is whitlockite. During Pul4 and Pul7 experiments, the stability field of plagioclase is entered but plagioclase does not typically nucleate. In only one experiment was plagioclase nucleation observed. More details of starting material preparation and

Table 1

Microprobe Analyses of Quenched Samples of Starting Compositions (wt.%)

	Pu 14[1]	Pul5[2]	Pul7[3]
Na_2O	2.85 ± 0.04[4]	2.11 ± 0.06	2.39 ± 0.03
MgO	8.76 ± 0.35	6.70 ± 0.20	10.36 ± 0.11
Al_2O_3	13.65 ± 0.66	10.50 ± 0.29	11.69 ± 0.16
SiO_2	56.63 ± 0.51	43.27 ± 0.58	53.45 ± 0.26
CaO	18.00 ± 0.05	26.80 ± 0.47	20.09 ± 0.14
P_2O_5	-	10.53 ± 0.40	1.40 ± 0.11[5]
Cl	-	0.0096 ± 0.014	___
F	-	0.058 ± 0.078	___
Total	99.89 ± 0.91	99.97 ± 0.92	99.38 ± 0.37
liquidus T	1272 ± 3°C	1330 ± 3°C	1286 ± 3° C

1 8 analyses of 3 samples

2 13 analyses of 2 samples

3 9 analyses of 3 samples

4 Errors are standard deviations of replicate analyses.

5 Pul7 P_2O_5 is slightly more inhomogeneous than other elements σ= 7%

microprobe analysis are contained in Appendices I and III of Benjamin (1979).

Spiking methods for the two basic starting compositions (Pul4 and Pul6) differed slightly. The plagioclase component of Pul4 was an An_{50} plagioclase glass containing 16ppm ^{239}Pu which was obtained from Los Alamos Scientific Laboratory. This glass was diluted (1:1) with synthetic diopside so that the resulting mixture contained 8ppm ^{239}Pu. The Pul4 was then spiked with a $SmCl_3$ solution (obtained from ICN, Inc.) to a concentration of 50ppm ^{151}Sm. It has been proposed that chlorine affects trace element partitioning (Harrison, 1977), and because some Cl remained after fusing, a second fusing in an open capsule (pinhole leak) was necessary to remove all Cl. Because of the difficulty of removing Cl from the system, both the Pu and Sm in Pul6 were added using nitrate solutions (obtained from New England Nuclear and ICN, respectively). Upon heating (after spiking) the nitrate decomposes to a lanthanide or actinide oxide, thereby eliminating the Cl problem. Although nominally identical in Pu and Sm, the Pul7 samples contain 1.5-2 times less Pu and Sm than Pul4. The reason for such a large discrepancy is unknown, although a major portion (~60%) of the Pul6 material leaked from its container during melting following spiking and was rendered unusable. It may be that Pu and Sm homogenization was not complete at this point and that the "lost" material was ~2x enriched in Pu and Sm over Pul4.

Individual sample runs (~5mg) consisted of growing crystals from melts contained in Pt capsules (Style A, Figure 2 of Benjamin, 1979) or in specpure graphite (United Carbon Products) capsules sealed in evacuated silica glass tubes. Samples were generated using a programmable Astro 1000A furnace, and temperatures were monitored with a Pt-Pt,Rh (S-type)

thermocouple checked against a calibrated thermocouple at the CIW Geophysical Laboratory (Benjamin, 1979). The temperatures reported here are slightly higher (~10°C) than those of Benjamin (1979) because of better calibration of the strip-chart recorder used to monitor furnace temperature.

To grow large (>~30μ) crystals and to help evaluate our approach to equilibrium, several thermal histories were used to nucleate and grow crystals: (1) 2-12 hours at ~10°C above the liquidus followed by a slow cooling (3-5°C/hr) to 55-65°C below the liquidus; (2) 2 hours at 10°C above the liquidus, drop to ~5°C below the liquidus for 12-15 hours followed by slow cooling to ~60°C below the liquidus; (3) ~2 hours at 10°C above the liquidus, drop to ~60°C below the liquidus and hold for 2-14 days. Schematics of these thermal histories are shown in Figure 1. The third method is sometimes complicated by plagioclase nucleation. Typical phase compositions are given in Table 2. Percent crystallization was determined by comparing the glass and mineral compositions after crystallization with the starting composition, using the method of Benjamin (1979).

The oxygen fugacity of the experimental charges was typically controlled using a cobalt-cobalt oxide (Co-CoO) buffer. This buffers the fO_2 at about 10^{-9} bar at the temperatures of these experiments (Myers and Gunter, 1979). When more oxidizing conditions were desired, either the Pt capsule was left unsealed (pinhole leak, fO_2 = 0.2 bar) or a hematite-magnetite buffer (HM) was used ($fO_2 \cong 10^{-2}$ bar; Heubner, 1971). For conditions more reducing than Co-CoO, samples were run in a graphite crucible inside a sealed and evacuated silica glass tube. The fO_2 of this low-pressure, graphite-containing system is ~10^{-22} bar. For more details on the oxygen fugacity of this system see Appendix II. Sealed,

Figure 1

This figure shows the three thermal histories used to grow pyroxene and whitlockite crystals. In method (1) the sample is taken to a temperature (T_i) above the liquidus for 1-2 hours and slowly cooled (3-4°C/hr) to a temperature (T_F) which yields a reasonable amount of crystallization. Method (2) is similar to method (1) except that an intermediate step is added in which the sample is abruptly lowered to a temperature (T_I) just below the liquidus for 10-15 hours in order to nucleate crystals. Method (3) is simply an abrupt drop from above the liquidus to the final temperature (T_F).

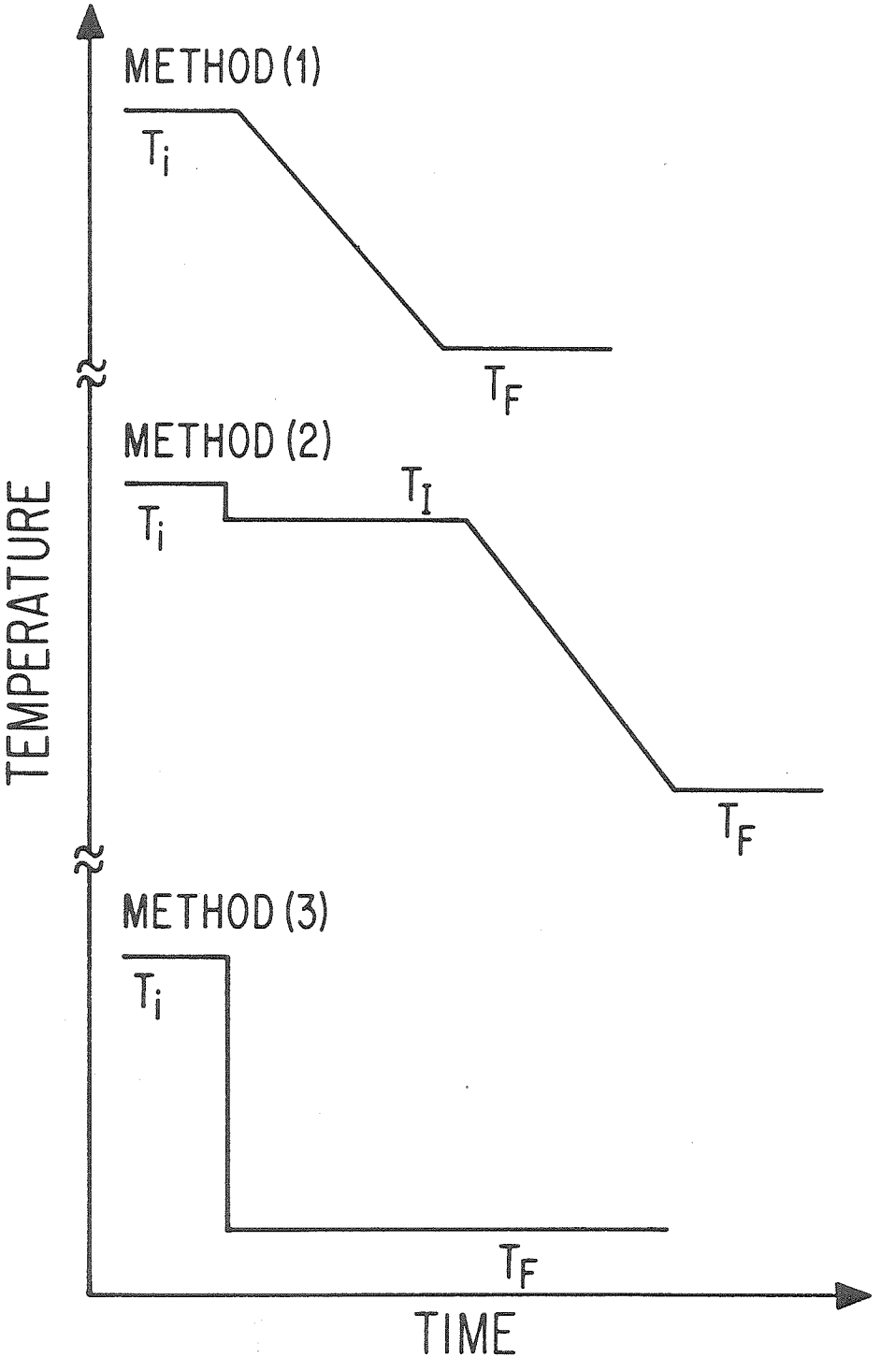
METHOD (1)
T_i
T_F
METHOD (2)
T_I
T_i
T_F
METHOD (3)
T_i
T_F
TEMPERATURE
TIME

Table 2

Typical Compositions of Crystals and Coexisting Glass (wt.%)

	Pul4		Pul5		Pul7	
	CPX	Glass	Whitlockite	Glass	CPX	Glass
Na_2O	0.22 ± 0.03	3.39 ± 0.03	0.35 ± 0.04	2.32 ± 0.03	0.19 ± 0.03	3.32 ± 0.03
MgO	17.88 ± 0.13	5.78 ± 0.06	3.61 ± 0.04	7.06 ± 0.06	18.14 ± 0.13	6.83 ± 0.07
Al_2O_3	3.33 ± 0.03	16.13 ± 0.11	*	11.52 ± 0.12	2.37 ± 0.05	15.34 ± 0.05
SiO_2	59.24 ± 0.27	57.56 ± 0.23	0.28 ± 0.01	47.21 ± 0.24	54.68 ± 0.27	52.55 ± 0.26
CaO	23.93 ± 0.05	16.75 ± 0.07	50.09 ± 0.10	23.78 ± 0.07	25.06 ± 0.08	18.92 ± 0.04
P_2O_5	-	-	45.49 ± 0.27	6.19 ± 0.06	-	2.00 ± 0.03
Total	99.60 ± 0.31	99.61 ± 0.27	99.82 ± 0.29	98.08 ± 0.29	100.44 ± 0.32	98.96 ± 0.28

*Below detection limit

unbuffered capsules typically yielded a ^{Pu}D intermediate to those obtained with the Co-CoO and air buffers. Over the fO_2 range 0.2 to 10^{-9} there is a significant increase in Pu^{+3}/Pu^{+4} (Benjamin, 1979); consequently it appears that variable amounts of trace organic contaminants reduce the fO_2 of the sealed capsules below the fO_2 of air.

In order to evaluate the effectiveness of the oxygen buffer, buffers of quenched samples are routinely mounted in epoxy and polished for petrographic examination. To maintain the fO_2 in equilibrium with Co-CoO requires the survival of both phases. For example, a leak in the Pt capsule will allow oxygen to enter the system and completely oxidize the Co metal. None of the samples used in this study show evidence of capsule leakage. However, in two long runs (15B-11Co and 15B-12Co) no Co metal was found; instead, all Co appears to have alloyed with Pt. At the temperatures of these experiments Co and Pt show complete solid solution, and during long runs Co from the buffer will alloy with the Pt container. Microprobe analysis of the Pt alloy associated with the CoO of 15B-12Co showed 20 mole % Co in the Pt. This solid solution with an accompanying reduction in the activity of Co will increase the fO_2 of the system but the exact amount is not known. Fission track maps of 15B-11Co and -12Co showed very little contrast in track densities between crystal and glass, indicating that the Pu^{+4}/Pu^{+3} ratio was sufficiently high to lower $^{Pu}D_{whit}$. Consequently, $^{Pu}D_{whit}$ results for the longer method (2) thermal histories were not possible.

Another complication in the buffering procedure is that the Co-CoO buffers of three runs (14A-11Co, 14A-13Co, and 14A-14Co) were accidentally wrapped in a nichrome foil instead of Pt or $Pt_{95}Au_5$. An X-ray spectrum of the foil showed that it contained Ni, Cr, Fe and Co. The abundances of

these elements in the foil are approximately in the order given. The main effect of this accident will be a tendency for the fO_2 to be below that of the Co-CoO buffer. Ni will remain in the reduced state but both Fe and Cr will oxidize and reduce CoO to Co. If all CoO was reduced, then the fO_2 for these samples is undetermined but was between the fO_2 of Co-CoO ($\sim 10^{-9}$bar) and Cr-Cr_2O_3 [$\sim 5 \times 10^{-18}$bar (Robie et al., 1978)]. Because of the fragile condition of the buffer, epoxy encapsulation and polishing was not possible and the presence of CoO was not determined; SEM X-ray spectra showed that Cr_2O_3 was definitely present. This accident should not affect the results of these runs unless significant Pu^{+4} still exists at 10^{-9}bar. Preliminary results from graphite capsule experiments indicate that very little Pu^{+4} still exists at $fO_2 = 10^{-9}$ bar.

A compilation of the thermal histories, percents of crystallization and oxygen buffers for all runs used in this study is given in Table 3. Nearly all Pul4 samples contain ~20% crystals. Exceptions are 14A-4D which crystallized plagioclase and 14A-11Co, -14A, -3D which simply contain more diopsidic pyroxene. The reason for increased crystallization in some samples is uncertain, since final temperatures (T_F) for these samples are similar to other samples with less crystallization. No evidence for quench crystals is observed. One possible explanation is that the amount of crystallization during fractional crystallization is different from that when equilibrium is maintained. Samples such as 14A-11Co, -3D, which were rapidly cooled, may have nucleated and grown pyroxenes at lower temperatures than the average sample. If pyroxene nucleation occurred near the final temperature (T_F), the amount of crystallization may more closely approximate that of equilibrium crystallization rather than fractional crystallization.

Table 3

Pu-Sm Partitioning Experiments

Sample	Ti(°C)	τi(hr)	TI(°C)	τI(hr)	Tf(°C)	τf(hr)	°C/hr	%XL[1]	Thermocouple
14A-1Co*	1283	2	-	-	1216	1.6	3.8	4.3 ± 4.3*	TC2
14A-2HM	1281	13	-	-	1213	1	2.9	20.6 ± 0.5	TC3
14A-5HM	1282	1	1273	21.5	1211		3.0	21.8 ± 1.2	TC5
14A-8A	1281	2	1273	13.5	-	-	-	0.8 ± 1.4	TC5
14A-11Co#	1281	2	-	-	1214	46	750	27.5 ± 0.5	TC5
14A-13Co#	1278	2	1268	15	1204	0	2.9	20.5 ± 0.9	TC5
14A-14Co#	1277	2	1268	17	1209	3	2.8	20.3 ± 0.7	TC6
14A-14A	1277	1	1268	2.3	1213	2.7	4.1	26.2 ± 1.4	TC5
17A-6Co	1293	3.8	1278	17.5	1215	7.5	4.18	29 ± 1	TC5
17A-7Co	1293	3.5	1278	15.0	1214	9.0	4.24	28 ± 1	TC6
17A-8Co	1294	3.0	1279	17	1214	3.3	4.25	27 ± 1	TC6
15B-2Co	1341	10.6	-	-	1254	0.6	3.8	9.3 ± 0.5	TC2
15B-6Co	1332	39.5	-	-	1244	1.2	3.9	9.8 ± 0.8	TC3
15B-6A(air)	1332	11	-	-	1246	2	3.86	10.1 ± 0.7	TC3
15B-7Co	1334	4	-	-	1245	13.5	2.97	10.5 ± 0.3	TC3
15B-11Co	1328	3.5	1314	9.7	1239	13	2.88	10.0 ± 0.7	TC6
15B-12Co	1329	2.5	1314	11.5	1236	8.5	2.93	9.9 ± 0.8	TC6
14A-1D**	1299	1.3	-	-	1218	13(days)	-	19.9 ± 0.9	D1
14A-2D								21.3 ± 2.8	
14A-3D	1278	6	-	-	1207	4-5(days)	-	27.6 ± 1.0	D2
14A-4D	1280	12	-	-	1207	10-13(days)	-	51.8 ± 12.8***	D2
14A-5D	-	-	-	-	1229	14(days)	-	-	D2

*Co contamination in sample. † T's and τ's are as defined in Figure 1.
**14A-1D, -2D run side-by-side and are nominally identical.
***contains plagioclase. # indicates nichrome "buffer".
1 %XL ≡ percent crystallization; determined as in Benjamin (1979)

B. Determination of Pu and Sm Partition Coefficients

Partition coefficients are determined by measuring the ratio (crystal/glass) of nuclear particle track densities produced by the element of interest in some suitable detector. A fragment of glass, containing crystals is mounted in epoxy and polished until crystals are exposed and the glass surface is flat and unpitted. In the case of Pu, a sheet of mica, which is used as a fission track detector, is placed on the sample and the mica and sample are irradiated with thermal neutrons in a nuclear reactor, fissioning the ^{239}Pu. Fission fragments from the top 10 microns of the sample recoil into the mica and produce trails of lattice damage (tracks) which can be chemically etched to be optically visible (Fleischer et al., 1975). These tracks can then be counted using either an optical or scanning electron microscope. The measured partition coefficient (D_m) is then,

$$Dm = \frac{(\text{tracks/cm}^2)\ \text{crystal}}{(\text{tracks/cm}^2)\ \text{glass}} .$$

Corrections for differences in particle range (Section C, this chapter) and amounts of crystallization transform D_m into the "true" partition coefficient, D (Benjamin, 1979). In this study the Pu fission tracks were counted, from SEM photographs of the detector mica. Reactor irradiations and mica etching followed Benjamin (1979).

The Sm partition coefficients are measured using the same principle but a different technique (Mysen and Seitz, 1975; Benjamin et al., 1977; Holloway and Drake, 1977). Here the detected particle is a beta and the detector is photographic emulsion. A polished section of the ^{151}Sm-bearing sample is placed on a "nuclear emulsion" (Ilford, Ltd.; K5; 25μ) which is sensitive to beta particles. A 500g weight is placed on the sample to ensure good contact. The betas expose the photographic

plate which can then be developed. A typical exposure is shown in Figure 2. The amount of reduced Ag in the photographic image is approximately proportional to the amount of ^{151}Sm in the sample. In this case, therefore,

$$Sm_{Dm} = \frac{\text{(concentration Ag) crystal}}{\text{(concentration Ag) glass}} \quad .$$

The Ag content of the Sm image is measured by counting the Ag L X-rays generated by the electron bean of an SEM. A detailed description of this technique is given in Appendix I. The area scanned was typically $(23\mu)^2$ for pyroxenes and $(16\mu)^2$ for whitlockites. For data reported here, emulsions were typically developed for five minutes in Ilford D-19. Temperature was rather constant (typically 20-23°C). Figure 3 shows the changes in %Ag with development time. Percent Ag vs. development time is emulsion-batch dependent and for this reason, the development time given above is shorter than those in Appendix I. Typical samples are exposed to give 20-25% the count rate of Ag metal. Errors for individual analyses are based on statistical fluctuations in the beta fluence as determined by replicate analyses of a plate of the same emulsion batch exposed by a homogeneous ^{151}Sm source to also give 20-25% the Ag metal count rate. More details of the procedure used to estimate the counting statistics standard deviation are given in Appendix I, but the data there are for a different emulsion batch. The precision (σ = 3-5%) of replicate analyses obtained in these exposures also sets an upper limit on the amount of variability in nuclear emulsion sensitivity from point to point on a given plate. The typical precision of replicate (five) glass analyses of crystallized samples (σ~5%) agrees with that obtained from of a homogeneous source.

Partition coefficients of Sm were typically determined using two

Figure 2

This figure shows reflected light photo of a polished Pu17 sample (A) with one large pyroxene crystal (bottom) and two small crystals (top). The pyroxenes have the highest reflectivity, the glass is darker and the scratched area is epoxy. Immediately below is a beta map (B) of the sample. The beta map is a mirror image of the sample. The dark areas (glass) of the beta map indicate high ^{151}Sm concentrations. The lighter areas (crystals) indicate less ^{151}Sm. Sample size is ~ 1mm diameter.

A

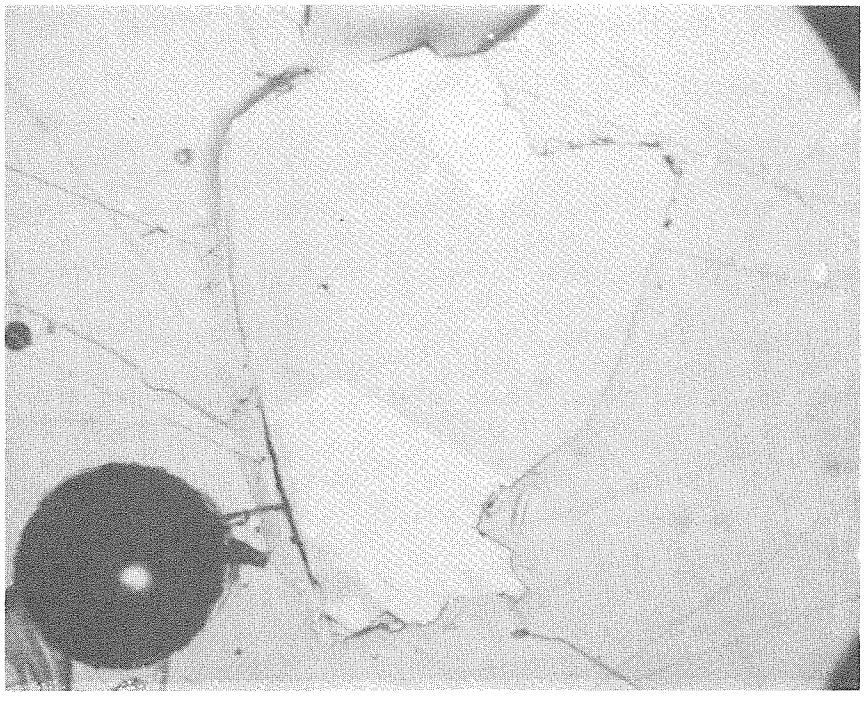

B

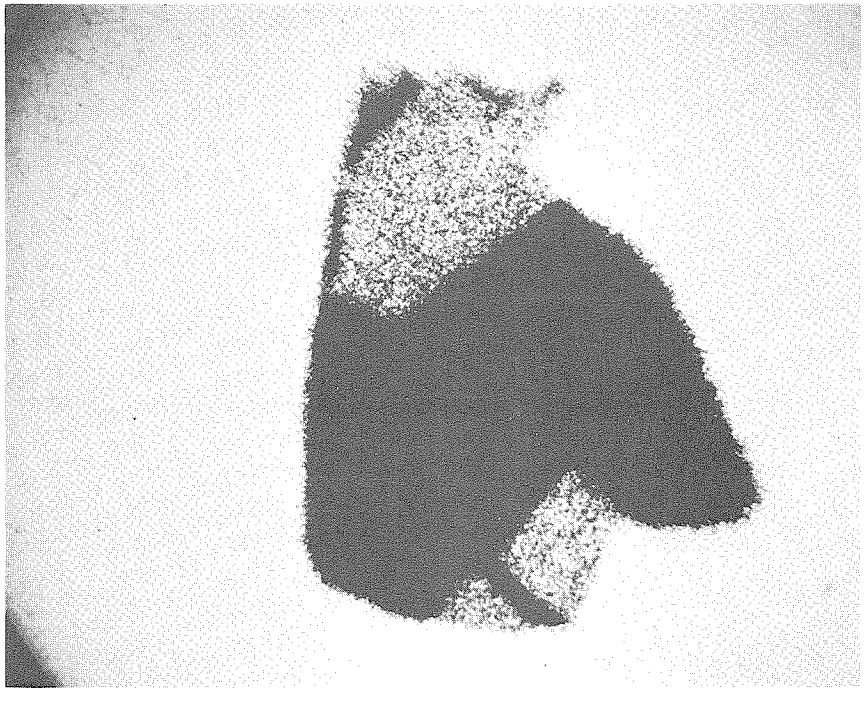

Figure 3

This figure shows the change in Ag counting rate with developing time for Ilford K5; 25μ emulsions. The emulsions of this study were typically developed for 5 minutes in Ilford D-19 developer. The scatter in the Ag counting rates, relative to any smooth trend, primarily reflects plate-to-plate variability in the Ag counting rate for constant exposure and development conditions. The data shown here come from a different emulsion batch than was used for most partition coefficient determinations.

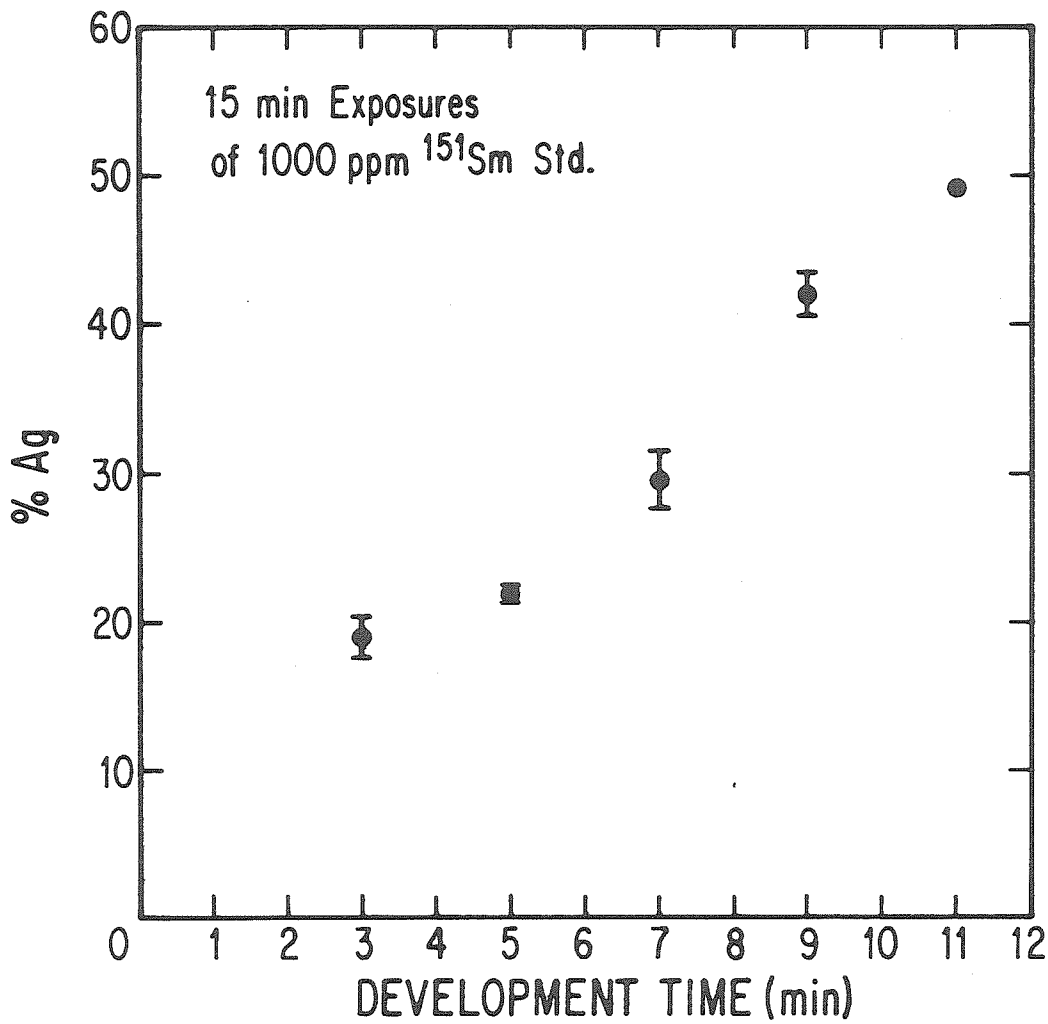
15 min Exposures
of 1000 ppm 151Sm Std.
% Ag
60
50
40
30
20
10
0
1
2
3
4
5
6
7
8
9
10
11
12
DEVELOPMENT TIME (min)

exposures (one for crystal and one for glass). Exposure times were adjusted so that the crystal of one exposure gives approximately the same Ag count as the glass of the second exposure. In this case,

$$Sm_D = \frac{\text{(concentration Ag) crystal}}{\text{(exposure time) crystal}} \Big/ \frac{\text{(concentration Ag) glass}}{\text{(exposure time) glass}} .$$

If the two exposures are timed such that the concentrations of Ag in the crystal and glass exposures are equal, then

$$Sm_D = \frac{\text{(exposure time) glass}}{\text{(exposure time) crystal}} .$$

A comparison of one-exposure and two-exposure Sm_D's typically give good agreement and differences are not systematic (see Table 4), suggesting that the nonlinearities in emulsion response described in Appendix I are usually not significant. Using the maximum observed low %Ag nonlinearity (Appendix I), one-exposure D's could be low by up to 40%, but the results from the two exposure technique should be correct. Typical exposure times are 5 hrs-crystal and 2 hrs-glass (diopside) and 45 min-crystal and 6 hrs-glass (whitlockite). Using the two exposure technique with equal (~ 20% Ag metal) Ag counting rates for both crystals and glass, the expected counting statistics standard deviation for a D value based on a single crystal measurement and five glass analyses with a 5% standard deviation for each analysis is 6%. Comparison of D values from exposures of the same sample on two different emulsion plates is complicated because the same crystals show complex zoning (discussed in detail in results section) and because there may be small differences ($\pm$ 20 microns) in the locations analyzed in the two plates. Nevertheless, as shown in Table 5, reasonable agreement is obtained in such comparisons. All D values in Table 5 are from the two exposure method. For variations

due entirely to counting statistics the average difference in two measurements should be 1.2σ , whereas 1.4σ is observed for the average of eight pairs of measurements. However, individual differences of 3σ are observed, and the possibility cannot be ruled out that the overall analytical error in ^{Sm}D is underestimated by a factor of ~ 1.5.

Table 4

Comparison of ^{Sm}D's Using One and Two Exposures

Sample	One Exposure	Two Exposure
14A-13Co		
CPX1-B	0.336 ± 0.043	0.270 ± 0.019
1-E	0.346 ± 0.044	0.309 ± 0.022
CPX1-A	0.304 ± 0.039	0.309 ± 0.022
CPX2-A	0.300 ± 0.038	0.268 ± 0.019
2-B	0.339 ± 0.043	0.343 ± 0.024
14A-14Co		
CPX1-A	0.278 ± 0.035	0.259 ± 0.018
1-B	0.273 ± 0.035	0.298 ± 0.021

Table 5

Comparison of Sm Analyses from Different Emulsions

Sm_{Dcpx}

Sample	Emulsion #1	Emulsion #2	$\frac{\Delta^*}{\sigma}$
14A-14Co			
CPX1-A	0.259 ± 0.019	0.322 ± 0.024	2.63
CPX1-B	0.298 ± 0.022	0.287 ± 0.021	0.52
CPX2-B	0.382 ± 0.029	0.378 ± 0.028	0.14
CPX3	0.292 ± 0.022	0.382 ± 0.029	3.10
14A-2HM			
CPX1-B	0.403 ± 0.030	0.370 ± 0.028	1.14
CPX2-A	0.293 ± 0.022	0.360 ± 0.027	2.48
CPX2-B	0.311 ± 0.023	0.331 ± 0.025	0.8
CPX3	0.487 ± 0.037	0.462 ± 0.035	0.71

* $\Delta = \left| Sm_D\#1 - Sm_D\#2 \right|$; σ = counting statistics standard deviation

Average $\frac{\Delta}{\sigma} = 1.4$

C. Spatial Resolution and Particle Ranges

The spatial resolution of these two particle mapping techniques is reasonably good. The "average" fission fragment range is about 3.5 mg/cm^2 (Northcliffe and Schilling, 1970) for an assumed total kinetic energy of 200Mev. In typical silicates this corresponds to a range (and resolution) of about ten microns.

The range-energy relations for beta particles are not so straightforward. Betas have a definite maximum range ($\overline{R}max$), but their attenuation in a thick absorber is approximately exponential so that, unlike fission fragments, few betas actually penetrate as far as their maximum energy would indicate. The mean range ($\overline{R}$) of a monoenergetic electron is given by:

$$\overline{R} = 0.412E^n \; ; \; n = 1.265 - 0.0954 \ln E \quad (0.01 < E < 3Mev).$$

(Katz and Penfold, 1952). Hence, for E = 0.076 Mev (Emax, ^{151}Sm), an $\overline{R}_{max}$ = 8.39 mg/cm^2 is calculated. However, since betas have a broad energy spectrum a more useful quantity is d 1/2, the absorber thickness necessary to stop 50% of the betas. In a typical silicate mineral, this corresponds to about eight microns (Evans, 1955). More details on the spatial resolution expected from ^{151}Sm betas are given in Appendix IV. In general only crystals $\gtrsim$ 30μ are considered usable. The smallest crystal on which data are reported is a 22μ wide whitlockite. No dependence of ^{Sm}D upon crystal size has been observed. This is shown in Figure 4 for whitlockite. It is also true for clinopyroxene.

Range corrections for fission fragments are made using the method of Benjamin (1979). This range correction is only applied to whitlockites since the pyroxene correction is very small ($\sim$ 1%). In the absence of detailed electron ranges for absorbers of different atomic number, the

Figure 4

This figure shows a plot of ^{Sm}D vs. crystal width (smallest dimension) for Pul5 whitlockites. One crystal is only 22 microns wide, but most crystals are > 30 microns wide. No obvious correlation of ^{Sm}D with crystal size is observed.

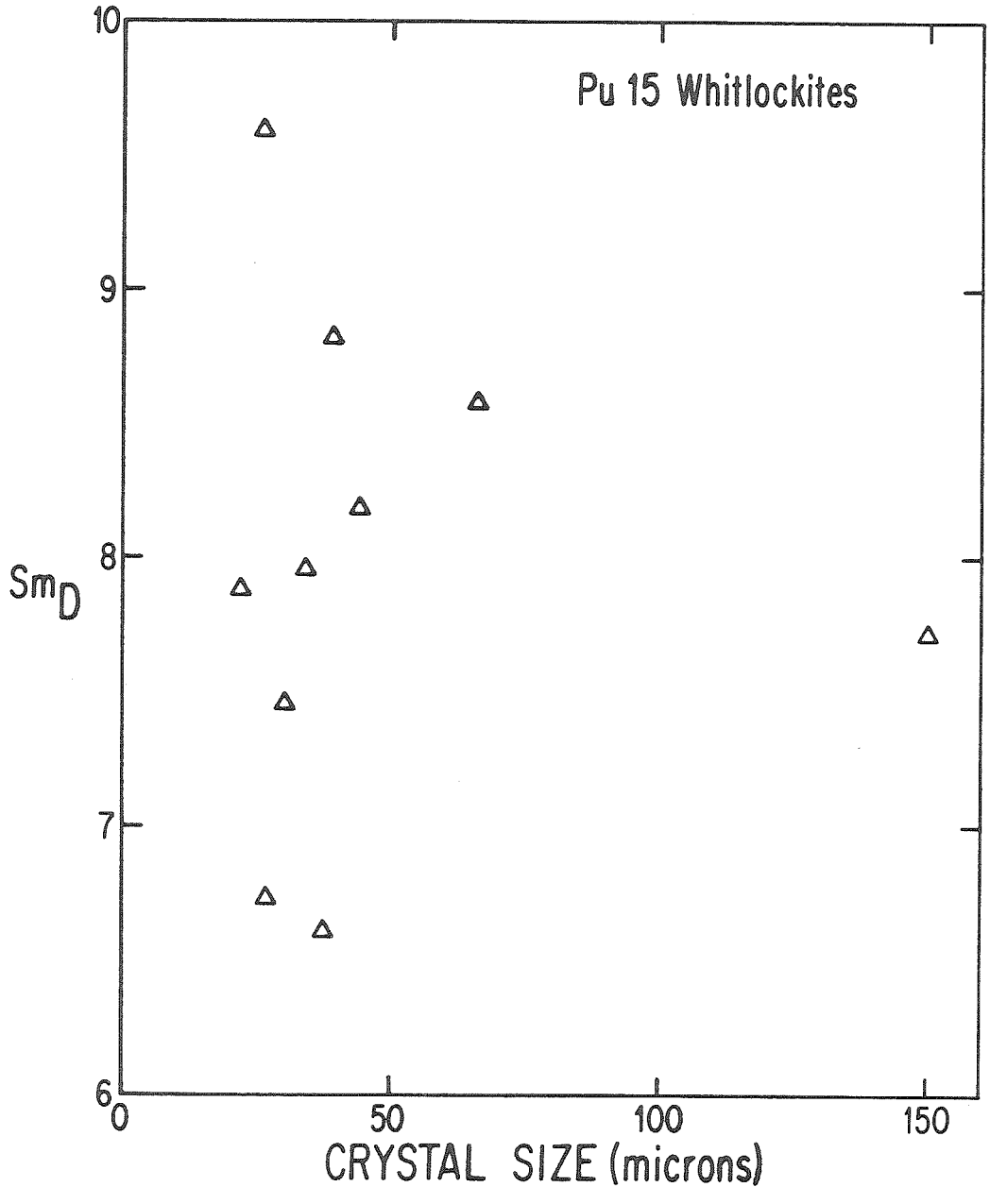
Pu 15 Whitlockites
10
9
8
7
6
Sm_D
0
50
100
150
CRYSTAL SIZE (microns)

semi-empirical calculations of Nelms (1956) were used to estimate differences in ^{151}Sm β ranges between minerals and glasses. Since calculated range differences for crystal-glass pairs were always $\leq$ 1%, no range corrections are made on the Sm data.

D. Nucleation

Although not considered to be a problem in the DiAnAb system (see, for example, Lindstrom and Weill, 1978), there have been difficulties at various times during this study in nucleating diopside. Some difficulties have been encountered with whitlockite as well. Three samples closely approximating the Pul4 (cpx) composition (one Pul3 and two Smut 32's from the study of Benjamin, 1979) were held 20°C above the liquidus for 20-24 hrs. before slow cooling was initiated to grow pyroxenes. These three samples were supercooled ~45°C below the liquidus without pyroxene nucleation. The only experimental difference between these samples and those with crystals appeared to be time above liquidus. In addition, two Pul5 (whit) samples were held ~17-20°C above the liquidus for 40-50 hours before slow cooling. The crystals from these runs were dendritic in texture, implying that there was a large amount of supercooling before nucleation followed by very rapid crystal growth. Infrared spectroscopic analysis of one of the Smut 32 samples showed negligible (~0.005%) water to lower the liquidus. Nucleation can be aided by reducing the superliquidus temperature of the samples. One Smut 32 experiment grew pyroxenes after 24 hours at 8-10°C above the liquidus and one Pul5 grew non-dendritic whitlockites after 40 hours at ~10°C above the liquidus. Both of these experiments used a method (1) thermal history (Figure 1).

Nucleation was also a problem in graphite capsule experiments (see also Appendix II). In this case, however, only 2 hours at ~25°C above the liquidus was sufficient to inhibit nucleation in two experiments, even at temperatures 70°C subliquidus. During this study, nucleation in graphite capsules has only been accomplished through "seeding" - either with $Pt_{95}An_5$ foil or with a diopside crystal; in 40% (2 of 5) of the Pt-

seeded experiments even this was not sufficient for nucleation.

Cooling method (2) was designed to insure that severe undercooling was not a problem in the normal (Pt container) experiments. It was found that 12-15 hours at ~5°C below the liquidus was sufficient to nucleate diopside in 3 out of 3 attempts for both Pul4 and Pul7 compositions. A single experiment with the Pul5 composition showed that this method was also adequate to nucleate whitlockite. Once diopside or whitlockite has been nucleated, larger crystals can be grown by slow cooling.

The observation that a Pt seed is often sufficient for nucleation in the graphite capsule experiments indicates heterogeneous nucleation. In the graphite-Pt-seed runs that did nucleate diopside, all crystals appear to originate at the Pt-silicate liquid interface. Under highly reducing conditions the Pt at this interface is actually a molten Pt-Si alloy (see Appendix II). Thus, the relationship of Pt to the nucleation of diopside in the higher fO_2 experiments (where Pt exists as solid Pt metal) is unclear.

Prior to the graphite experiments, the possibility was considered that destruction of homogeneous nucleation sites and/or rearrangements of the silicate liquid structure were responsible for the inability to grow diopside. The correlation of no nucleation with time above the liquidus supported this view. In an effort to check this, IR absorbtion spectra of several samples were taken to see if changes (in shape, intensity or position) of the 1000 cm^{-1} silicate band were correlated with thermal history. These experiments were inconclusive since the shape and intensity of the 1000 cm^{-1} feature are extremely dependent upon the particle size of the silicate glass. Repetitive grindings in a SiC mortar and pestle continued to produce changes in both peak shape and intensity

without ever, apparently, coming to steady state.

III. EXPERIMENTAL RESULTS

A. Interfacial Equilibrium

Because of the sluggish nature of intracrystalline diffusion (e.g. see McCallister et al., 1979), diffusive crystal-liquid equilibrium is not possible during the time scale of the experiments reported here (~ 1 day). The assumption behind the experiments of this study is that equilibrium will always be closely approached at the crystal-liquid interface, with no diffusive equilibrium within the crystal (i.e. fractional crystallization). Crystals grown by pure fractional crystallization will have compositional gradients that are predictable. The change in the chemical composition of the liquid from which the crystals grew is also predictable. In the case where $^{M}D_{xl}<1$ the concentration of trace element M in the first crystal is less than the concentration of M in the melt. Additional crystallization will further concentrate M in the melt and more M will enter into the crystal (at the interface, $^{M}C_{xl} = {}^{M}C_{liq}$). Thus, crystals will be zoned with the concentration of M increasing from core to rim. Conversely, if $^{M}D_{xl}>1$, M will be concentrated in the crystal, depleting the melt and causing the concentration of M in crystals to decrease from core to rim. The equations describing the concentration of elements in crystals and melt during fractional crystallization are given by Albarede and Bottinga (1972).

In order to attain interfacial equilibrium, homogenization of the liquid (by diffusion and convection) must be rapid with respect to crystal growth. If crystal growth is too rapid, incompatible elements ($^{M}D_{xl}<1$) will be concentrated at the crystal-liquid interface and compatible elements ($^{M}D>1$) will become depleted. In this situation a boundary layer,

depleted in compatibles and enriched in incompatibles, will form around the crystal and measured partition coefficients for such a crystal will be artificially high for incompatible elements and artificially low for compatible elements. During extremely rapid growth irregularities on the crystal surface which are closer to the outer edge of the boundary layer will grow preferentially and the crystal will become dendritic. The only sample used in this study which contained dendritic crystals was 14A-11Co which was cooled at a rate of 750°C/hr.

The assumptions of interfacial equilibrium and fractional crystallization have support from the study of Benjamin (1979). Benjamin showed that the variability of Pu and minor element (Na, Al) D values for pyroxenes grown at 20kbar was adequately explained by fractional crystallization. Because of complications in the experiments reported here, the assumption of interfacial equilibrium will be discussed further during presentation of the experimental results.

One means of documenting approach to equilibrium is through reversal experiments. To reverse the experiments of this thesis would require that a crystal, spiked with Pu and Sm above equilibrium concentrations, equilibrate with a melt at a subliquidus temperature. McKay (1977) successfully reversed the partitioning of Sr and Ce between plagioclase and liquid in 580 hours. Drake (1972), however, was not able to completely equilibrate Ca in plagioclase, even after 800 hours. Lindstrom and Weill (1978) attempted to reverse Ni partitioning into diopside. Lindstrom and Weill found "equilibrated" rims on their pyroxenes whose thickness did not increase with time (run duration up to 11 days), apparently ruling out diffusive equilibration. They interpreted these rims as equilibration by dissolution and reprecipitation of unequilibrated crystals.

Samples which are raised to a subliquidus temperature but never totally molten can be identified by the presence of a large number of small (~ 10μ) crystals. The results of Lindstrom and Weill (1978) suggested that a reversal experiment could be performed if small crystals highly concentrated in Sm would dissolve and reprecipitate on larger crystals, minimizing the surface free energy of the system. The reprecipitated rims should be a nearly ideal test of equilibrium since their growth rate should be very slow (i.e. the dissolution rate of the smaller crystals). Consequently, 14A-5D was raised to a temperature of 1229°C and held for two weeks. Unfortunately, even after two weeks no obvious increase in crystal size occurred. The largest pyroxene crystal was about 15μ -too small for either Pu or Sm analysis. Thus, equilibria in the experiments discussed here have not been confirmed by reversals.

B. Pyroxenes

1. Samarium and Aluminum

The measured Sm partition coefficients for Pul4 diopside pyroxenes are shown in Figure 5. As shown by Table 3, the samples in Figure 5 have similar final temperatures (T_f) and D's should be comparable. Error bars have been assigned based on the statistical fluctuations in the beta fluence (see preceding chapter and Appendix I). All Pul4 Sm analyses were made using two exposures (one for glass and one for crystal) on the same emulsion so that the Ag counting rates (~ 20% Ag metal) from glass and crystal would be comparable. The mean $^{Sm}D_m$ from all cooling methods [(1), (2), and (3) - see preceding chapter] is 0.347 $\pm$ 0.009 (error of mean). The variation in the data is 2-3 times that expected from the analytical uncertainty of the Sm measurements, if only statistical errors governed the spread. The mean of the method (2) Sm analyses is about 8% lower than the method (1) mean and 24% lower than the mean of the method (3) sample. The 0.462 datum has been excluded from the method (1) average since it lies 18σ from the mean. Because disequilibrium crystal growth will result in larger ^{Sm}D's (see Section A, this chapter) and because nucleation problems should be better controlled using method (2) (see preceding chapter), the discussion will first focus on the method (2) samples.

There is a $\pm$ 20% spread in the method (2) Sm data which is not entirely due to analytical imprecision. Figure 6 shows that pyroxenes with larger ^{Sm}D also tend to have larger ^{Al}D. Some scatter is introduced because the crystals are zoned (see Figure 7) and because the quality of the optical microscope of the microprobe makes it difficult to obtain a microprobe analysis on the same spot analyzed for Sm. This positional

Figure 5

This figure shows a breakdown of the Pul4 Sm data by sample and by crystal. Analyses labeled A, B, C, etc. refer to different areas on the same crystal. Samples generated by cooling methods (1), (2), and (3) are distinguished and the mean $^{Sm}D_{cpx}$ for each method is given (associated error is error of mean). Error bars are assigned based on the reproducibility of analyses of a homogeneous ^{151}Sm glass which was exposed to give the same Ag counting rate as the samples shown here. The precision of each analysis is $\pm$ 6%. Sample Pul4A-8A was not slow cooled but only held below the liquidus long enough to nucleate crystals. These crystals are small (~ 40μ)and the ^{Sm}D values reported are probably upper limits. Sample 14A-14A is included with method (1) runs because the time at T_I (~ 2 hrs.) was found to be insufficient for nucleation. Bracketed analyses of 14A-13Co, -14Co are replicate analyses of the same emulsion, taken on different days. The mean for the method (1) samples does not include the 14A-2HM-CPX-3A analysis (see text).

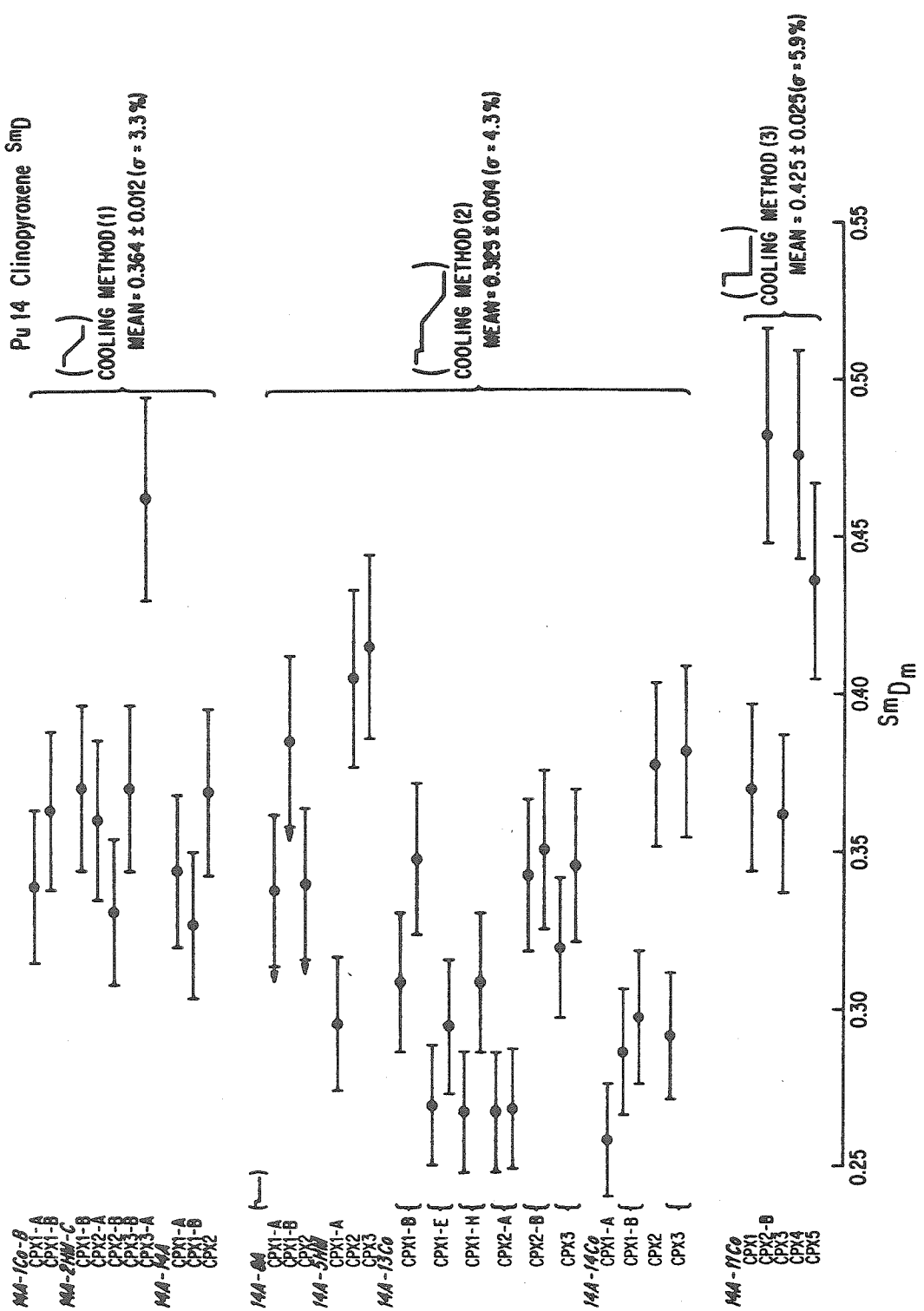
Pu 14 Clinopyroxene SmD
COOLING METHOD (1)
MEAN = 0.364 ± 0.012 (σ = 3.3 %)
COOLING METHOD (2)
MEAN = 0.323 ± 0.014 (σ = 4.3 %)
COOLING METHOD (3)
MEAN = 0.425 ± 0.025 (σ = 5.9 %)
14A-1Co-B
CPX1-A
CPX1-B
14A-2HW-C
CPX1-B
CPX2-A
CPX2-B
CPX3-B
14A-1AA
CPX3-A
CPX1-A
CPX1-B
CPX2
14A-4M
CPX1-A
CPX1-B
CPX2
14A-5HW
CPX1-A
CPX2
CPX3
14A-13Co
CPX1-B
CPX1-E
CPX1-H
CPX2-A
CPX2-B
CPX3
14A-14Co
CPX1-A
CPX1-B
CPX2
CPX3
14A-11Co
CPX1
CPX2-B
CPX3
CPX4
CPX5
0.25
0.30
0.35
0.40
0.45
0.50
0.55
SmDm

Figure 6

This figure shows point-by-point $^{Sm}D_m$ vs. $^{Al}D_m$ data for the method (2) Pul4 pyroxenes. Box symbols are for 14A-14Co pyroxenes; others are 14A-13Co. Sm error bars (6%) are the same as Figure 5; Al error bars (~ 1%) are assigned from microprobe counting statistics. Because of zoning, positional uncertainties are probably larger than the uncertainty due to counting statistics (see text). Typical positional errors in ^{Al}D are estimated at 2-5%. Although there is some scatter, the crystals with larger $^{Sm}D_m$'s tend to have larger $^{Al}D_m$'s as well. The line shows the range in D values expected during 20% fractional crystallization ($^{Al}D = 0.18$ and $^{Sm}D = 0.35$).

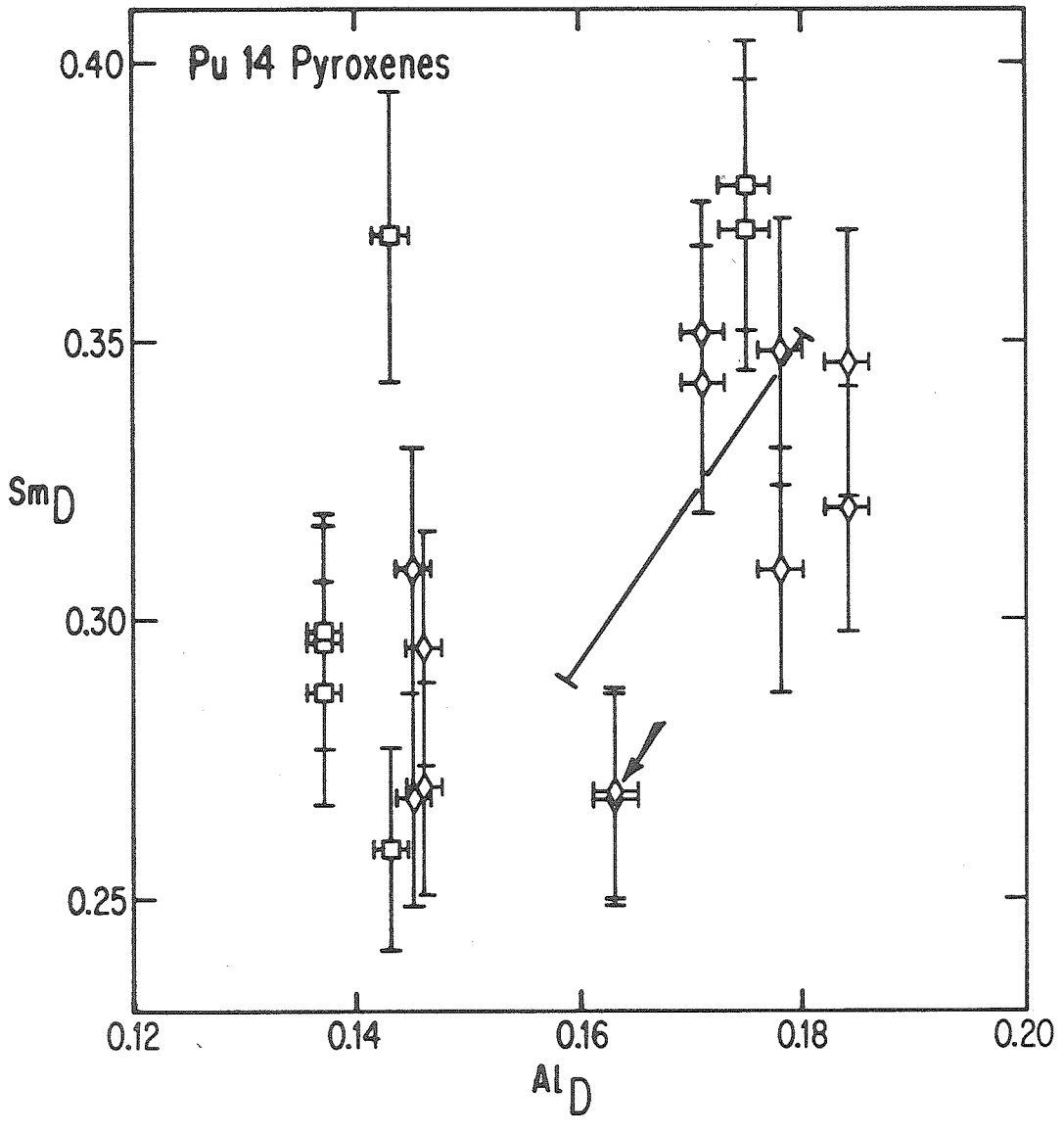
Pu 14 Pyroxenes
0.40
0.35
0.30
0.25
Sm D
0.12
0.14
0.16
0.18
0.20
Al D

uncertainty is estimated to be worth 2-5% for ^{Al}D, which is larger than the microprobe counting statistics error (~ 1%). An extreme case of positional uncertainty is the set of two analyses marked by an arrow. Two other Al analyses in the same general area yield ^{Al}D of 0.147 and 0.170. Only one other analysis (box symbol in upper left of Figure 6) deviates greatly from a correlation trend of ^{Sm}Dm and ^{Al}Dm. A second ^{Sm}D analysis of this pyroxene on the same emulsion (plotted directly beneath the discrepant point) yielded a much lower ^{Sm}Dm, in agreement with the correlation. 14A-5HM, another two-stage sample, was not included, since the oxygen fugacity of the hematite-magnetite buffer differs from the reducing conditions of meteorite formation.

Presumably the same factors which cause ^{Al}D to increase also affect ^{Sm}D. One possible cause for changes in Dm's is fractional crystallization. Given the amount of crystallization and assuming that ^{Sm}D and ^{Al}D are known, the amount of change in Dm's during fractional crystallization may be calculated (Albarede and Bottinga, 1972). The bar in Figure 6 was calculated assuming $^{Sm}D = 0.35$ and $^{Al}D = 0.18$ (~ the largest values from Figure 6; during fractional crystallization, the last crystals to grow have the highest D) and shows the maximum amount of change in Dm's after 20% fractional crystallization. The range in Dm's is larger than can be accounted for by fractional crystallization, although the extreme values still presumably correspond to the first and last formed crystals. The inadequacy of fractional crystallization in explaining Al zonation is shown in more detail by Figure 7, which compares the Al profile of a pyroxene grain with a calculated profile assuming fractional crystallization and $^{Al}D = 0.19$ (the largest value from Figure 6). The measured Al profile is steeper than the model would predict. A similar Al profile

Figure 7

This figure shows part of a microprobe Al traverse across cpx-1 of 14A-13Co. The Al data are contrasted to the calculated profile produced by $^{Al}D = 0.19$ during 20% fractional crystallization. Error bars are based on the microprobe counting statistics. Microprobe beam size was ~ 2 microns. The poor fit of the calculated curve to the data indicates either an increase in ^{Al}D with decreasing temperature or a departure from equilibrium. The interior points of the traverse are equivalent to ~ 2 wt.% Al_2O_3.

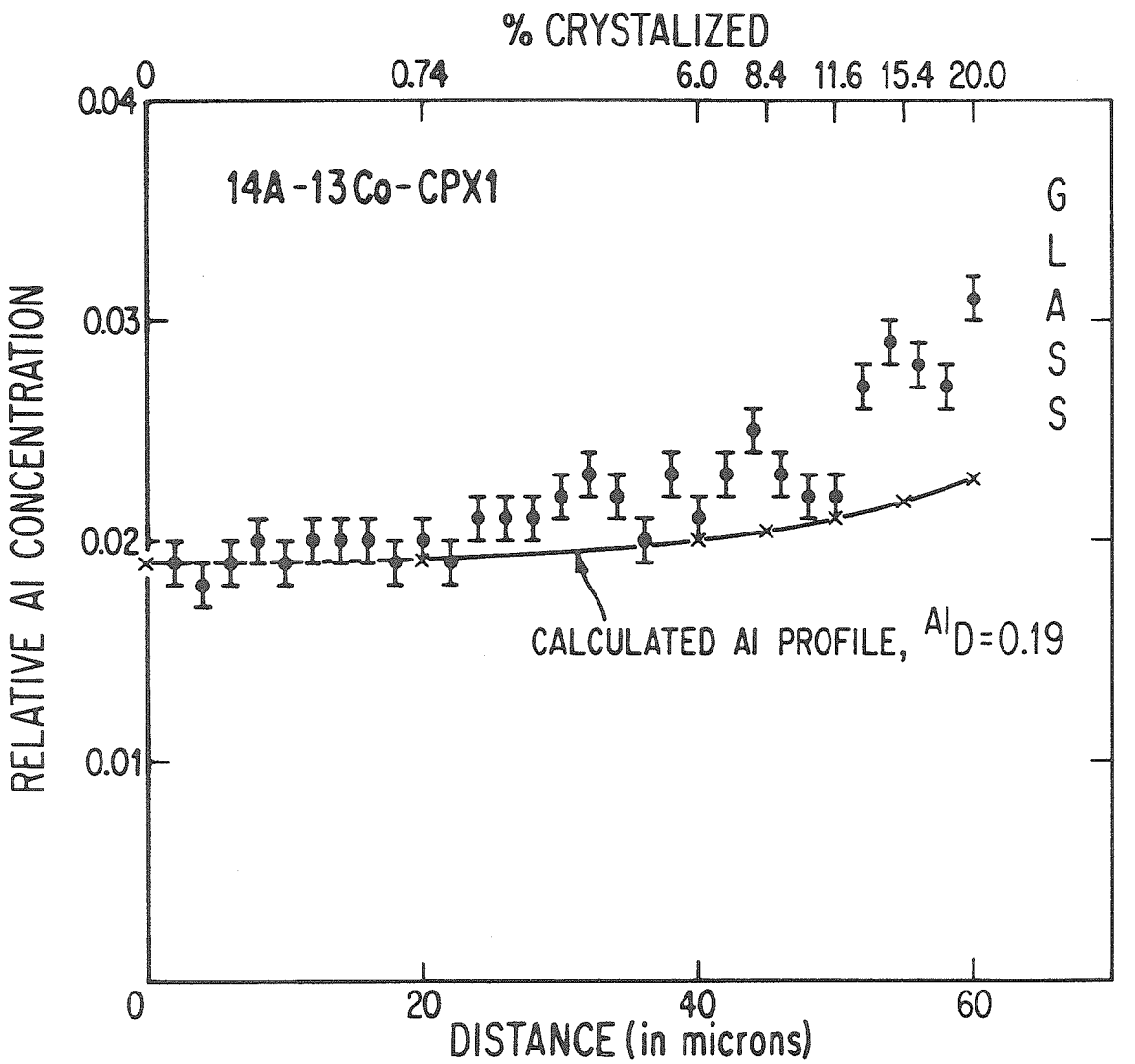
% CRYSTALIZED
0
0.74
6.0
8.4
11.6
15.4
20.0
14A-13Co-CPX1
GLASS
RELATIVE Al CONCENTRATION
0.04
0.03
0.02
0.01
CALCULATED Al PROFILE, $^{Al}D=0.19$
0
20
40
60
DISTANCE (in microns)

was also seen by Benjamin (1979) for 20kbar pyroxenes. The calculated profile in Figure 7 would not be noticeably changed if ^{Al}D were assumed to be either 0.30 or 0.10 rather than 0.19. Sm zoning is more difficult to document (two typical Sm analyses would cover the traverse in Figure 7), but ^{Sm}D and ^{Al}D appear to be correlated (Figure 6) and, in general, pyroxene cores yield lower ^{Sm}Dm than do rims. The discrepancy between the observed and calculated Al profiles in Figure 7 indicates either a departure from equilibrium or an increase in ^{Al}D with decreasing temperature. Because of the importance and the difficulty of documenting the approach to equilibrium, the possibility of disequilibrium will be discussed in more detail.

The simplest means of generating a correlation between $^{Sm}D_m$ and $^{Al}D_m$ by a disequilibrium process is rapid crystal growth. If a crystal grows faster than elements in the melt can diffuse, a boundary layer enriched in incompatible elements is produced. Since the concentration of an element in a crystal is proportional to the concentration of that element in the liquid from which that crystal grew, abnormally high D's can be produced in this manner (Albarede and Bottinga, 1972).

Tests of the importance of this type of kinetic disequilibrium are (1) to grow crystals at different cooling rates and (2) to search for compositional gradients in the liquid from which the crystal grew. Benjamin (1979), using the same cooling rates as this study (~ 3°C/hr.), was unable to observe gradients in the Pu concentration of his 1bar glasses; nor was he able to observe differences in the D's of phosphates grown at < 20°C/hr. In growing pyroxenes at 20kbar, cooling rates of 70°C/hr. were necessary to produce ~ 50% effects in elements (U and Th) with D's as low as 0.002 (Benjamin, 1979). This cooling rate is ~ 20X more rapid than the

experiments of this study. Although these results are not applicable to Sm per se, the lower D's and larger atomic weights (possibly indicating slower diffusion relative to Sm) of these elements would be expected a priori to accentuate the effects of kinetic disequilibrium.

As an additional check, Pu 14A-13Co (a method (2) sample) was quenched immediately after termination of cooling (within 5 minutes) and compositional gradients in Al were searched for near a crystal-glass interface using the electron microprobe. Although not as direct as searching for Pu or Sm gradients, the Al data have the advantage of better spatial resolution (~ 2μ).

Figures 8, 9, and 10 show the results of two Al traverses across cpx-1 of 14A-13Co, which appears to be a composite of ~4 individual pyroxene crystals. One side of the crystal (AA') shows essentially no Al gradient within 10μ of the crystal, but the opposite side (BB') shows a definite gradient with Al concentration increasing as the crystal is approached. This boundary layer is at least 10μ wide and indicates that crystal growth was rapid compared to the diffusion of Al in the melt. Even on the "no gradient" side the Al concentration of the glass is variable and may represent an "old" boundary layer that has not completely remixed with the main mass of melt. Quantitative microprobe analyses (30μ spot) of the 14A-13Co glass show variable Al_2O_3 with a range from 15.0 to 18.4% Al_2O_3. This is not seen in samples which set at the final temperature for times on the order of hours before quenching. Consequently, it appears that liquid Al compositional inhomogeneities are removed on an hour time scale at 1200°C. Within the crystal the Al traverses are complex and the "gradient" side shows evidence of oscillatory zoning. Whether this is further evidence of rapid crystal growth or normally

Figure 8

This figure shows cpx-1 of 14A-13Co, a composite crystal composed of several (~ 4) pyroxenes. The line AB designates the Al traverse of Figure 9. The line A'B' is the Al traverse of Figure 10.

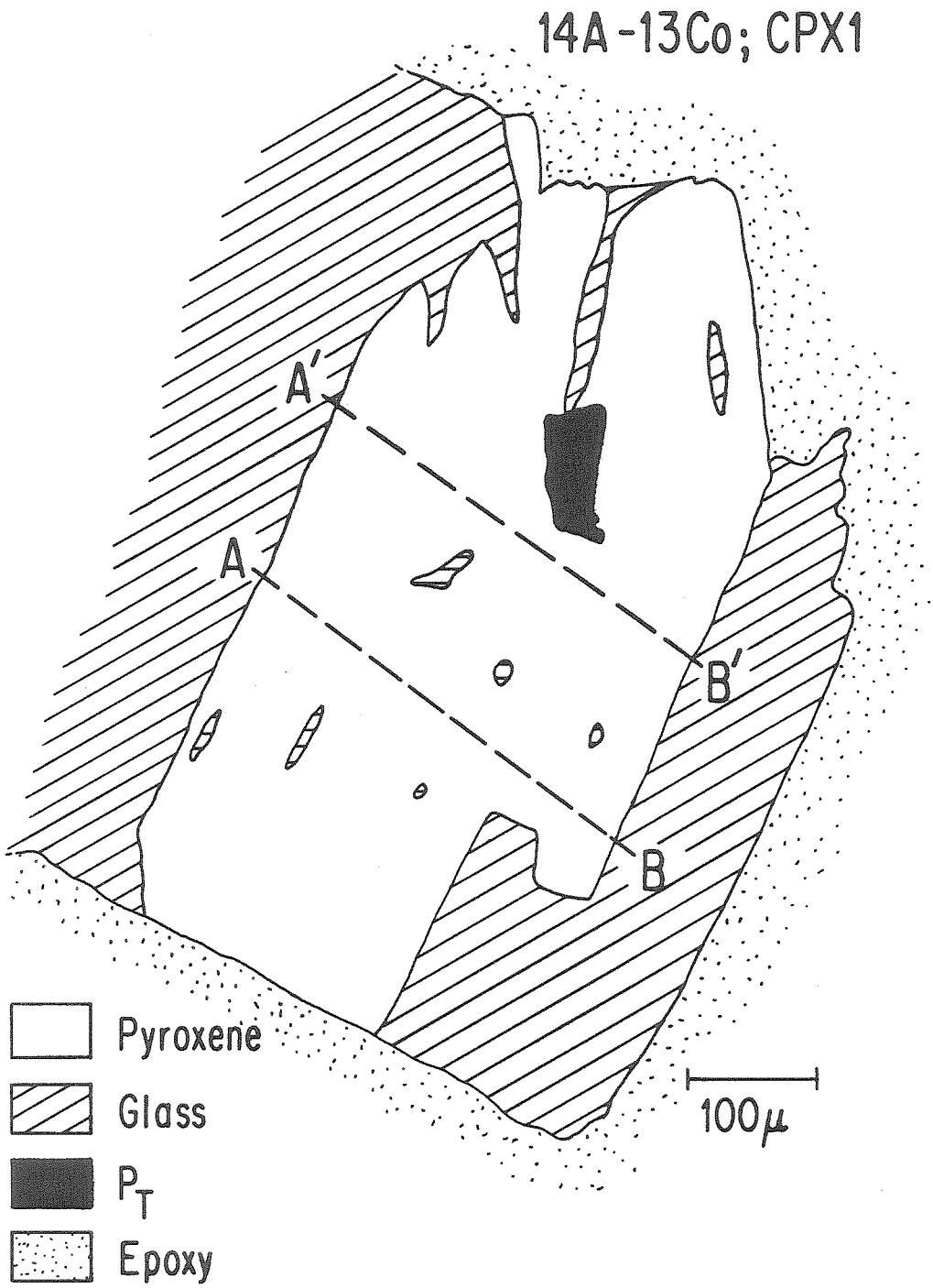
14A-13Co; CPX1
A'
A
B'
B
Pyroxene
Glass
P_T
Epoxy
100μ

Figure 9

This figure shows Al analyses from microprobe traverse #1(A-B) across cpx-1 of 14A-13Co. Representative error bars are shown on two points. High Al points within crystal are small glass inclusions. The glass near point B is ~ 14% enriched in Al over the point a class and decreases with distance from the crystal. This indicates that the B side crystal growth was rapid compared to Al diffusion in the melt. Note change of scale on vertical axis.

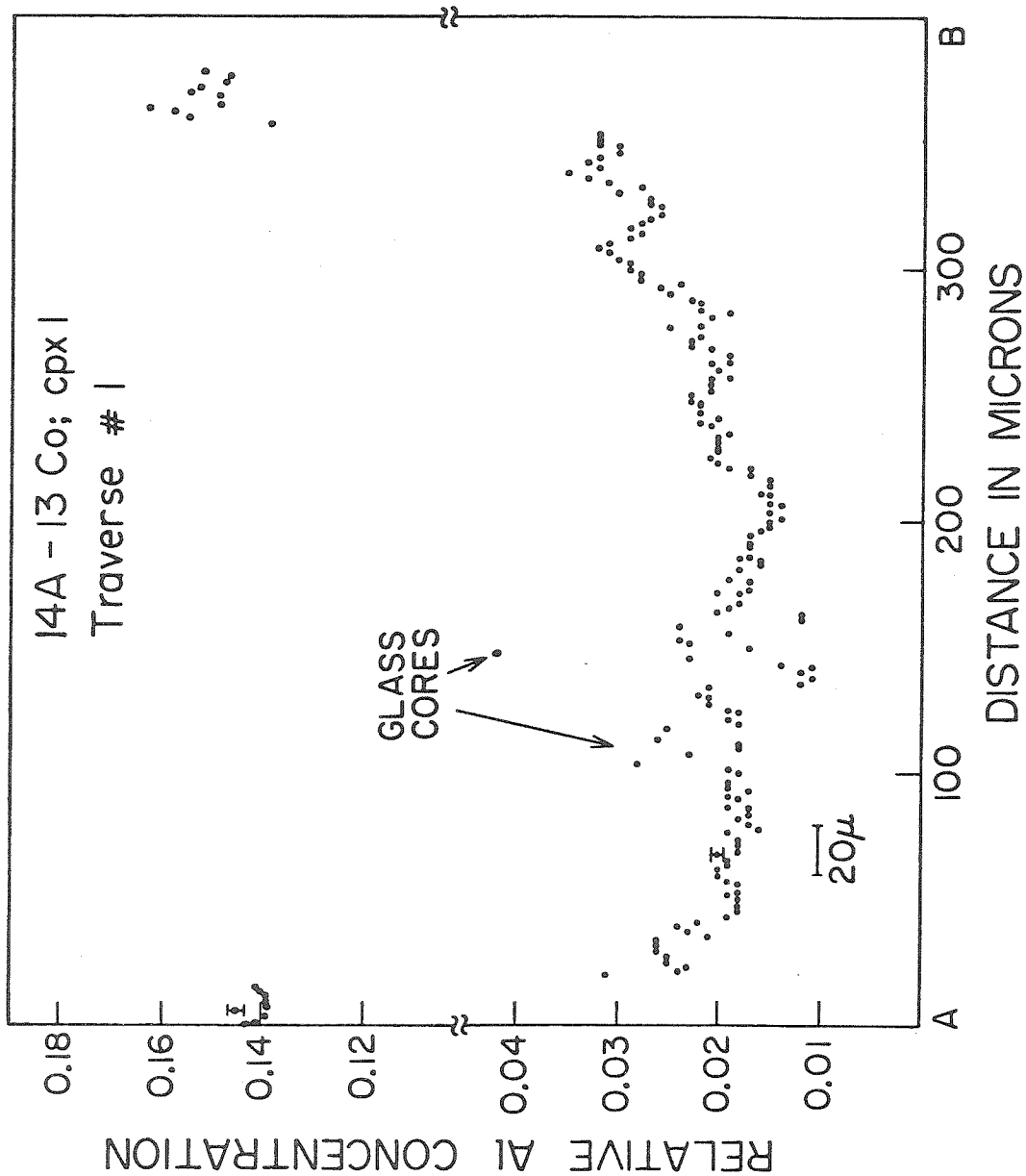
14A - 13 Co; cpx 1
Traverse # 1
GLASS CORES
20μ
RELATIVE Al CONCENTRATION
0.18
0.16
0.14
0.12
0.04
0.03
0.02
0.01
A
100
200
300
B
DISTANCE IN MICRONS

Figure 10

This figure shows a second Al traverse (A'B') across cpx-1 of 14A-13Co. Oscillatory zoning is pronounced and a steep Al gradient in the glass is observed at B'. Note change of scale on the vertical axis.

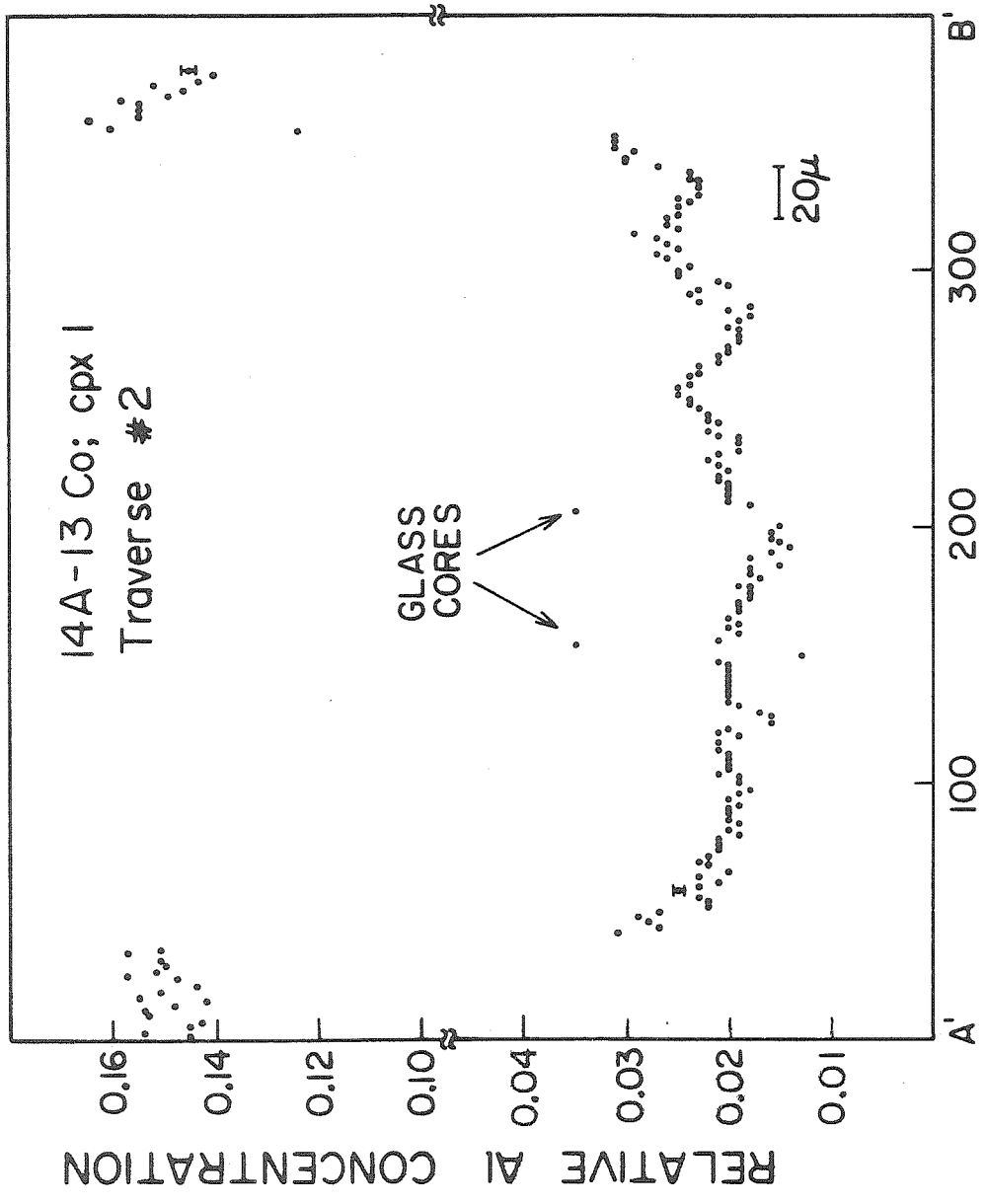
14A-13 Co; cpx 1
Traverse #2
GLASS CORES
20μ
RELATIVE Al CONCENTRATION
0.16
0.14
0.12
0.10
0.04
0.03
0.02
0.01
A'
B'
100
200
300
DISTANCE IN MICRONS

zoned crystals which have grown together is uncertain. The important conclusion from the 14A-13Co Al profiles is that even early nucleation of crystals is not sufficient to prevent supercooling and rapid crystal growth in this system.

It is not clear to what extent Sm partitioning has been affected by the rapid crystal growth demonstrated by the Al results of 14A-13Co. With 10μ spatial resolution, a 10μ boundary layer enriched in Sm by 10% would be difficult to detect considering the precision of a typical analysis (± 5%). However, a set of six Sm glass analyses taken in approximately the same locations as the variable (15.0 - 18.4%) quantitative Al analyses do not show the same variability. Beam sizes for the Sm and Al analyses were similar (20-30μ). The glass areas showing high Al_2O_3 gave average or below average Sm concentrations. The standard deviation of the six Sm analyses was ± 5% (the same as expected from counting statistics) - and better than the standard deviation of the Al analyses (± 8%). This suggests that Sm diffusion may have been rapid enough to keep pace with crystal growth while Al diffusion was not. As discussed previously for Figure 6, this suggestion is compromised by the inability to take Sm and Al analyses on exactly the same spot. Additionally, a significant amount of Sm variability could exist within the precision of the analyses (± 5%).

2. Na-Al Correlations

A different argument against kinetic control of ^{Sm}D in diopside comes from the Na partitioning data. If one assumes that the highest ^{Al}D's and ^{Sm}D's in Figure 6 are the result of rapid crystal growth, then the boundary layers must have been enriched in Al, Sm, and Na and depleted in Ca and Mg. If Na substitution is primarily as jadeite, then Na should

be important in maintaining charge balance during Al substitution and the Na concentration should proportionally increase with Sm and Al. Figure 11 shows a plot of ^{Na}D vs. ^{Al}D for method (2) (two stage) pyroxenes. Na_D/Al_D is not constant and decreases with increasing ^{Al}D, the opposite of what would be expected during kinetic disequilibrium, if Na and Al diffuse at similar rates in the liquid. Figure 12 shows that the crystals with the highest Al content have a smaller percentage of the Al in the form of jadeite ($NaAlSi_2O_6$). In other words, as the pyroxene Al content increases, the Na/Al ratio decreases. The trend in Figure 12 is not easily understood in terms of kinetic disequilibrium and argues that the observed variations in D's do not simply reflect the influence of boundary layers. Searching for Na boundary layers faces the same difficulty as Sm in that large beam sizes (20-30μ) are necessary (to avoid Na volitilization) and result in poor spatial resolution. The validity of this argument for equilibrium is questionable if Na diffusion is much more rapid than Al. Although relative diffusion coefficients for Na and Al are not well known, recent data by Powell et al. (1980) suggest that Na diffuses at about half the rate of Al in basaltic melts. The variations in Na and Al partitioning presented in Figures 11 and 12 are therefore best interpreted as primarily due to differences in temperature of nucleation and/or growth of the analyzed pyroxenes. However, the Al profiles of Figures 9 and 10 show that some contribution from kinetic effects must still be present. A decrease in ^{Al}D with increasing temperature can be inferred from the one bar data of Hytönen and Yoder (1961) who observed an increase in the solubility of Ca-tschermakite ($CaAl_2SiO_6$) in diopside with decreasing temperature in the system diopside-Ca-tschermakite. Additionally, Benjamin

Figure 11

This figure shows a plot of $^{Na}_{Dm}$ vs. $^{Al}_{Dm}$ for 14A-13Co, -14Co pyroxene analyses. Errors are microprobe counting statistics. Although $^{Na}_{D}$ and $^{Al}_{D}$ correlate, the $^{Na}_{D}/^{Al}_{D}$ ratio changes from ~ 0.35 to 0.3. This is the opposite sense to that expected if $^{Na}_{D}$ and $^{Al}_{D}$ were controlled by kinetic disequilibrium. Triangles represent 14A-13Co analyses.

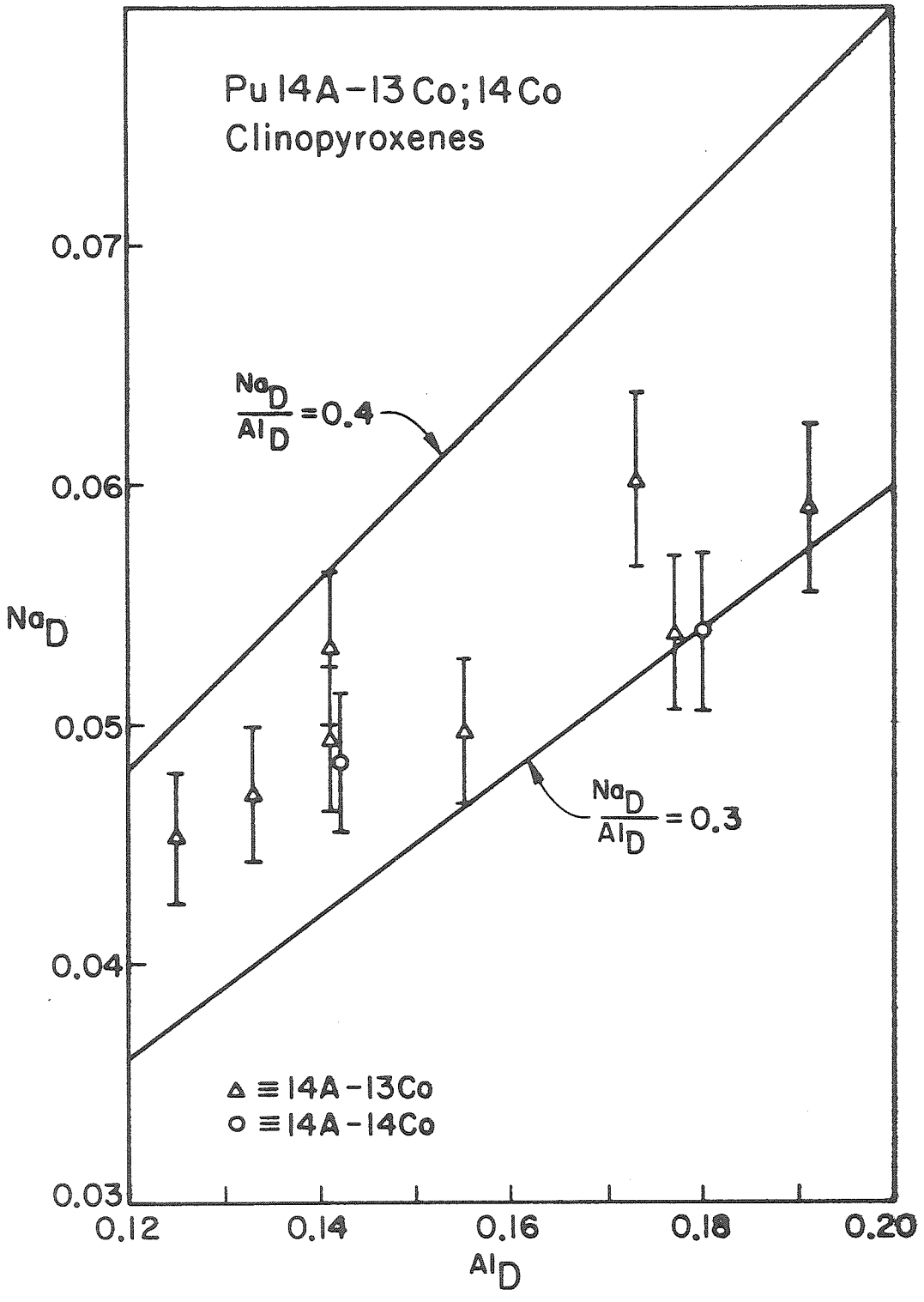
Pu 14A-13Co; 14Co
Clinopyroxenes
$\frac{Na_D}{Al_D} = 0.4$
$\frac{Na_D}{Al_D} = 0.3$
△ ≡ 14A-13Co
○ ≡ 14A-14Co
Na_D
Al_D
0.07
0.06
0.05
0.04
0.03
0.12
0.14
0.16
0.18
0.20

Figure 12

This figure shows the fraction of Al in method (2) pyroxenes that exists as jadeite solid solution. Errors (5-6%) are from the pyroxene Na counting statistics. The Al is assumed to exist only as jadeite ($NaAlSi_2O_6$) and Ca-tschermakite ($CaAl_2Si_2O_6$). As %Al in the pyroxene increases the percentage of jadeite decreases. This is the opposite of what would be expected if the D's of this study were controlled by kinetic disequilibrium.

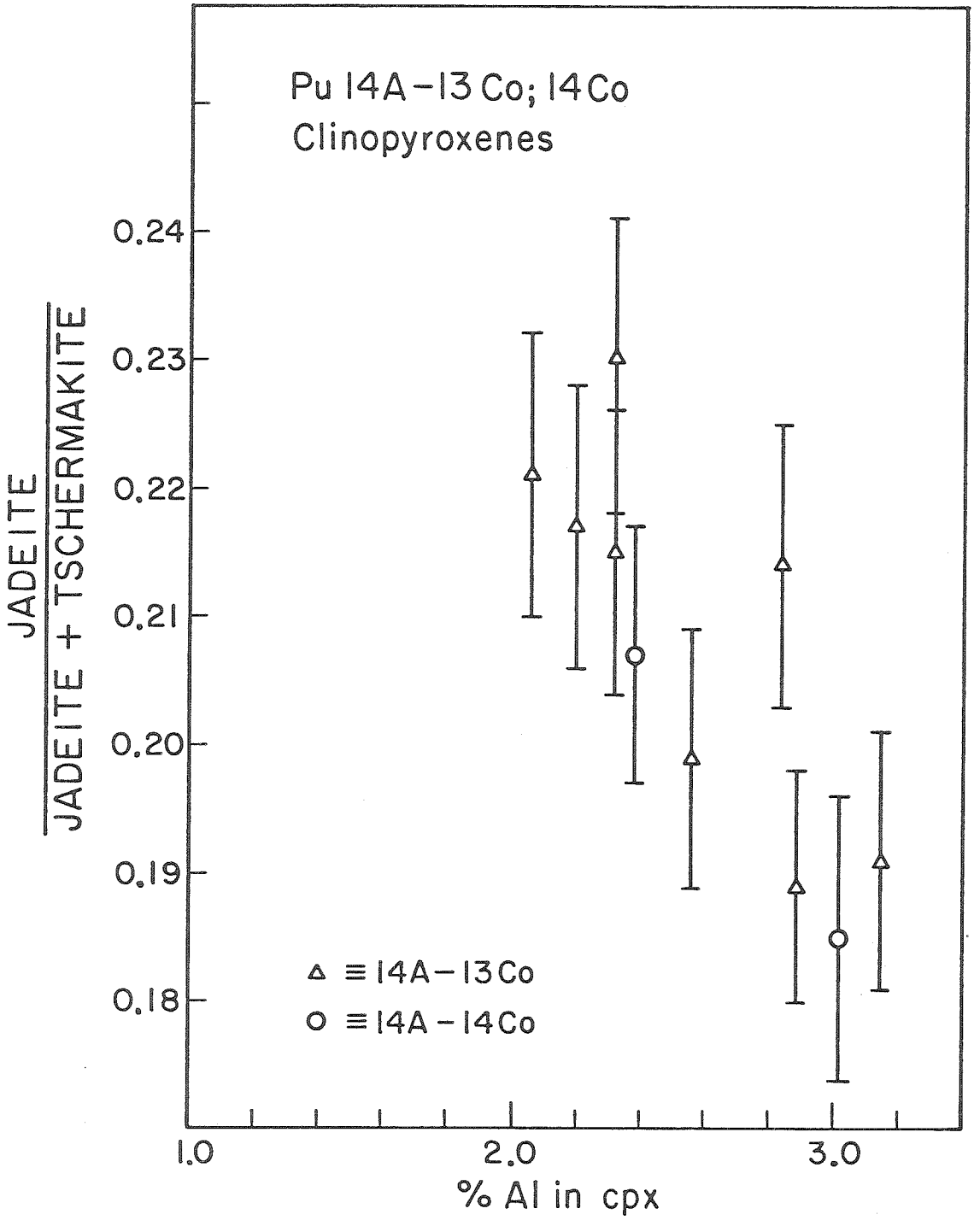
Pu 14A-13Co; 14Co
Clinopyroxenes
JADEITE / JADEITE + TSCHERMAKITE
0.24
0.23
0.22
0.21
0.20
0.19
0.18
△ ≡ 14A-13Co
○ ≡ 14A-14Co
1.0
2.0
3.0
% Al in cpx

(1979) noted that the Al zoning of his 20kbar pyroxenes was too large to be explained by fractional crystallization, although Na zoning agreed well with a fractional crystallization model. Benjamin's Al data could also be explained by increasing ^{Al}D with decreasing temperature.

If ^{Al}D and ^{Na}D are primarily influenced by temperature rather than kinetic disequilibrium, then the ^{Sm}D-^{Al}D correlation of Figure 6 should also be due to temperature. (The range of the data in Figure 6 was too large to be explained by fractional crystallization.) This is also the most reasonable interpretation of the difference between the method (1) (one-stage) and method (2) (two-stage) ^{Sm}D data (Figure 5). The average method (2) ^{Sm}D value is slightly lower and, moreover, the standard deviation of the method (2) D values is ~ 2.5X that of the method (1) pyroxenes. If nucleation occurred at a lower temperature for the method (1) samples (due to greater supercooling), then crystals would grow at a lower temperature and over a smaller temperature range. If ^{Sm}D increases with decreasing temperature in the same manner as ^{Al}D, then the method (1) pyroxenes should have a larger average ^{Sm}D with less spread. This interpretation is consistent with Drake and Holloway (1977), who noted that $^{Sm}D_{cpx}$ increased with decreasing temperature, but does not preclude kinetic disequilibrium effects.

3. Experiments of Extended Duration

As a further effort to check the approach to equilibrium of the method (2) samples, several samples (14A-1-4D) were generated using method (3) (rapid drop and hold) but were left at final temperature for one to two weeks to see if there was any tendency for equilibration either by crystal dissolution and reprecipitation or by diffusion. In either case,

if the crystals grown by a sudden drop in temperature are not in equilibrium with the co-existing melt, then equilibrated rims should form. The thickness of the rims would be determined either by the volume of crystal which dissolved and reprecipitated or by the rates of diffusion in pyroxene. None of these samples was buffered because of the large loss of Co to the Pt container over these time periods (see preceding chapter). 14A-1D and 14A-2D were hung side by side during a single furnace run and are nominally identical. 14A-1D was irradiated to measure ^{Pu}D and 14A-2D was used for Sm analysis. The Pu track map of 14A-1D showed no rim but the low fission track densities of the pyroxenes ($\sim 5 \times 10^6/cm^2$) would make the recognition of a rim difficult. The beta map of 14A-2D, however, did show rimmed pyroxenes - or at least showed reverse zoning of Sm. As illustrated in Figure 13, cores of 14A-2D pyroxenes yielded ^{Sm}D values of 0.36-0.39; rim ^{Sm}D values ranged between 0.21-0.25 - the lowest $^{Sm}Dcpx$ values measured for Pul4 pyroxenes. Figure 14 shows that Al concentrations in 14A-2D; cpx-1 are up to ~ 30% lower near crystal-glass contacts than in the crystal core. 14A-1D the companion sample to 14A-2D also showed low-Al rims; ^{Al}Dm values for cores ranged from 0.13-0.17 (within the rage of method (2) runs) while ^{Al}D from rims averaged 0.11-0.12, consistent with the 14A-2D data. 14A-3D, an independent method (3) sample, is also reverse zoned in Sm (rimmed?) but ^{Sm}Dm values range from 0.32 (rim) to 0.43 (core), overlapping but slightly higher than the method (2) samples.

14A-4D differs from the other 1-2 week runs in that plagioclase nucleation occurred. The ^{Sm}Dm cpx values for this run range from 0.24-0.32. The presence of plagioclase and the large amount of crystallization in this run (~ 50%) complicate the interpretation of the measured D's.

Figure 13

This figure shows $^{Al}D_m$ and $^{Sm}D_m$ data for two samples which were stepcooled from above the liquidus to ~ 1200°C. Error bars are standard deviations of six and four analyses of cores and rims, respectively. Sm and Al data do not come from exactly the same location and are meant to illustrate differences between cores and rims. A field encompassing the method (2) pyroxene data is shown for comparison. The core data plot slightly higher than the method (2) field. The rim data fall on an extention of the method (2) trend.

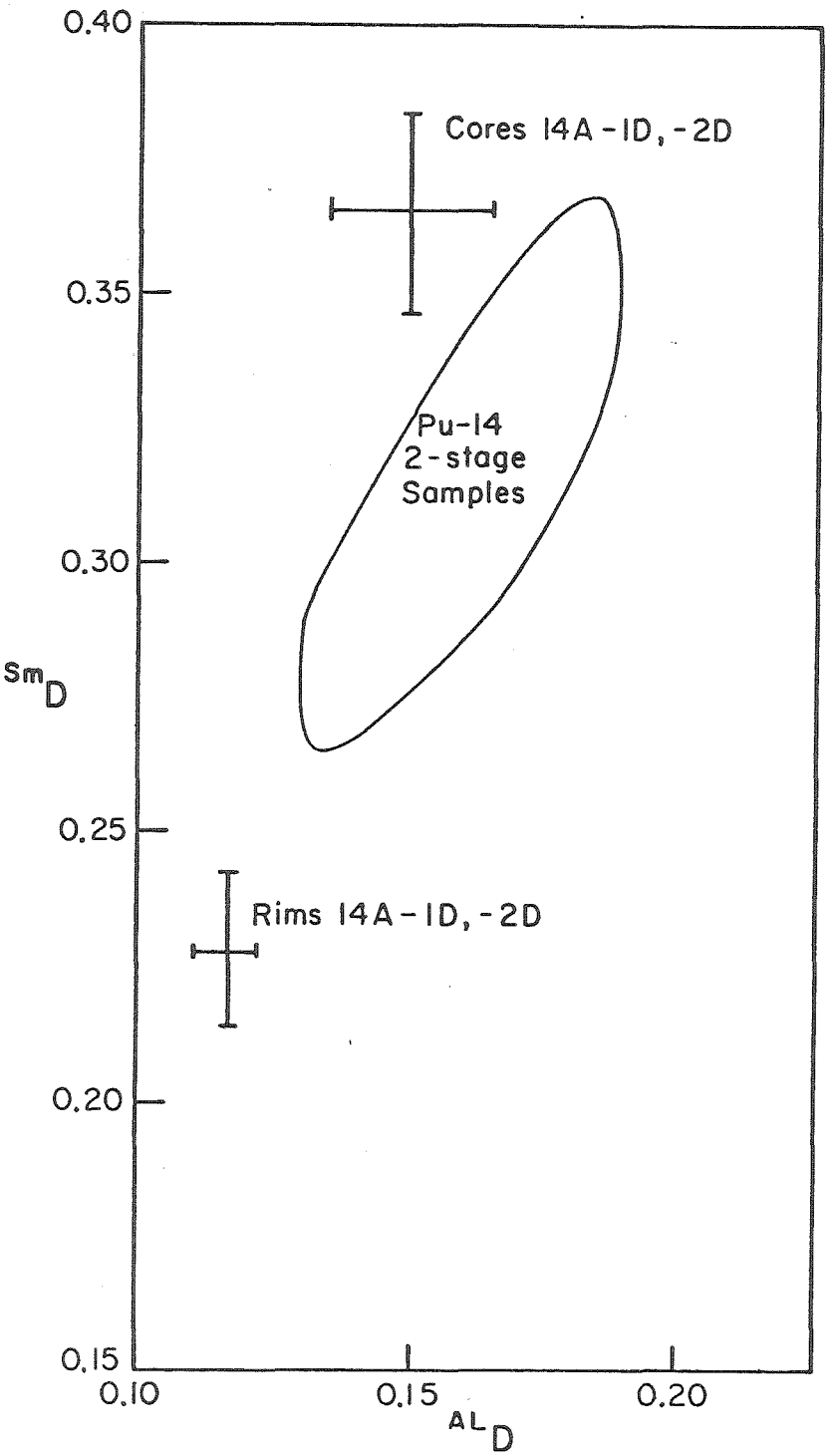
0.40
0.35
0.30
0.25
0.20
0.15
0.10
0.15
0.20
$^{Sm}_{D}$
$^{AL}_{D}$
Cores 14A-1D, -2D
Pu-14
2-stage
Samples
Rims 14A-1D, -2D

Figure 14

This figure shows a microprobe Al traverse across cpx-1 of 14A-2D. Note change of scale on the vertical axis. The crystal is reversed zoned in Al with a high Al core. Note the large differences (~ 25%) in Al concentration between opposite sides of glass inclusions. Error bars are shown on 2 points. The highest core Al concentrations correspond to $Al_D \sim 0.17$. Inset shows the crystal traverse.

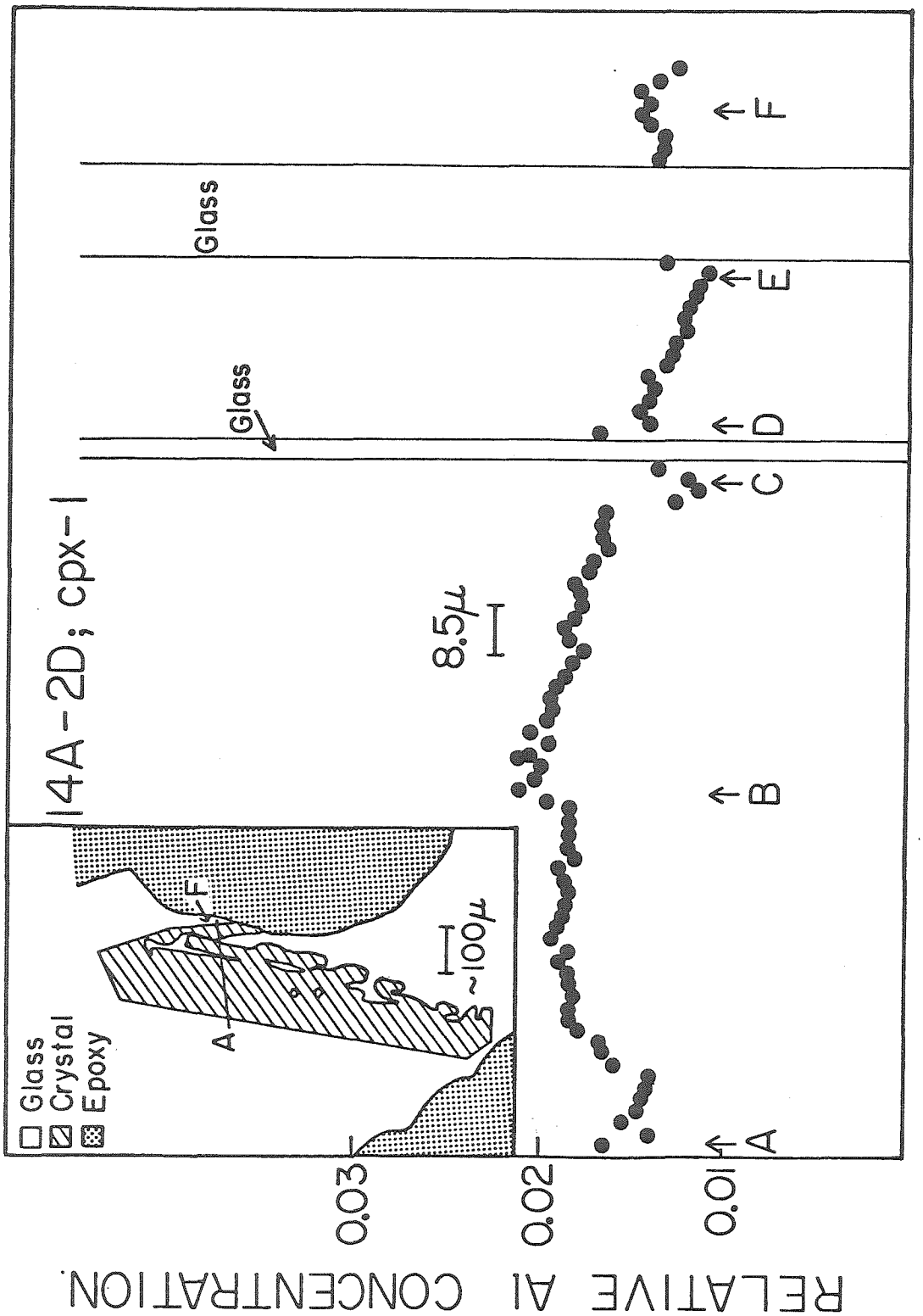
RELATIVE Al CONCENTRATION
0.03
0.02
0.01
14A-2D; cpx-1
Glass
Glass
Glass
Crystal
Epoxy
8.5μ
~100μ
A
B
C
D
E
F
A
F

No low-Sm rims are observed, but the significance of this is uncertain, because of the complex crystallization sequence. Crystallization apparently occurred in the following manner: (1) temperature is dropped and diopside is crystallized (20-30%); (2) eventually plagioclase nucleates and the composition of the liquid moves back to the Di-An-Ab cotectic; (3) more diopside and plagioclase crystallize until the sample is ~ 50% crystalline - 10% plagioclase and 40% diopside. This extra crystallization will raise the Sm concentration in the liquid and will artifically lower the Sm_{Dm}'s (see preceding section) unless the pyroxenes measured were the last pyroxenes to crystallize. This is difficult to determine since these two pyroxene populations have not been distinguished petrographically.

The first observation from these experiments is that zoning of Sm and Al still persists after 2 weeks and that total equilibration did not occur. Are the low-Sm, low-Al rims equilibrated with the liquid? Figure 14 would seem to indicate that the answer is no. If measurable equilibration has occurred then pyroxene Al concentrations should be very similar near all glass contacts. Except possibly for the first 2μ into the crystal from the glass boundary, this is not true (compare A,C,D,E,F). The concentration of Al in area D is 25% higher than area C. Similarly the Al concentration in area F is 23% higher than area E. The Al profile also places constraints on Sm. Since Sm diffusion within diopside should be dependent on Ca, Al, and Si diffusion (to maintain charge balance), diffusive equilibration of Sm and Al could not have produced a sharply-bounded 10μ rim such as A or C. Rimming by dissolution and reprecipitation of smaller pyroxenes faces the same problems as diffusion, in that pyroxene Al concentrations at crystal-glass interfaces are variable. For this model to be viable, areas A and C must have formed under quite

different conditions. Specifically, area C would have to have grown either at a higher temperature (i.e. lower ^{Al}D) or from an Al-depleted melt relative to A. Additionally, the "precipitation" model would probably also require that areas such as D be dissolving (or remaining unchanged) while precipitation occurs elsewhere on the same crystal (e.g. area E).

An alternative explanation for the Al profile of Figure 14 is that the low-Al areas (e.g. A and C) were the first portions to crystallize. Originally, the crystal would have been extremely skeletal (or several unconnected crystals) which filled in (or connected) during subsequent crystallization, with area B being the last to form. This model gives a natural explanation to the Al discontinuity at B, which is otherwise difficult to understand. Such a crystal would be reverse zoned (e.g. Al increasing from A to B) with the "rims" yielding the lowest ^{Sm}D and ^{Al}D values.

Thus, these experiments have failed to demonstrate appreciable equilibration of diopsidic clinopyroxene when held at 1218°C for ~ 2 weeks. This is consistent with the conclusions of Lindstrom and Weill (1978) who saw no measurable diffusion of Ni in diopside after 11 days at 1286°C. This is also consistent with the results of McCallister et al. (1979) who (with poor resolution) saw no Ca diffusion in diopside after 56 days at 1200°C. Additionally, Huebner et al. (1975) attempted to measure Ca and Mg diffusion constants by making microprobe traverses across grains of an augite-orthopyroxene mixture. Even after 26 days at 1266°C, these authors saw no diffusion on a scale larger than 3μ.

In summary, no appreciable equilibration of diopsidic pyroxene has been observed in the long-duration experiments. The reverse zoning of Sm and Al is best explained by early skeletal crystal growth and

subsequent filling of the interiors of the skeletal crystals by further crystallization. The low Sm, Al rims are interpreted as early, high temperature growth. The suddenness of the temperature drop makes this scenario seem unlikely, but the thermal relaxation time of the furnace (~ 2 minutes) does not preclude this possibility. The other alternative is that all other samples (with higher ^{Sm}D and ^{Al}D) are further out of equilibrium than 14A-1D, -2D. This seems unlikely since other samples' cooling rates (and presumably crystal growth rates) were much slower. The crystal cores are interpreted as having crystallized at lower temperatures (T_f?) Since the range in ^{Sm}D and ^{Al}D (core-rim) is too large to be explained by fractional crystallization, the cores could represent disequilibrium growth although the core D values (Figure 13) are close to those measured with lower cooling rates.

4. Summary and Interpretation of Variations in D Values

In summary, two points concerning equilibrium must be reemphasized: (1) prolonged (1-2 week) experiments show little evidence of pyroxene-melt equilibration and (2) crystal growth in 14A-13Co was sufficiently rapid to prevent interfacial equilibrium of Al (and probably Na as well) at the 10-20% level. The Sm homogeneity ($\pm$ 5%) of the 14A-13Co glass indicates that Al equilibration may be more difficult than for Sm. Overall, the range in ^{Sm}D and ^{Al}D is larger than can be accounted for by fractional crystallization but is qualitatively consistent with $^{Al}D_{cpx}$ and $^{Sm}D_{cpx}$ increases (with decreasing temperature) observed by Hytönen and Yoder (1961) and Drake and Holloway (1977), respectively. The preceding data do not define the degree to which $^{Sm}D_{cpx}$ has been affected by kinetic disequilibrium, but the Pu-Sm partitioning systematics

indicate that disequilibrium effects are not large (see following section). The preferred Dcpx values in the 1210-1270°C temperature range follow the correlation of Figure 6, with (^{Sm}D, ^{Al}D) ranging from (0.28, 0.142) to (0.34, 0.180) and the highest values interpreted as representing the lowest temperature.

5. Comparison with Literature Sm Partition Coefficients

Of the REE partitioning studies in the literature, the experimental conditions of Grutzeck et al. (1974) are the most comparable to those reported here. For two compositions in the DiAnAb system at 1265°C, Grutzeck et al. reported ^{Sm}Dcpx values of 0.26 $\pm$ 0.03 and 0.32 $\pm$ 0.17 (errors are standard deviations), in agreement with ^{Sm}Dcpx values reported here. The major difference between this study and that of Grutzeck et al. is the amount of Sm added to the Di-An-Ab system (50 ppm ^{151}Sm vs. 1-2 wt.% "cold" Sm). The agreement in ^{Sm}D values between these two studies supports the Grutzeck et al. (1974) contention that their partition coefficients are applicable at the lower REE concentrations (~ ppm) more typical of geological systems. Other experimental ^{Sm}Dcpx studies are those of Tanaka and Nishizawa (1975) Drake and Holloway (1977), Mysen (1977), and Nicholls and Harris (1980).

The experimental conditions and results of these studies are summarized in Table 6. Also summarized in Table 6 are phenocryst-matrix partition coefficients determined on natural samples (Schnetzler and Philpotts, 1970). The ^{Sm}Dcpx results reported here are lower than or approximately equal to the values reported from other experimental studies and fall within the large range of values from natural samples.

Table 6

Reference	$^{Sm}D_{cpx}$	Experimental Conditions
Grutzeck et al. (1974)	0.26-0.32	DiAnAb; 1265°C; 1 bar
Tanaka and Nishizawa (1975)	0.51-0.77	Tholeilite; 1200°C; 20 kbar
Drake and Holloway (1977)	0.35-2.68	DiAnAb; Fe-free and natural andesite; 900-1070°C; 2-12 kbar (P_{H_2O})
Mysen (1977)	0.75	Plag.-fosterite-silica; 20 kbar (P_{H_2O}); 950°C
Nicholls and Harris (1980)	0.3 -1.1	Hydrous and anhydrous basalt and andesite; 15-30 kbar; 1000-1380°C
Schnetzler and Philpotts (1970)	0.09-1.81	Natural samples· phenocryst-matrix

6. Plutonium

Following analysis of Sm by beta radiography, the two-stage samples 14A-13Co and 14A-14Co and the rapidly cooled [method (3)] sample 14A-11Co were irradiated with neutrons (see Chapter II). The resulting fission track maps on affixed mica detectors were used to determine ^{Pu}D. Pyroxene Pu analyses were taken as close to the areas analyzed for Sm as possible. The positional correspondence of the Sm and Pu analyses is much better than that of the Sm and Al determinations. This primarily reflects the greater difficulty in finding exact locations using the microprobe than with the SEM. Areas of Pu analyses (for pyroxenes) are ~ 6X larger than the Sm analyses, in order to have enough tracks for adequate precision ($< \pm$ 10%).

Pu differs from Sm in that multiple valence states are present in silicate melts. Sm exists as Sm^{+3}, but Pu can exist as Pu^{+2}, Pu^{+3}, and Pu^{+4}. Although Pu^{+2} is thought to be relatively unimportant in silicate melts (see Benjamin, 1979; Appendix VI), the presence of both Pu^{+3} and Pu^{+4} makes ^{Pu}D dependent upon fO_2. Although these samples were generated in the presence of nichrome and were probably at a lower fO_2 than the Co-CoO buffer (see Chapter II), the agreement in ^{Pu}D between these samples, the 1 bar Co-CoO buffered samples of Benjamin (1979) and preliminary results for pyroxenes grown at $fO_2 \sim 10^{-22}$ implies that negligible Pu^{+4} exists at oxygen fugacities less than 10^{-9}.

Figure 15 shows a plot of ^{Sm}Dm vs. ^{Pu}Dm for method (2) pyroxenes. A better correlation is observed between ^{Sm}Dm and ^{Pu}Dm than between ^{Sm}Dm and ^{Al}Dm. This may reflect either that the Pu analyses had a smaller positional error than the Al analyses or that Pu and Sm have more similar properties. An averaging of the Pu data yields a mean ^{Pu}Dm of 0.167

Figure 15

This figure shows the correlation between $^{Pu}D_m$ and $^{Sm}D_m$ for method (2) pyroxenes. Sm error bars are errors of the mean for replicate Sm analyses (same emulsion) and Pu error bars are Pu track-counting statistics. Box symbols are 14A-13Co pyroxenes; circles are 14A-14Co pyroxenes. Because of the limited number of Pu tracks, the areas of the Pu analyses are larger than for the Sm analyses but Pu and Sm analyses are as close together as possible. Note the good correlation between $^{Pu}D_m$ and $^{Sm}D_m$ with $^{Sm}D \sim 2\ ^{Pu}D$. The heavy bar shows the amount of change expected during 20% fractional crystallization for $^{Sm}D = 0.35$ and $^{Pu}D = 0.20$.

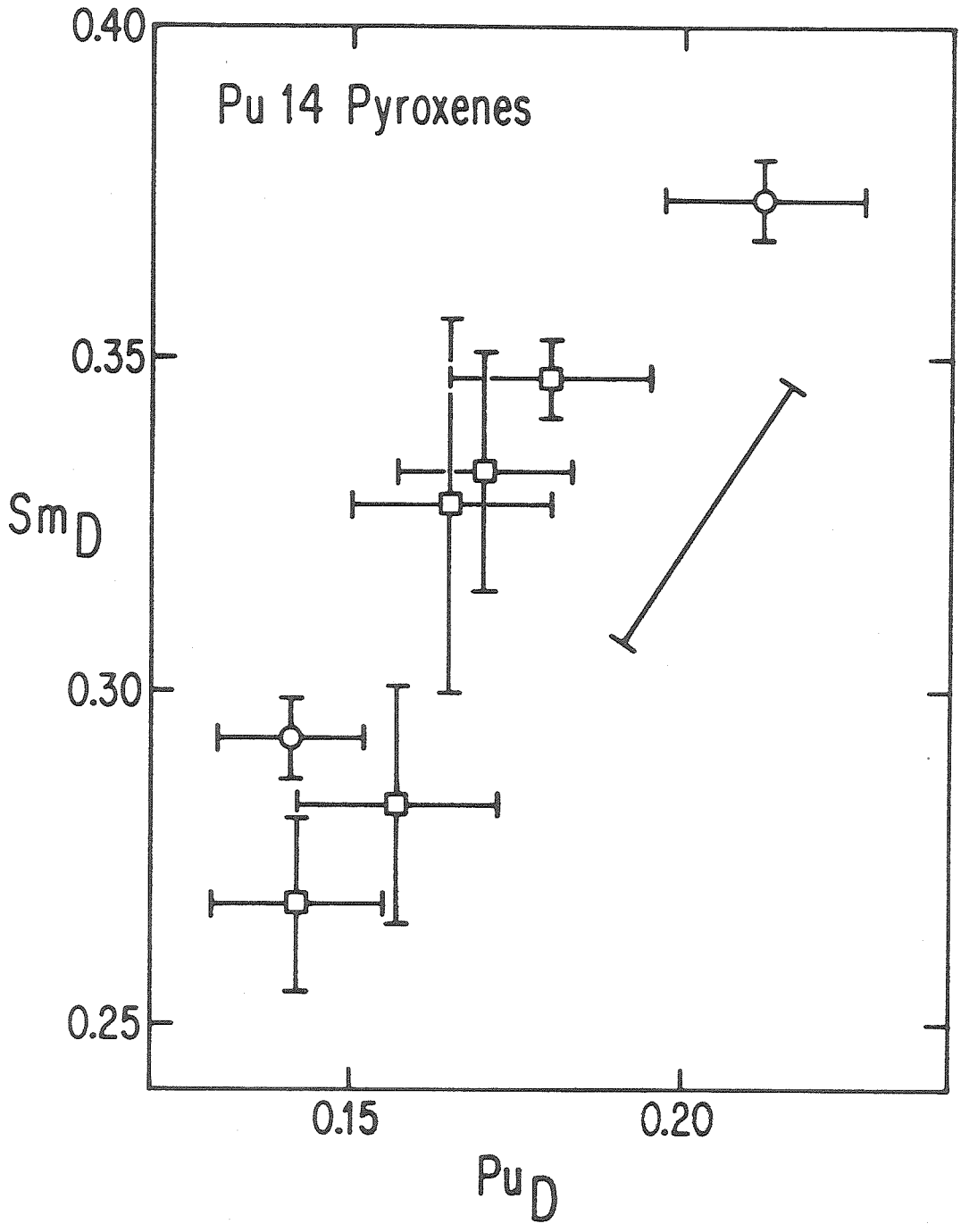
Pu 14 Pyroxenes
0.40
0.35
0.30
0.25
Sm D
0.15
0.20
Pu D

with a standard deviation of 14.7%, somewhat larger than expected from analytical uncertainty (8-10%). As in the case of Sm, no Pu inhomogeneity is observed in the 14A-13Co glass, an argument for a close approach to equilibrium. Three Pu analyses from the glass region of 14A-13Co which showed high Al_2O_3 contents and three Pu analyses from a glass region that showed the lowest Al concentrations, were identical within counting statistics ($\pm$ 5%). The spread in the partition coefficients of Figure 15 is too large to be attributible to fractional crystallization alone and is interpreted as the effect of temperature, following the discussion in Section 4. Figure 16 is the same as Figure 15 but analyses from 14A-11Co (the most rapidly cooled sample) have been added to extend the range of the data. Even over ~ a range of a factor of two in Sm_{Dm}, the correlation of Sm_D/Pu_D persists. This is surprising since the 14A-11Co sample would not be expected to represent a close approach to equilibrium. Although dendritic crystals do exist in 14A-11Co, these were too small to analyze. The 14A-11Co crystals analyzed and shown in Figure 16 may represent the last-grown crystals. If so, these crystals could have grown the least rapidly and at the lowest temperature. They show the highest D's as would be predicted from a low temperature of growth.

Figure 16 suggests that the Sm and Pu partition coefficients are not controlled by kinetic disequilibrium (see section A, this chapter). For example, if the "true" partition coefficients of Sm and Pu were 0.28 and 0.15, respectively, then the higher Dm values in Figure 16 could be interpreted as the artifacts of rapid crystal growth. In this case, the larger the Dm values, the more rapid the growth; a scenario that is consistent with 14A-11Co [a method (3) sample] having the largest Dm's.

Figure 16

This figure is the same as Figure 15 with the addition of 14A-11Co pyroxenes [method (3)] to extend the range of Pu and Sm data. Box symbols represent 14A-13Co pyroxenes, circles are 14A-14Co pyroxenes and diamond symbols represent 14A-11Co pyroxenes. The solid line (slope = 1.9) is drawn through the origin and 14A-13Co; cpx-2B, and fits the data well. The dashed line shows the path predicted if the D values were controlled by kinetic disequilibrium (see text). Surprisingly, the method (3) (drop and hold) pyroxenes show a close approach to equilibrium, although the higher (on the average) D values imply lower crystallization temperatures as would be expected. The relation $^{Sm}D \simeq 2\,^{Pu}D$ appears to hold over a range in ^{Sm}D of nearly a factor of two.

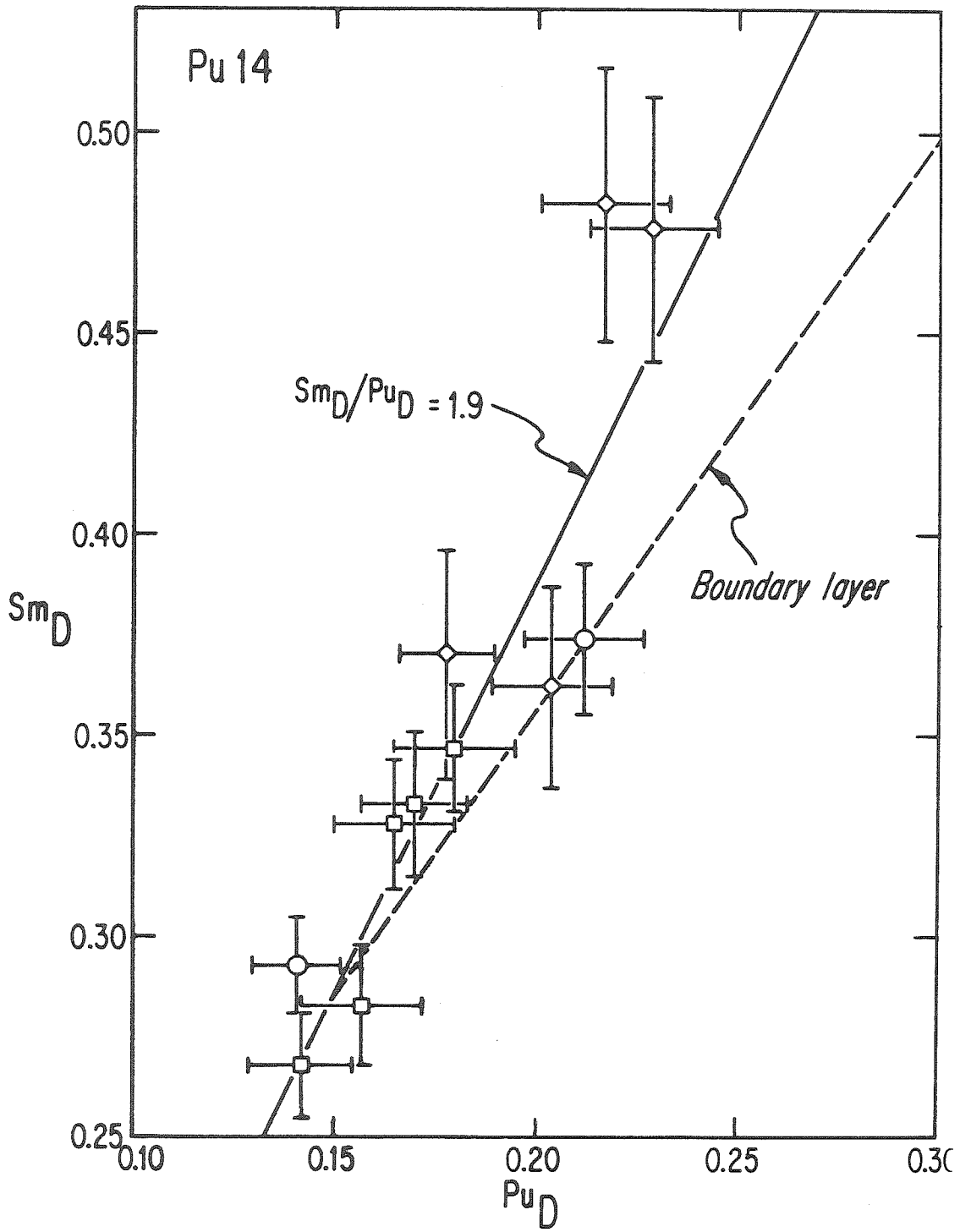
Pu 14
0.50
0.45
0.40
0.35
0.30
0.25
Sm_D
Sm_D/Pu_D = 1.9
Boundary layer
0.10
0.15
0.20
0.25
0.30
Pu_D

The dashed line in Figure 16 is an attempt to model rapid crystal growth. Burton et al. (1953) have shown that, at steady state with infinite liquid, the relationship between the apparent (measured) partition coefficient $^{M}D_m$ for element M and the true partition coefficient ^{M}D is given by:

$$^{M}D_m = \frac{^{M}D}{^{M}D + (1 - {}^{M}D)\, e^{-\Delta}} \quad ; \quad \Delta = V\delta/J_m$$

where $\underline{V}$ is the crystal growth rate, J_m is the diffusion coefficient of M in the melt and $\underline{\delta}$ is the width of the boundary layer. $^{Sm}D_m$ and $^{Pu}D_m$ have been calculated for crystal growth rates sufficient to produce the observed change in ^{Sm}D ($\Delta \equiv 0$-0.77) and are shown by the dashed line. J_{Sm} and J_{Pu} are assumed to be equal. Although this model is certainly oversimplified, it demonstrates the important general point that, as kinetic disequilibrium increases, the slope of the ^{Sm}D vs. ^{Pu}D trend should approach unity. This is because the concentration of $\underline{M}$ in the boundary layer will be higher for elements with low ^{M}D and, as crystal growth rate increases, the concentration of M in the boundary layer, $^{M}C_{\delta}$, approaches $(^{M}C_1/^{M}D)$, where $^{M}C_1$ is the concentration of M in the liquid beyond the boundary layer. At the lowest D values the kinetic disequilibrium trend fits the data well. However, at larger D values the kinetic disequilibrium trend clearly diverges from the slope = 2 line and begins to approach unity. The critical assumption of this model is the assignment of $J_{Sm} = J_{Pu}$. If $J_{Sm} > J_{Pu}$ then the kinetic disequilibrium trend will diverge from the slope = 2 line earlier. If $J_{Sm} < J_{Pu}$ the kinetic disequilibrium model might fit the data quite well for a certain value of J_{Sm}/J_{Pu}, but for lower ratios the trend will diverge in the opposite sense to that shown on Figure 16. The case of $J_{Sm} < J_{Pu}$ is more unlikely; since Pu^{+3}

is both larger (slightly) and heavier than Sm^{+3}, it is expected that $J_{Sm} \geq J_{Pu}$, but relative diffusion coefficients of Pu and Sm are not available. This assumption is consistent with the alkaline earth diffusion data of Hofmann and Magaritz (1977) for a basaltic melt. These authors saw a monotonic decrease in J with atomic number (i.e. mass and size) for Ca, Sr, and Ba. Thus, unless J_{Sm} is less than J_{Pu} by exactly the right amount, (the direction necessary for the disequilibrium curve to better fit the data) kinetic disequilibrium does not appear to have affected ^{Pu}D and ^{Sm}D values during pyroxene growth.

The most reasonable interpretation of the ^{Sm}D vs. ^{Pu}D trend, as well as the ^{Al}D–^{Sm}D trend discussed earlier, therefore, is that it is due to the combined effects of fractional crystallization and temperature. Since fractional crystallization cannot be responsible for more than half the spread in the data (see Figure 15), temperature appears to be the dominant effect. Since $^{Sm}D \approx 2^{Pu}D$, this requires that

$$\frac{d\ ^{Sm}D^{cpx}}{dT} \approx 2\ \frac{d\ ^{Pu}D^{cpx}}{dT}$$

This is an interesting result and implies that the molar enthalpies of the Sm and Pu substitution reactions are nearly equal, i.e.

$$\Delta\overline{H}^{\circ}\ Sm;cpx \approx \Delta\ \overline{H}^{\circ}\ Pu;cpx.$$

This similarity in $\Delta\overline{H}^{\circ}$ of substitution probably indicates similar substitution mechanisms. This is expected since Pu^{+3} and Sm^{+3} have similar ionic sizes [1.00 and 0.96 Å , respectively (Shannon, 1976)]. The substitution mechanism as given by Grutzeck et al.(1974) is

$$CaMgSi_2O_6(s) + X^{+3}(\ell) + Al^{+3}(\ell) \rightarrow XMgAlSiO_6(s) + Ca^{+2}(\ell) + Si^{+4}(\ell)$$

where X = Pu or Sm.

This is a simple reaction which both preserves charge balance and allows Pu and Sm to substitute into a crystal site of similar size to their own ionic radii.

7. Effect of Phosphorus

Benjamin (1979) showed that the addition of $Ca_3(PO_4)_2$ to the Di-An-Ab system greatly lowered Dcpx values for the actinide elements (Th and U). For Th and U, the addition of 15 or 25 wt.% $Ca_3(PO_4)_2$ (~ 5 and 8 wt.% P_2O_5) lowered $^{Th,U}D_{cpx}$ by an order of magnitude. No direct evaluation of the effect of P_2O_5 on Pu partitioning is possible from the Benjamin (1979) data. However, pyroxenes grown from P-bearing melts at 20kbar yielded a ^{Pu}D which was 3-4X smaller than that of pyroxenes grown in a P-freemelt at one bar.

Because of the significant effect of P at the 5-8% P_2O_5 level on actinide partitioning, experiments were undertaken to see whether a smaller amount of P_2O_5 would also significantly affect actinide D's and to check whether the $^{Sm}D_{cpx} \approx 2\ ^{Pu}D_{cpx}$ correlation was composition invariant (see preceding section). Because Mysen et al. (1981) saw changes in the Raman spectra of silicate glasses when ~ 1 wt.% P_2O_5 was introduced, this was considered to be enough P_2O_5 to affect trace element partitioning but not enough that whitlockite would become a liquidus phase. Consequently, 3 wt.% $Ca_3(PO_4)_2$ was added to a Pul6

composition (Di_{60} An_{20} Ab_{20}) to make Pul7, which contained 1.4 wt.% P_2O_5 but whose liquidus phase was still clinopyroxene. Fortuitously, the Pul7 liquidus is only ~ 10°C higher than that of Pul4. Because of this, there is a great deal of overlap in the thermal histories of Pul4 and Pul7, and, consequently, differences between the two systems should primarily depend upon composition rather than temperature.

The Sm and Al data show a great deal of overlap with the data of the P-free system. Figure 17 shows a comparison of the Pul4 and Pul7 ^{Sm}D and ^{Al}D data. The ^{Al}D values are essentially unchanged, although there is a tendency for the ^{Sm}D values to be smaller in the P-bearing system. Figure 18, a plot of ^{Sm}D vs. ^{Pu}D, better shows that this is indeed the case. The P-bearing Pul7 data show a trend which differs significantly from the P-free system. The slope of ($^{Sm}D/^{Pu}D$) cpx has changed from 1.9 to 2.6 (~ 30% difference) with the addition of ~ 1.5 wt.% P_2O_5, and $^{Pu}D_{cpx}$ has been lowered by about a factor of two. This large change in ^{Pu}D with a much smaller change in $^{Sm}D/^{Pu}D$ implies that ^{Sm}D has also been lowered by ~ 1.5x. This comparison between the Pul4 and Pul7 (Figure 18) should not be affected by percent crystallization. Although the Pul7 (P-bearing) samples in general contain more crystallization that the Pul4 samples (~ 30% as opposed to 20%), 14A-11Co, which was used to extend the range of the Pul4 data, is also ~ 30% crystalline.

The mechanism by which these changes occur is not certain but may represent a complexation of Pu and Sm by phosphate groups in the liquid. In this model Pu must be more tightly bound to the complexing ligands than Sm and, therefore, less available for partitioning into pyroxene. This would be consistent with the greater spatial extent of the Pu 5f orbitals (as compared to the Sm 4f orbitals) which would facilitate

Figure 17

This figure is the same as Figure 6 but Pul7 pyroxene data have been added for comparison. ◇ ≡ 14A-13Co; □ ≡ 14A-14Co; ● ≡ 17A-6Co; ◆ ≡ 17A-7Co; ■ ≡ 17A-8Co. Data points represent individual crystals and errors are assigned as in Figure 6. Note the difference in error bars for the 17A-7Co;-8Co ^{Sm}D analyses. The errors for these samples are larger because the one exposure method was used to determine ^{Sm}D. Although little change is seen in ^{Al}D, ^{Sm}D has decreased by ~ 1.5x (see text).

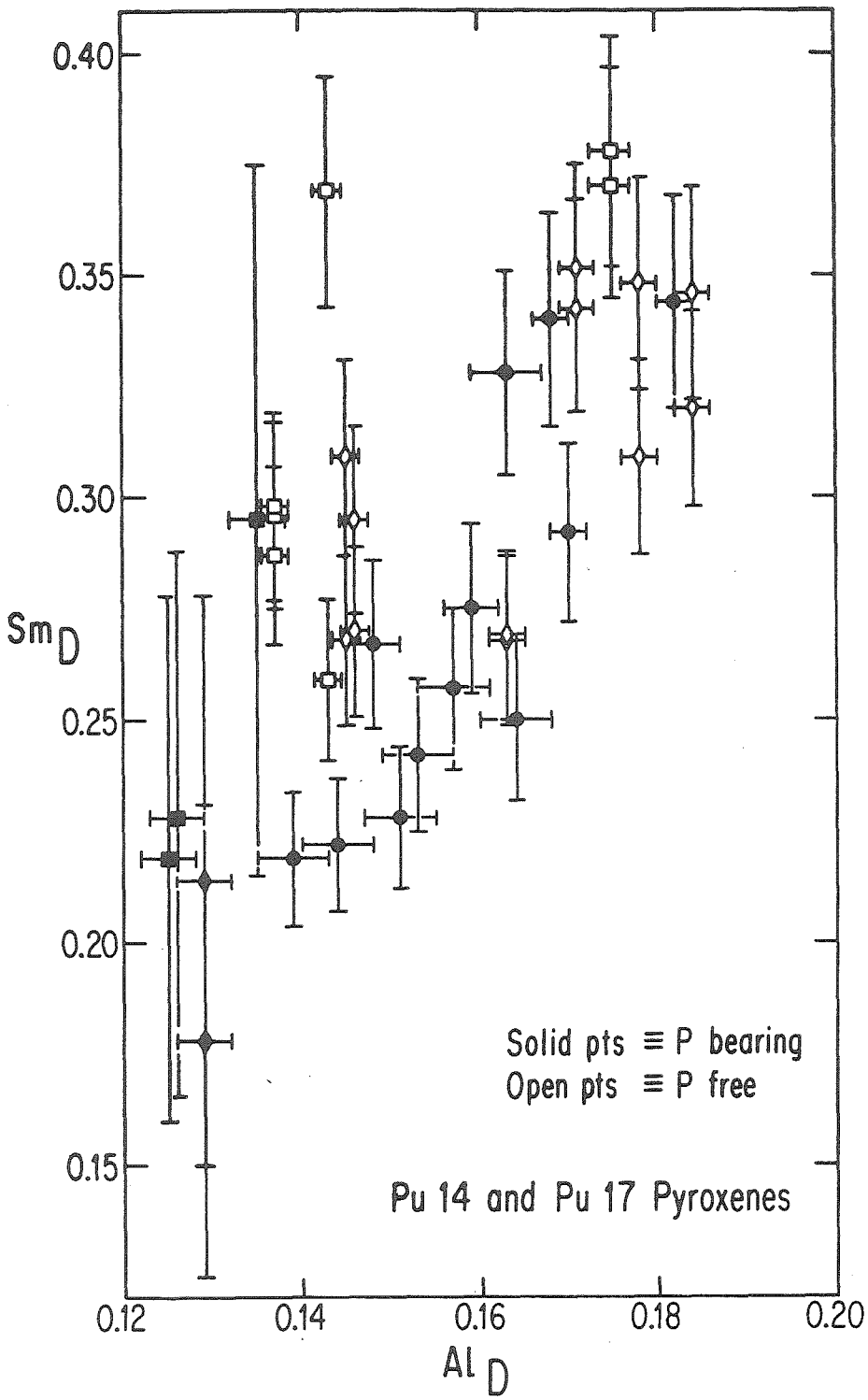
0.40
0.35
0.30
0.25
0.20
0.15
Sm D
0.12
0.14
0.16
0.18
0.20
Al D
Solid pts ≡ P bearing
Open pts ≡ P free
Pu 14 and Pu 17 Pyroxenes

Figure 18

This figure is the same as Figure 16 with the addition of the Pul7-6Co,-7Co data (dark symbols); ◆ ≡ 17A-6Co, ● ≡ 17A-7Co. The Pul7-7Co Sm error bar is an error of the mean of two analyses of the same exposure. 17A-6Co Sm errors are as in Figure 17. Pu errors are counting statistics. Open symbols represent Pul4 samples, as in Figure 16.

Although there is a large overlap of ^{Sm}D values, there is little or no overlap of the Pu data between Pul4 and Pul7. A least-squares line through the P-bearing data passes close to the origin and has a steeper slope than the P-free data, such that for Pul7 pyroxenes $^{Sm}D \cong 2.6\ ^{Pu}D$.

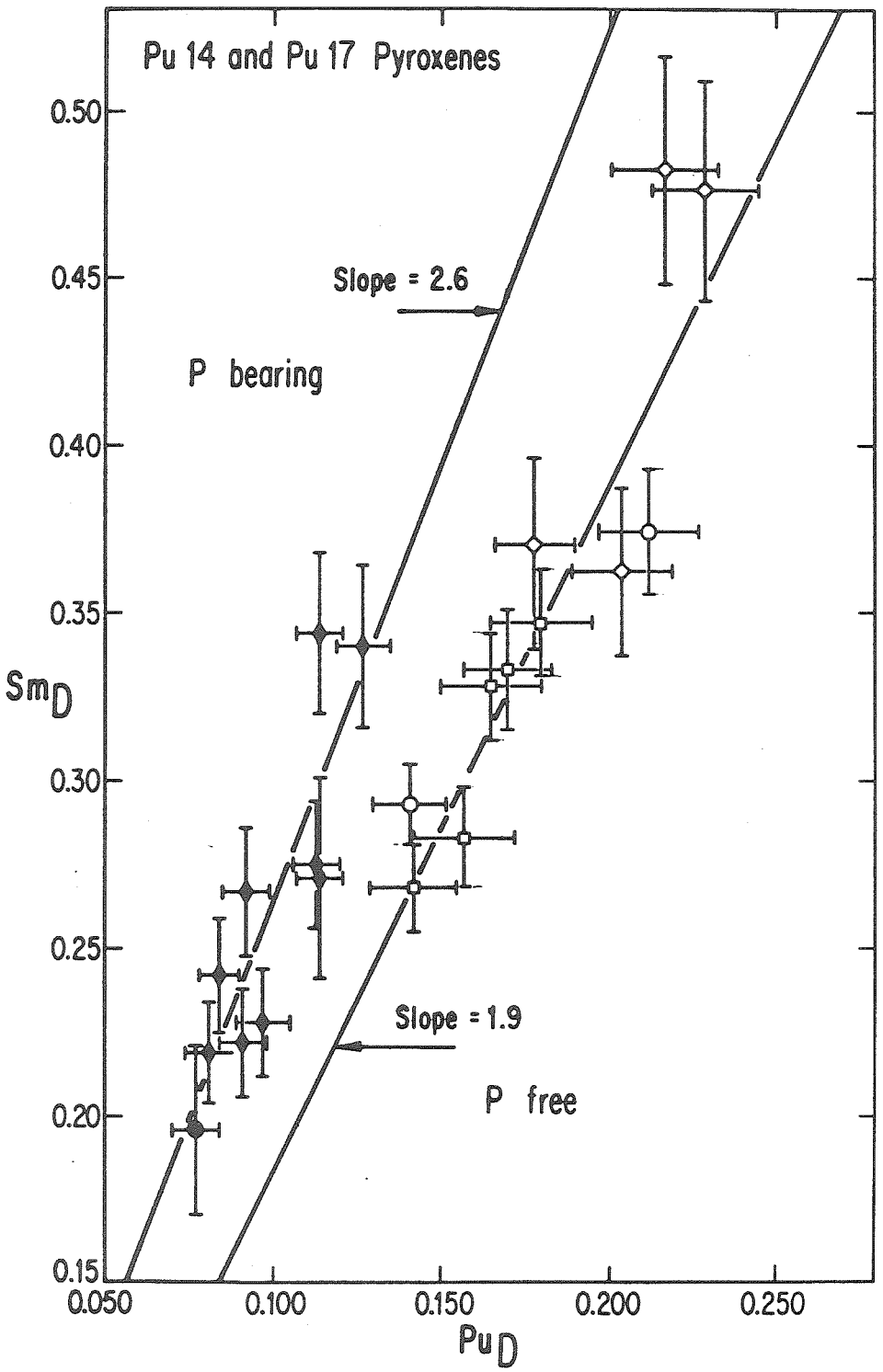
Pu 14 and Pu 17 Pyroxenes
Slope = 2.6
P bearing
Slope = 1.9
P free
Sm D
Pu D
0.50
0.45
0.40
0.35
0.30
0.25
0.20
0.15
0.050
0.100
0.150
0.200
0.250

complexing (Cotton and Wilkinson, 1962). Since U and Th are also greatly affected by P_2O_5 (Benjamin, 1979), it may be that the actinides in general are more susceptible to complexing agents than the lanthanides. This is at least true in aqueous solution where the actinides readily form complexes while the lanthanides do not.

Another alternative for the change in $^{Pu}D/^{Sm}D$ is that Pu behaves like a REE and that the REE pattern of diopside has been significantly changed by the addition of P_2O_5 to the melt. Although the shape of the REE pattern of a given mineral is generally considered to be rather similar (even though absolute D values may change), the REE phenocryst-matrix partition coefficient patterns of natural clinopyroxenes are not constant and can show changes in REE partition coefficient ratios of a factor of two (Schnetzler and Philpotts, 1970). More data would be required to support this speculation, however.

8. Summary of Pyroxene Data

Table 7 gives a summary of the adopted Pul4 and Pul7 partition coefficients. The lowest D values (when corrected for fractional crystallization) are assumed to be representative of the first crystals to nucleate and grow. The first order results from these data are as follows: (1) in the Di-An-Ab system, an analogue of natural basalts, $^{Sm}Dcpx \cong 2\,^{Pu}Dcpx$; (2) the addition of P_2O_5 to the Di-An-Ab system increases the difference in D's such that $^{Sm}Dcpx \cong 2.6\ ^{Pu}Dcpx$; (3) if Pu^{+3} diffuses at the same rate as (or slower than) Sm^{+3}, then kinetic disequilibrium does not appear to have been important in these experiments and the spread in the data may be reasonably interpreted as primarily due to the combined

Table 7

Summary of Pyroxene Data

	Pu_D	Sm_D	Al_D	Na_D	T(°C)	%XL
Pu14 (0% P_2O_5)	0.17 ± 0.02	0.31 ± 0.03	0.17 ± 0.02	0.059 ± 0.06	1250 ± 10	20
Pu17 (1.4% P_2O_5)	0.11 ± 0.01	0.26 ± 0.03	0.17 ± 0.02	0.055 ± 0.06	1260 ± 10	28

effects of temperature and fractional crystallization; and (4) Al (and perhaps other elements) shows the effects of kinetic disequilibrium during crystal growth.

The Sm data for the P-free system are in good agreement with the $^{Sm}D_{cpx}$ values reported by Grutzeck et al. (1974). The interpretation of the temperature dependence of $^{Al}D_{cpx}$ and $^{Sm}D_{cpx}$ are qualitatively supported by the work of Hytönen and Yoder (1961) and Drake and Holloway (1977). The most probable cause of the change in $^{Sm}D_{cpx}/^{Pu}D_{cpx}$ between the P-free and P-bearing systems is the greater tendency for the actinides to form complexes.

C. Whitlockite

1. Samarium

A grain by grain display of $^{Sm}D_m$'s for Pul5 whitlockites is given in Figure 19. Examples from both method (1) and method (2) cooling histories are shown. In this case, where $^{Sm}D > 1$, deviations from equilibrium due to rapid growth and formation of boundary layers will cause partition coefficients to be too low (see Section A, this chapter). As in the case of pyroxenes, Sm analyses were made using the two-exposure method. Exposures were made such that the Ag count rate was ~ 20% that of Ag metal. Analyses are slightly less precise because smaller areas were used for whitlockite analyses-$(16\mu)^2$. No difference is observed between method (1) and method (2) crystals, suggesting a close approach to equilibrium using method (1). The mean of all ^{Sm}D analyses is 7.81 ± 0.16 (error of mean). The analyses have a poorer precision (~ 1.9σ) than that expected from fluctuations in the beta fluence (see Appendix I and Chapter II). The only sample which shows consistent differences from the mean is 15B-6Co, whose analyses are all lower than 7.0. 15B-6Co does not differ significantly in % crystallization or cooling rate from the other samples, but was held above the liquidus much longer than usual (see Table 3). If this extended superliquidus time inhibited nucleation (see Chapter II), the 15B-6Co ^{Sm}D's may have been affected by rapid crystal growth. Alternatively, those 15B-6Co crystals which were analyzed may have grown later than average and were less affected by fractional crystallization (see Section A, this chapter). In any event, the $^{Sm}D_m$'s of the method (2) whitlockites do not have a higher average ^{Sm}D than the method (1) whitlockites as would be expected if nucleation problems and kinetic disequilibrium were important during whitlockite

Figure 19

This figure shows a grain-by-grain summary of all whitlockite Sm partition coefficients. Error bars for all samples but 15B-2Co and 15B-6Co were assigned in exactly the same manner as for the Pul4 and Pul7 analyses and are $\pm$ 6.5%. Because 15B-2Co and 15B-6Co were analyzed using a different emulsion batch, errors were based on the precision of multiple analyses of the 15B-2Co and -6Co glasses. For those two samples errors are $\pm$ 10%. Method (2) whitlockites do not have larger ^{Sm}Dm's than method (1) whitlockites, implying that nucleation and kinetic disequilibrium problems were not significant. All samples have ~ 10% crystallization.

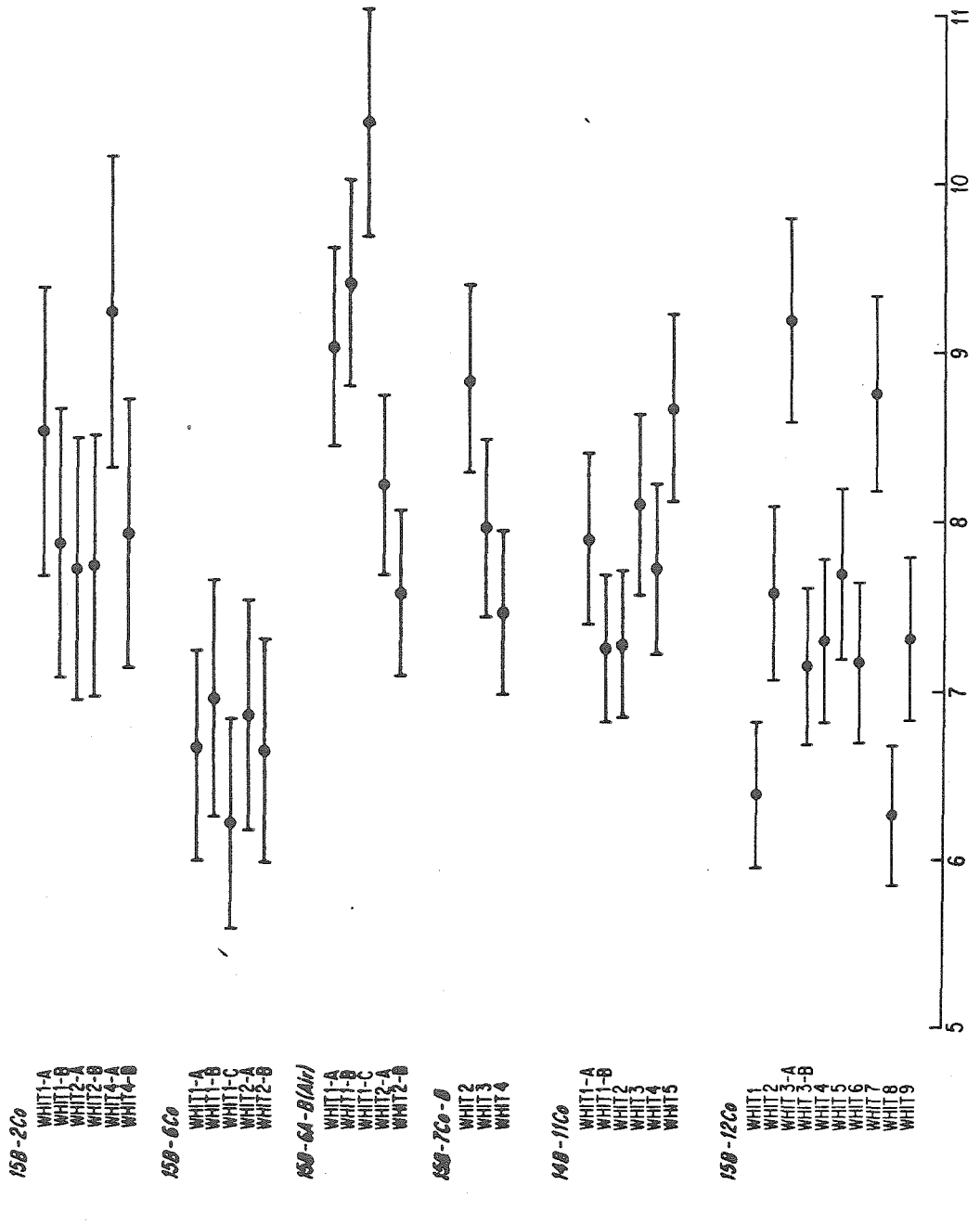
Pu 15 Whitlockite SmD
COOLING METHOD(1)
MEAN = 7.95 ± 0.25
(σ = 3.1%)
COOLING METHOD(2)
MEAN = 7.61 ± 0.020
(σ = 2.6%)
15B-2Co
WHIT1-A
WHIT1-B
WHIT2-A
WHIT2-B
WHIT4-A
WHIT4-B
15B-6Co
WHIT1-A
WHIT1-B
WHIT1-C
WHIT2-A
WHIT2-B
15B-6A-B(Air)
WHIT1-A
WHIT1-B
WHIT1-C
WHIT2-A
WHIT2-B
15B-7Co-B
WHIT2
WHIT3
WHIT4
14B-11Co
WHIT1-A
WHIT1-B
WHIT2
WHIT3
WHIT4
WHIT5
15B-12Co
WHIT1
WHIT2
WHIT3-A
WHIT3-B
WHIT4
WHIT5
WHIT6
WHIT7
WHIT8
WHIT9
5
6
7
8
9
10
11

crystallization. This is especially true if 15B-6Co is excluded. Without the 15B-6Co crystals the method (1) average becomes 8.4 $\pm$ 0.22 (error of mean).

Unlike the pyroxenes of the last section, the range of ^{Sm}D values for Pul5 whitlockites is not larger than that permitted by fractional crystallization. If the average ^{Sm}Dm were 8 after 10% fractional crystallization, then the true $^{Sm}Dwhit$ would be 6 with a range in ^{Sm}Dm from 6(rim to 10.2(core). This model is very close to what is actually observed; however, because crystal size does not increase linearly with % crystallization, the ^{Sm}Dm values are more representative of the crystal core than a crystal average. If $^{Sm}Dm = 7.81 \pm 0.16$ is taken to be representative of the crystal core, the corrected ^{Sm}D becomes 5.08 ± 0.07. Because the SEM beam may be larger than the crystal core, this calculation is an overcorrection and gives a firm lower limit to $^{Sm}Dwhit$.

The minor elements, Mg and Si, do not appear to be as straightforward as Sm. Figure 20 shows ^{Mg}Dm and ^{Si}Dm for four method (1) and two method (2) samples. No difference between the two sets of samples is seen, but the scatter of the data makes interpretation difficult. The Mg data are relatively precise ($^{Mg}Dm = 0.498 \pm 0.006$, σ mean = 1.3%) but the Si data are more variable ($^{Si}Dm = 0.00493 \pm 0.00011$, σ mean = 2.2%). In both cases there is more variation than can be explained by fractional crystallization. (For comparison, the dashed line in Figure 20 shows the range of Dm's expected during 10% fractional crystallization with $^{Si}D = 0.0057$ and $^{Mg}D = 0.52$.) If kinetic disequilibrium were responsible for the Mg and Si scatter and for the low ^{Sm}D values of 15B-6Co (see Figure 19), then the 15B-6Co ^{Si}D and ^{Mg}D might be higher than average.

A priori it might be expected that the method (2) samples would be

Figure 20

This figure shows a plot of ^{Si}Dm vs. ^{Mg}Dm for Pu15 whitlockites. The amount of scatter is large compared to the counting statistics errors of the microprobe, but no difference can be seen between the method (1) and method (2) whitlockites. The dashed line shows the amount of change in Dm's expected during 10% fractional crystallization. Unlike the Sm data, Si and Mg show more variability than can be accounted for by fractional crystallization.

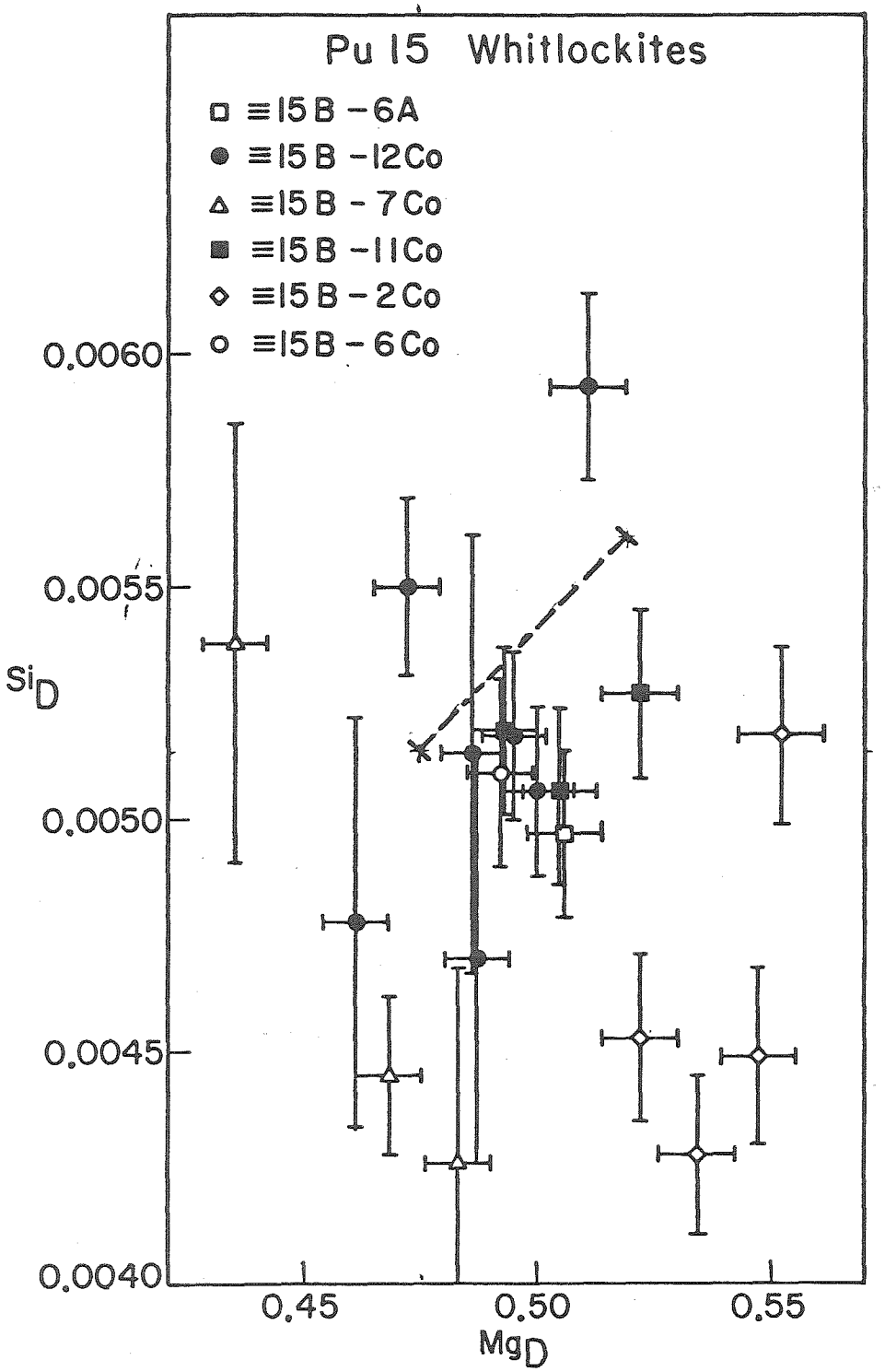
Pu 15 Whitlockites
□ ≡15B-6A
● ≡15B-12Co
△ ≡15B-7Co
■ ≡15B-11Co
◇ ≡15B-2Co
○ ≡15B-6Co
0.0060
0.0055
0.0050
0.0045
0.0040
Si D
0.45
0.50
0.55
Mg D

less subject to kinetic disequilibrium; however, this is not supported by Figure 20. ^{Si}D which should be the most susceptible to kinetic effects (100X smaller than ^{Mg}D) is perhaps slightly lower for the method (1) whitlockites. ^{Si}D [method (1)] averages 0.00470 $\pm$ 0.00012 (error of mean) while the average method (2) ^{Si}D is 0.00506 $\pm$ 0.00015.

Thus, the cause of the scatter in Figure 20 is not clear, and a plot of ^{Sm}D vs. ^{Mg}D (Figure 21) does not help clarify the situation. The Si and Mg data are complex and may result from several processes (fractional crystallization, change of D's with temperature, and kinetic disequilibrium) none of which dominates.

Figure 21

This figure shows a plot of $^{Sm}D_m$ and $^{Mg}D_m$ for Pul5 whitlockites. ^{Sm}D errors are assigned as in Figure 19 and ^{Mg}D errors are microprobe counting statistics. An exception is whit-1 of 15B-7Co whose errors are the standard deviations of two Sm analyses and four Mg analyses. No real trend is observable. The line through the data shows the amount of change expected in Dm's during 10% fractional crystallization, assuming $^{Sm}D = 6$ and $^{Mg}D = 0.5$.

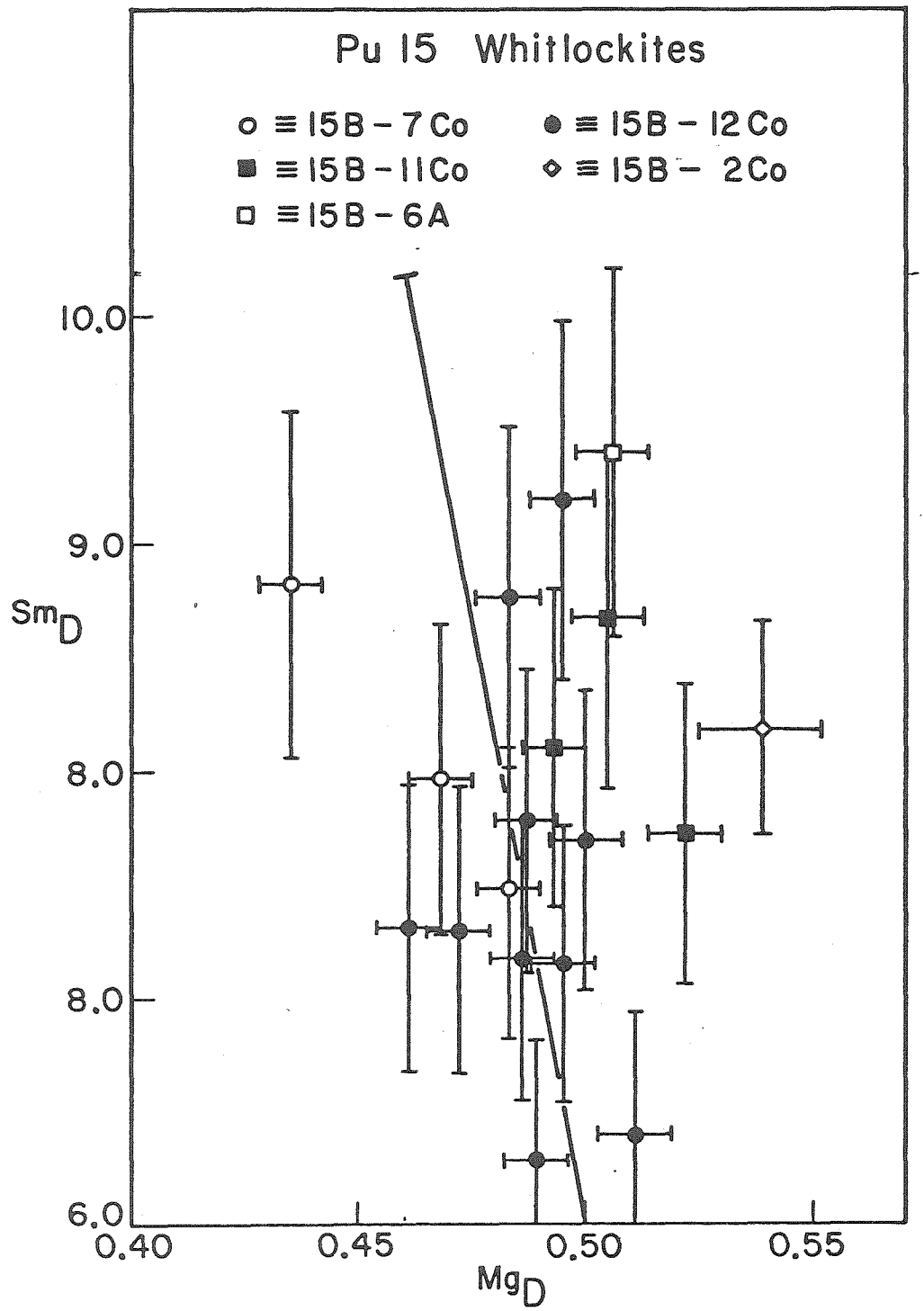
Pu 15 Whitlockites
○ ≡ 15B - 7Co
● ≡ 15B - 12Co
■ ≡ 15B - 11Co
◇ ≡ 15B - 2Co
□ ≡ 15B - 6A
10.0
9.0
8.0
8.0
6.0
Sm D
0.40
0.45
0.50
0.55
Mg D

2. Plutonium

Pu fission track maps were used to determine $^{Pu}D_{whit}$. As in the case of pyroxenes, care was taken to analyze the same areas as were used to determine $^{Sm}D_{whit}$. Figure 22 shows a plot of $^{Sm}D_m$ vs. $^{Pu}D_m$. No method (2) Pu data are included because of the ineffectiveness of the Co-CoO buffers (see Chapter II). Assuming that Pu behaves similarly to Sm, the similarity of $^{Sm}D_m$ between the method (1) and method (2) (two-stage) samples implies that nucleation and kinetic disequilibrium problems are not significant for the whitlockite system, and that the method (1) samples should yield a valid $^{Pu}D_{whit}$. The average of all $^{Pu}D_m$ is 4.56 $\pm$ 0.13 (σ mean = 2.8%). As in the case of Sm, assuming this value to be representative of the whitlockite core will result in $^{Pu}D_{whit}$ = 3.50 $\pm$ 0.08. The solid curve in Figure 22 shows the apparent change in ^{Pu}D and ^{Sm}D expected during 10% fractional crystallization assuming $^{Sm}D_{whit}$ = 5.08 and $^{Pu}D_{whit}$ = 3.50. The dashed line shows the amount of change during 10% fractional crystallization if ^{Sm}D = 5.9 and ^{Pu}D = 3.9. The slope of either curve is consistent with the trend of the data. The solid line fails to cover the entire range of the data, indicating that the D values may have been slightly (~ 10%) overcorrected for fractional crystallization. Because of this uncertainty, the preferred values for ^{Sm}D and $^{Pu}D_m$ are 6.4 $\pm$ 0.7 and 4.0 $\pm$ 0.4, respectively. These are the averages of the corrected (core-rim) D's (overcorrected) and the average Dm's (uncorrected) (see Benjamin et al, 1980).

As in the case of pyroxenes, whitlockite fractionates Pu and Sm. When corrected for fractional crystallization and fission fragment ranges, the Pu data from Figure 22 yield a $^{Pu}D_{whit}$ of 3.8 $\pm$ 0.4, in agreement with the 20kbar value of Benjamin (1979). Taking $^{Sm}D_{whit}$ as 6.4,

Figure 22

This figure shows a plot of $^{Sm}D_m$ vs. $^{Pu}D_m$ for Pul5 whitlockites. Sm error bars for 15B-2Co and -6Co are errors of the mean for multiple analyses of a given crystal; all other error bars are based on the counting statistics of individual analyses and the errors assigned to points in Figure 19. Data are from method (1) samples only - ● ≡ 15B-2Co; ■ ≡ 15B-6Co; ◆ ≡ 15B-7Co. The solid line shows the amount of apparent change in D's possible during 10% fractional crystallization with $^{Pu}D_{whit}$ = 3.5 and $^{Sm}D_{whit}$ = 5.08. The dashed curve is the same model with ^{Sm}D = 5.9 and ^{Pu}D = 3.9. Variations in the data are consistent with fractional crystallization, and show a much better correlation than either ^{Sm}D vs. ^{Mg}D or ^{Si}D vs. ^{Mg}D.

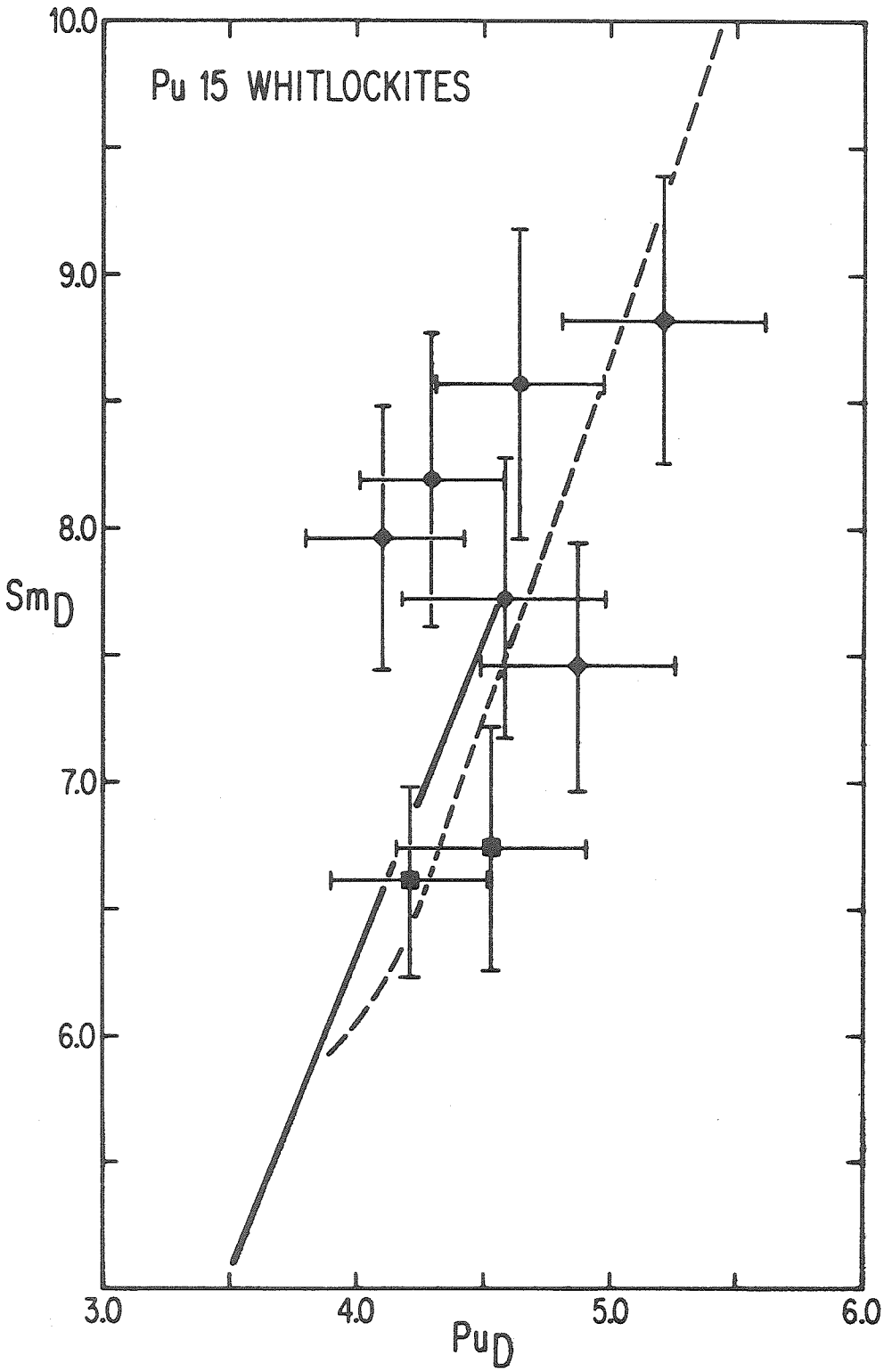
Pu 15 WHITLOCKITES
10.0
9.0
8.0
7.0
6.0
Sm D
3.0
4.0
5.0
6.0
Pu D

(Sm_D/Pu_D)whit is found to be 1.7, slightly lower than the (Sm_D/Pu_D) ratios found for pyroxenes.

IV. DISCUSSION

A. Pu-Light Rare Earth Fractionation in Geologic Systems

As discussed in the Introduction, the results of Marti et al. (1977) were the major impetus for starting this thesis. The data of Marti et al. indicated that Pu and Nd do not fractionate during normal igneous or solar nebula processess. A diverse suite of samples gave $^{244}Pu/Nd$ ratios of 6-8 X 10^{-5}(by atom). This study has indicated that Pu and Sm do fractionate during igneous processes and, therefore, the chemical coherence of Pu and the light rare earths requires further discussion.

Although the absolute magnitude of REE partition coefficients may be quite variable with changes in temperature, pressure and chemical composition, the relative D's for REE's tend to be less variable [see for example the review by Irving (1978)]. This assumption is particularly true for Sm and Nd which differ by only two in atomic number. Thus, because Sm_D/Nd_D is rather constant for a given mineral, Pu_D/Nd_D may be calculated from the experimental data, i.e.,

$$Pu_D/Nd_D = (Pu_D/Sm_D)\ (Sm_D/Nd_D).$$

Table 8 shows that Pu_D/Nd_D is not unity for any of the experiments in this study and that for both clinopyroxene and whitlockite Pu_D/Nd_D is close to 0.6(0.5-0.71). This permits Pu-Nd fractionation during partial melting or fractional crystallization, yet the data of Marti et al. still stand. In order to see if these two observations can be reconciled, let us now examine the samples analyzed by Marti et al. individually.

Table 8

Adopted Pyroxene Partition Coefficients

	Clinopyroxene (P_2O_5 = 0)	Clinopyroxene (P_2O_5 = 1.4%)	Whitlockite
Pu_D	0.17 ± 0.02	0.11 ± 0.01	3.8 ± 0.4
Sm_D	0.31 ± 0.03	0.26 ± 0.03	6.4 ± 0.7
Pu_D/Sm_D	0.55	0.42	0.59
Sm_D/Nd_D	1.29*	1.29*	1.0**
Pu_D/Nd_D	0.71	0.54	0.59

*Grutzeck et al. (1974)

**Estimated from Irving (1978)

1. Basaltic achondrites (eucrites)

This class of meteorites grossly resembles terrestrial basalts in their texture and chemistry (whence the name) and were probably produced by low pressure partial melting of a pyroxene-olivine-plagioclase mixture (Stolper, 1977) which, although not chondritic, may have had unfractionated (relative to chondrites) refractory LIL (large-ion-lithophile) element abundances. During partial melting (after the disappearance of any trace minerals which concentrate actinides and lanthanides) it is assumed that the only major reservoir of Pu and Nd in the solid residuum will be clinopyroxene. Because both ^{Pu}D and ^{Nd}D are small, equilibrium partial melting will produce a liquid that is essentially unfractionated in Pu and Nd relative to its source region. By mass balance,

$$(Pu/Nd)liq = (Pu/Nd)source \quad \frac{Xliq + {}^{Nd}Dcpx\ fcpx\ (1-Xliq)}{Xliq + {}^{Pu}Dcpx\ fcpx\ (1-Xliq)}$$

where Xliq is the mass fraction of partial melting and fcpx is the fraction of clinopyroxene in the solid residuum. If for Juvinas $0.15 \leq Xliq$ and $fcpx \leq 0.5$ (Stolper, 1977) and $^{Nd}Dcpx = 0.24$ and $^{Pu}Dcpx = 0.17$, then

$$1 \leq (Pu/Nd)liq \ / \ (Pu/Nd)source \leq 1.16$$

If the laboratory D values are higher than the D values applicable during eucrite genesis, the maximum fractionation is less than given here. If the laboratory D's are low by as much as a factor of two, the amount of Pu-Nd fractionation is still less than 25% (relative to the source) for Xliq = 0.15. Since refractory LIL elements are not easily volatilized and are difficult to fractionate in partial melting events (as in the case of Pu and Nd), the chance of the eucrite parent body having unfractionated relative abundances of these elements is good. This is

presumably the reason that many eucrites (including Juvinas which was analyzed by Marti et al.) have flat REE patterns when normalized to chondrites (Schnetzler and Philpotts, 1969) and Th/U ratios of 3.8 (Morgan and Lovering, 1973; Tatsumoto et al., 1973). Thus, on the basis of partition coefficients and simple assumptions about the eucrite parent body, Juvinas should (neglecting ^{244}Pu decay) have a (Pu/Nd) ratio within 20% that of chondrites, even though $Pu_D/Nd_D \neq 1$.

Additionally, the bracketing theorem of Benjamin et al. (1978) argues that since, in general, $U_D \leq Th_D < Pu_D < Sm_D$ or Nd_D, if a meteorite has a flat REE pattern, chondritic Sm/U and Th/U = 3.8, then the Pu/Nd or Pu/U ratio should be unfractionated as well. Those basaltic achondrites which meet these criteria appear to be reasonable choices for Pu/Nd or Pu/U determinations unless they are substantially younger than chondrites. This does not appear to be the case. ^{206}Pb-^{207}Pb ages of eucrites are indistinguishable from chondrites (Tatsumoto et al., 1973); initial $^{87}Sr/^{86}Sr$ ratios of eucrites actually tend to be lower than chondrites (Papanastassiou and Wasserburg, 1969; Sanz and Wasserburg, 1969), although the $(^{87}Sr/^{86}Sr)_I$ of St. Severin is nearly the same as BABI (Manhes et al., 1978); and the Nd isotopic systematics of Juvinas indicate that its age is unresolvable from those of chondrites, although with poor ($\pm$ 100 m.y.) resolution (Jacobsen and Wasserburg, 1980). It is concluded, therefore, that eucrites such as Juvinas should yield reasonable estimates of the $^{244}Pu/^{238}U$ and the $^{244}Pu/Nd$ ratio of the solar system.

2. Angra dos Reis (AdoR)

AdoR is an unusual meteorite--an achondrite which is 90% fassaitic clinopyroxene and which exhibits a cumulate texture (Prinz et al., 1977).

AdoR is thus often modeled as a pyroxene cumulate of some extraterrestrial magma chamber (Ma et al.,1977). If this were strictly true and AdoR contained no trapped liquid, then for equilibrium crystallization, the Pu/Nd ratio of AdoR should be 0.7 that of its parent magma for up to 50% crystallization (see Table 8). This model is difficult to reconcile with AdoR's high U concentration (~200 ppb) which, if $^{U}D_{cpx} \leq 0.02$ (Benjamin, 1979), would imply that its residual magma had a U concentration of ≥ 10ppm which is ~50 times greater than the U-rich Allende inclusions.

A more reasonable model is that the pyroxene cumulate also contained trapped, interstitial liquid. This is consistent with AdoR's mineralogy and texture. In this case the $^{Pu}/Nd$ of the crystal-liquid mixture is given by

$$(Pu/Nd)Ador = (Pu/Nd)liq \quad \frac{(1-Xcum) + {}^{Pu}Dcpx \quad Xcum}{(1-Xcum) + {}^{Nd}Dcpx \quad Xcum}$$

where Xcum is the fraction of the cumulate that is pyroxene. The $(Pu/Nd)_{liq}$ is a function of the amount of crystallization and is given by

$$(Pu/Nd)liq = (Pu/Nd)^* \quad \frac{{}^{Nd}D \quad f^* + (1 - f^*)}{{}^{Pu}D \quad f^* + (1 - f^*)}$$

where (Pu/Nd)* is the (Pu/Nd) ratio of the parent liquid prior to pyroxene crystallization and f* is the mass fraction of pyroxene crystallized. Combining these with the partial melting equation given earlier yields,

$$(Pu/Nd)AdoR \;/\; (Pu/Nd)source =$$

$$\frac{Xliq + fcpx \; {}^{Nd}Dcpx \; (1-Xliq)}{Xliq + fcpx \; {}^{Pu}Dcpx \; (1-Xliq)} \cdot \frac{(1-Xcum) + {}^{Pu}Dcpx \; Xcum}{(1-Xcum) + {}^{Nd}Dcpx \; Xcum} \cdot \frac{(1-f^*) + {}^{Nd}D \; f^*}{(1-f^*) + {}^{Pu}D \; f^*}$$

Since almost nothing is known about the AdoR parent magma, any assignment of values to Xliq, fcpx, f*, and Xcum will be rather arbitrary. Since pyroxene did crystallize from the AdoR melt, pyroxene was presumably

in the AdoR melt's source region. Whether the refractory LIL elements of this source region were fractionated relative to chondrites is also unknown. Because of these difficulties no numerical solutions to the model given above are attempted here.

Rather than explore model dependent solutions, it is perhaps more illustrative to consider the Ce/Nd ratio of Ador. Comparing the $^{Pu}D_{cpx}$ of this study to the REE D's of Grutzeck et al. (1974), $^{Ce}D_{cpx} < {}^{Pu}D_{cpx} < {}^{Nd}D_{cpx}$; implying that the Ce/Nd ratio may place a constraint on the amount of Pu/Nd fractionation. From the data of Schetzler and Philpotts (1969) and Nakamura (1974), (Ce/Nd)Ador / (Ce/Nd)chondrites = 0.77. Thus, as in the case of Juvinas, AdoR appears (somewhat fortuitously) to be a reasonable candidate for the solar system Pu/Nd ratio (within 20%), although its history is complex. The measured equality of the pyroxene and whitlockite (Pu/Nd) ratios (Marti et al., 1977) could still be explained since from Table 8, $(^{Pu}D/^{Nd}D)_{cpx} = 1.1\ (^{Pu}D/^{Nd}D)_{whitlockite}$. This similarity between $[(Pu/Nd)_{cpx} / (Pu/Nd)_{whit}]_{lab}$ and $[(Pu/Nd)_{cpx} / (Pu/Nd)_{whit}]_{Ador}$ would be difficult to achieve during fractional crystallization unless pyroxene and whitlockite both crystallized at the same time (co-crystallization). A more reasonable interpretation is that the pyroxene and whitlockite have undergone extensive subsolidus equilibration of Nd and Pu, consistent with the lack of major element zoning in the Ador pyroxene (Prinz et al., 1977). As in the case of Juvinas, the $^{207}Pb - {}^{206}Pb$ model age of Ador is indistinguishable from that of chondrites (Wasserburg et al., 1977; Tatsumoto et al., 1973).

This model, as well as the eucrite model, has assumed that $^{Sm}D_{cpx} = 0.31$ and $^{Pu}D_{cpx} = 0.17$, the values measured in the laboratory. Since these compositions are much different from the eucrites or Ador,

one might ask how partition coefficients might be expected to change with bulk composition. Because of a lack of detailed data, this is a difficult question to answer quantitatively, since there are differences both in composition and liquidus temperature between the starting materials used in this study and AdoR or eucrites. The qualitative answer is that $\ln(^{Sm}D_{cpx})$ decreases linearly with increasing temperature (Drake and Holloway, 1977) and that, at constant temperature, a melt with lower viscosity [i.e. lower SiO_2 and Al_2O_3 contents and (based on immiscible liquid partitioning) higher concentrations of network modifiers such as FeO and Na_2O] should have a smaller $^{Sm}D_{cpx}$ (Ryerson and Hess, 1978). These effects are, to some degree, cancelling. For example, as FeO is added to an Fe-free system, REE D's should decrease (Ryerson and Hess, 1978), but, because FeO addition lowers the liquidus in many geologically important systems, partitioning occurs at lower temperatures which should tend to increase D values.

Perhaps the major difference between the models for eucrites and AdoR described here and the true petrogenesis of these rocks, is mineralogy. Although the liquidus phases of the AdoR parent magma are not well known, none is likely to have been diopside. Also, Stolper (1977) concluded that pigeonite was the pyroxene phase of the eucrite source region. Pigeonite (sub-calcic pyroxene) has much lower ^{Sm}D and ^{Nd}D values than diopside. Based on phenocryst-matrix data on natural samples, Schnetzler and Philpotts (1970) give 0.049 and 0.100 for $^{Nd}D_{pig}$ and $^{Sm}D_{pig}$, respectively. If no calcic pyroxene existed in the AdoR magma and eucrite source regions, then Pu and Nd partitioning should be controlled by pigeonite and plagioclase [which also has $^{Nd}D \leq 0.1$ (Drake, 1972)]. Because these minerals have lower D's, fractionation of Pu and Nd is

likely to be much more difficult during partial melting than if diopsidic pyroxene were stable. Similarly, the REE's of cumulates of sub-calcic pyroxene would be dominated by small amounts of trapped liquid, rather than by the cumulate phase itself. For these reasons the model described earlier for the eucrites appears to put reasonable limits on the amount of Pu-Nd fractionation that could have occurred during the formation of these rocks. The eucrites and perhaps even AdoR appear to be viable candidates for determining the Pu/Nd ratio of the solar system.

3. Allende coarse-grained inclusions

The Allende type A and B coarse-grained inclusions (Grossman, 1975) are very complex objects which are believed by some to be the first condensates from the solar nebula (Marvin et al., 1970). These inclusions have the lowest known $^{87}Sr/^{86}Sr$ ratios (Gray et al., 1973). Marti et al. (1977) measured melilite from an Allende type-B coarse-grained inclusion and found it to have a Pu/Nd ratio very similar to the values of AdoR and Juvinas, again implying chemical coherence of Pu and Nd. This result requires interpretation, however. The Sm-Nd isotopic system of this inclusion appears to have been disturbed (G. Lugmair, pers. comm.) raising the possibility of xenon loss which would produce a low Pu/Nd ratio.

In summary, it appears that, although ^{Pu}D does not in general equal ^{Nd}D, Pu and Nd are difficult to fractionate in ordinary igneous processes. This is because both ^{Pu}D and ^{Nd}D are small ($\sim<0.3$) for common silicate minerals and because phosphates and other trace minerals containing Pu and Nd are generally assumed to be assimilated by the magma during the

early stages of partial melting (Carmichael et al., 1974). The differences between this laboratory study and the real world appear to be such as to further decrease ^{Pu}D and ^{Nd}D, making fractionation even more difficult. Thus, of the samples analyzed by Marti et al., the eucrite Juvinas appears to be an excellent candidate for determining an early solar system Pu/Nd ratio, but both AdoR and the Allende melilite appear to have had a more complex origin. Since Juvinas appears to have an age comparable to that of chondrites (Lugmair et al., 1976), the discrepancy in Pu/U between the Marti et al. data and St. Severin still stands. In an effort to resolve this discrepancy, the next section will discuss other Pu/U determinations from the literature to see if any pattern emerges.

B. Other measurements of $^{244}Pu/^{238}U$

The conclusion of Podosek (1970a) was that Pu and U chemically fractionate, since his St. Severin whole-rock $^{244}Pu/^{238}U$ ratio of 0.015 was substantially different from the 0.035 value measured on whitlockite of the same meteorite by Wasserburg et al. (1969a). Since Pu and Nd were observed not to fractionate, Marti et al. (1977) reasoned that the $^{244}Pu/^{238}U$ ratio of the early solar system could be calculated using their AdoR data, i.e.

$$(^{244}Pu/^{238}U)_{solar} = (^{244}Pu/Nd)_{AdoR}\ (Nd/^{238}U)_{chondrites}.$$

This method yielded a $^{244}Pu/^{238}U$ ratio of 0.004 which was a factor of four lower than the 0.015 value of Podosek (1970a, 1972).

This discrepancy between 0.015, measured on a chondrite, and the 0.004 value which purports to be "chondritic" is made more perplexing by the conclusion of the preceding section which claimed that the Juvinas Pu/Nd ratios (and perhaps the AdoR and Allende data as well) were essentially unfractionated from chondritic. In an attempt to resolve this discrepancy, an evaluation of the available Pu/U data will now be made. Since the data of Marti et al. have been discussed in some detail in the preceding section and Introduction, emphasis will be placed on other sources.

1. Eucrites

The only eucrites for which $^{244}Pu/^{238}U$ data exist are Juvinas and Pasamonte. The Juvinas fission Xe concentrations of Marti et al. (1977) and the U data of Morgan and Lovering (1973) yield a $^{244}Pu/^{238}U$ ratio of 0.004, in agreement with the calculated value of Marti et al. The

Pasamonte data of Hohenberg et al. (1967) and the U data of Unruh et al. (1977) give a ratio of 0.0047, in good agreement with Juvinas. Thus, although sampling errors may be large, these two eucrites appear to have rather low $^{244}Pu/^{238}U$ ratios that are identical to the ratio calculated from Pu/Nd data.

2. AdoR

It was mainly the AdoR Pu/Nd data which were used to calculate the 0.004 value of Marti et al., and it is of interest, therefore, to compare the results of this calculation to a measured $^{244}Pu/^{238}U$ ratio on the same meteorite. The fission Xe data of Hohenberg (1970) and the U data of Tatsumoto et al. (1973) combine to yield a $^{244}Pu/^{238}U$ ratio of 0.0065. This is somewhat higher than 0.004 but still significantly different from 0.015. The amount of Pu-U fractionation during the formation of Ador is unknown but, based on Ce/U, is likely to have been about 20%, assuming an unfractionated source. The AdoR U concentration of Tatsumoto et al. (1973) is in good agreement with the analyses of Morgan and Lovering (1973) and Bhandari et al. (1971) and is ~27% higher than the U analyses of Wasserburg et al. (1977). The fission Xe concentration of Hohenberg (1970) is in good agreement with that of Lugmair and Marti (1977).

3. Allende coarse-grained inclusions

Ganapathy and Grossman (1976) suggested that coarse-grained Allende inclusions (types A and B (Grossman, 1980)) should yield a valid initial $^{244}Pu/^{238}U$ ratio. They based their arguments on the primative nature of these objects (Gray et al., 1973) and their observation that refractory LIL elements in coarse-grained inclusions were unfractionated. Prior to

this Podosek and Lewis (1972) had measured a $^{244}Pu/^{238}U$ ratio of 0.087 on an uncharacterized mixture of Allende inclusions, but the most viable interpretation of this measurement appears to be that the sample contained a large number of fine-grained inclusions which are known to have fractionated LIL abundances (Grossman and Ganapathy, 1976b; Ganapathy and Grossman, 1976) and fractionated Th/U ratios (Chen and Tilton, 1976; Tatsumoto et al., 1976). Additionally, Ganapathy and Grossman (1976) noted that the U content of the Podosek and Lewis (1972) sample was only ~0.1 that of most coarse-grained inclusions (Grossman and Ganapathy, 1976a), implying that this sample was nonrepresentative.

Drozd et al. (1979) measured the $^{244}Pu/^{238}U$ ratio of a large Type B inclusion. Their value of 0.016 agreed remarkably well with the 0.015 ratio of Podosek (1970a) and appeared to substantiate the views of Ganapathy and Grossman. However, Boynton (1978) pointed out that the Th/U ratios of coarse-grained inclusions appeared to be shifted towards higher values than chondrites. His tabulation of Th/U ratios (Mason and Martin, 1974; Chen and Tilton, 1976; Tatsumoto et al., 1976) with an average Th/U = 7-8 was twice that of chondrites (Morgan and Lovering, 1968). Boynton attributed this difference to the incomplete condensation of U (Boynton, 1978). Grossman (1980) disagreed with Boynton's interpretation and suggested that the inclusions with high Th/U ratios tabulated by Boynton were nonrepresentative. However, regardless of the mechanism of fractionation, additional data appear to substantiate Boynton's observation that the Th/U of coarse-grained Ca-Al-rich inclusions tends to be high. Figure 23 shows a histogram of Th/U ratios for coarse-grained inclusions. Data are either direct Th/U determinations or are inferred from $^{208}Pb/^{206}Pb$ ratios (Chen and Wasserburg, 1980). The average Th/U

Figure 23

This figure shows a histogram of Th/U ratios for Allende coarse-grained Ca-Al-rich inclusions. Data are from Mason and Martin (1974), Chen and Tilton (1976), Tatsumoto et al. (1976), Stapanian (1980) and Chen and Wasserburg (1981). The mean of all data is Th/U = 6.6 or 1.75 X chondritic. Since Th and U are fractionated in these objects, they may not be good sources for $^{244}Pu/^{238}U$ ratios.

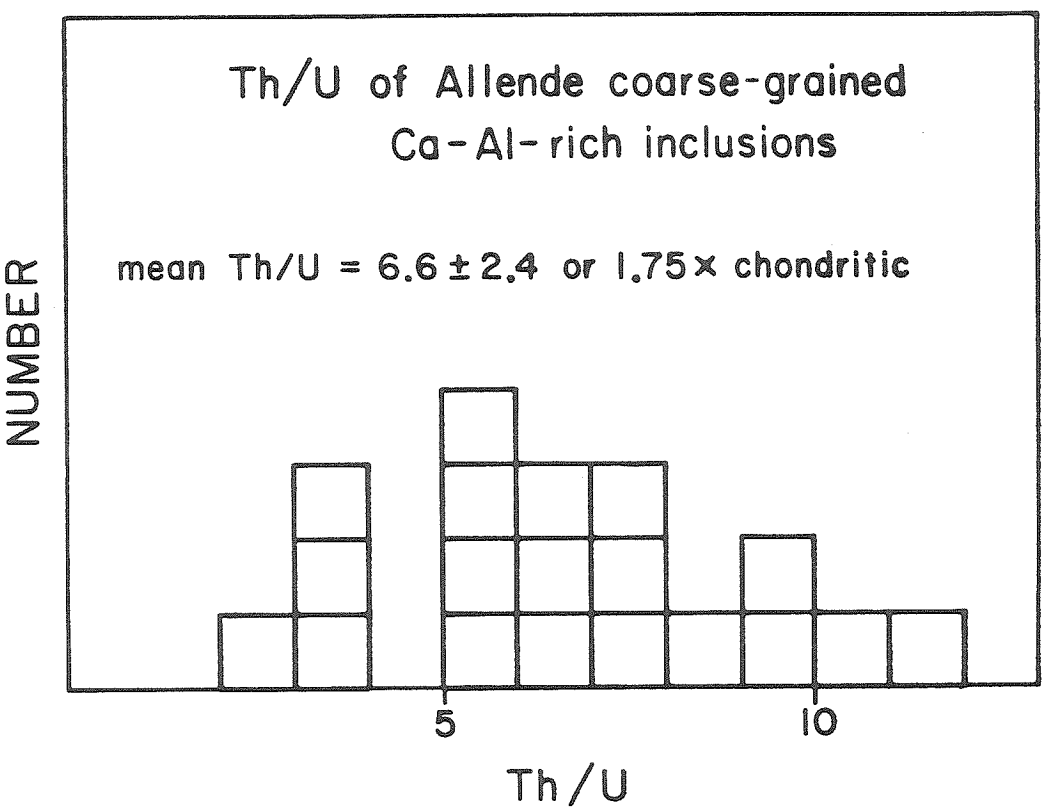
Th/U of Allende coarse-grained
Ca-Al-rich inclusions
mean Th/U = 6.6 ± 2.4 or 1.75× chondritic
NUMBER
5
10
Th/U

of 6.6 is 1.75 times that of Cl chondrites. If Th and U are fractionated, Pu and U may be also. This makes interpretation of the Drozd et al. (1979) $^{244}Pu/^{238}U$ ratio difficult.

4. The St. Severin chondrite

Although the Podosek (1970a) ratio is the most often quoted, other St. Severin $^{244}Pu/^{238}U$ determinations exist as well. The Podosek method (1970b) has the following advantages: (1) no assumption about the trapped xenon composition is necessary; (2) no determinations of absolute concentrations of xenon are required; and (3) the Pu and U are determined on the same sample. As Jones and Burnett (1979) have pointed out, these considerations appear to make the Podosek method superior to more conventional techniques. However, unless errors are systematic, it is expected that whole-rock Xe analyses of unirradiated chondrites would, with poorer precision, yield $^{244}Pu/^{238}U$ ratios comparable to the Podosek technique.

One possible systematic error is the assumption of AVCC (average carbonaceous chondrite) as the trapped xenon composition. If the trapped composition has a higher $^{136}Xe/^{132}Xe$ ratio than AVCC (e.g. air), then by choosing AVCC as a trapped composition, the calculated amount of fission ^{136}Xe will be too high and the calculated $^{244}Pu/^{238}U$ ratio will be high as well. Conversely, if the actual trapped composition has a $^{136}Xe/^{132}Xe$ ratio less than AVCC, the calculated $^{244}Pu/^{238}U$ ratio will be too low. Since Alaerts et al. (1979) have presented evidence that the trapped xenon of LL-chondrites has a slightly lower $^{136}Xe/^{132}Xe$ ratio than AVCC, $^{244}Pu/^{238}U$ calculations involving "conventional" analyses will be be made (1) assuming AVCC to be the trapped composition and (2) assuming the trapped composition of Alaerts et al.

Five whole-rock xenon analyses of St. Severin exist in the literature: two by Wasserburg et al. (1969a), two by Marti et al. (1969), and one by Alaerts et al. (1979). Table 9 gives the xenon data and $^{244}Pu/^{238}U$ ratios of these samples. As would be expected, the data have a greater spread and are less precise than Podosek's, but somewhat unexpectedly the $^{244}Pu/^{238}U$ ratios are much lower--regardless of the assumption of the trapped composition. Although the scatter is large, the tendency toward lower $^{244}Pu/^{238}U$ ratios is seen in all four St. Severin analyses from three laboratories. Taken at face value these data would suggest that the Podosek St. Severin ratio was high.

Two other irradiated St. Severin samples have also been analyzed using the Podosek technique. An unpublished xenon analysis of an Alexander et al. (1972) St. Severin sample was kindly provided by S. Niemeyer. This St. Severin aliquot was most probably left over from an earlier whitlockite study (Lewis, 1975) and had its magnetic fraction removed during a Franz separation (S. Smith, pers. comm.; Zaikowski, 1980). Since many whitlockites are associated with metal and troilite (Jones and Burnett, 1979; Manhes et al., 1978), this St. Severin sample may be depleted in whitlockite. If whitlockite contained only a minor amount of the Pu in St. Severin [as it does U (Jones and Burnett, 1979)], any whitlockite removal should make only a very small (~10%) difference in the $^{244}Pu/^{238}U$ ratio. A least-squares extrapolation of the 1100, 1200, 1400, and 1500°C xenon releases (1300°C release was lost) yields a $^{244}Pu/^{238}U$ ratio of 0.0065. The slope of the regression line is mainly determined by the 1100 and 1200°C releases; the 1400 and 1500°C releases are close enough to AVCC to be compatible with a range of $^{244}Pu/^{238}U$ ratios. If the regression line is required to pass through AVCC, the calculated $^{244}Pu/^{238}U$

Table 9

St. Severin Aliquot	Wt. (g)	^{132}Xe x10^{12}cc/g(STP)	$^{244}Pu/^{238}U$*† trapped ≡ AVCC	≡ Alaerts et al.
Wasserburg et al. (1969) - Light	0.432	19 ± 3	0.010 ± 2	0.011 ± 2
Wasserburg et al. (1969) - Dark	0.435	35 ± 5	0.006 ± 1	0.009 ± 2
Marti et al. (1969) - Ia	1.0	20.5 ± 1.5	0.0029 ± 6	0.0047 ± 6
Marti et al. (1969) - Ib	1.9	27 ± 3	0.0038 ± 8	0.0062 ± 10
Alaerts et al. (1979) - bulk	0.7895	27.3 ± 3.2	0.0012 ± 4	0.0036 ± 6
		Average =	0.0035 ± 20	0.0059 ± 23

*(132/136) sp = 0.7; U = 12ppb; ^{136}Xe yield from ^{244}Pu ≡ 6%; Fission Branching Ratio = 1.25×10^{-3}

Because spallation corrections are small, errors assigned are from the ^{132}Xe measurements and error in (136/132) m. Errors are typically 20-30% and are given for the last decimal place.

†The ^{136}Xe fission yield used to calculate $^{244}Pu/^{238}U$ is 6%. The fission yield used by Podosek (1972) was 5.6%. Using 6% instead of 5.6% will lower the Podosek (1972) $^{244}Pu/^{238}U$ ratio from 0.0154 to 0.0144.

ratio is 0.0043. If the regression line is required to pass through the trapped component of Alaerts et al. (1979), a $^{244}Pu/^{238}U$ ratio of 0.0040 is calculated--not significantly different from AVCC.

This discussion is complicated by the recent observation of Hohenberg et al. (1981) that the trapped xenon of the dark lithology of St. Severin is neither AVCC nor the composition of Alaerts et al. (1979), but one which is slightly enriched in ^{129}Xe, ^{130}Xe, and ^{134}Xe relative to AVCC. In the case of the dark St. Severin Xe analyses of Hohenberg et al. (1981) (analyzed using the Podosek (1970) technique), assuming AVCC as the trapped component gives a $^{244}Pu/^{238}U$ ratio of 0.007. If the 1325°C release (the most precise, non-radiogenic release inconsistent with AVCC) is taken as the trapped component, the $^{244}Pu/^{238}U$ ratio is raised to 0.014, in good agreement with Podosek (1972). If the Hohenberg et al. (1981) 1325°C release with a higher $^{136}Xe/^{132}Xc$ ratio than AVCC is the actual trapped component of the unirradiated samples, the $^{244}Pu/^{238}U$ ratios calculated for them are too high (see discussion at beginning of Section). Summarizing, two different analytical techniques for $^{244}Pu/^{238}U$ tend to give different results, even for the same meteorite. Five whole-rock analyses of unirradiated St. Severin average 0.005 ± 2 and two step-wise thermal releases of irradiated samples give $^{244}Pu/^{238}U$ ratios of 0.014 - 0.015. A third irradiated sample which had its magnetic fraction removed gave an intermediate value (0.0065).

Alaerts et al. (1979) noted that, within error, their total-rock concentration of ^{136}Xe fission in St. Severin could be accounted for by assuming that all the ^{244}Pu resided in whitlockite and by prorating the whitlockite ^{136}Xe fission data of Lewis (1975). If this is true, then

the $^{244}Pu/^{238}U$ ratio of St. Severin my be calculated,

$$(^{244}Pu/^{238}U)\ \text{St. Severin} = {}^{U}X_{whit}\ (^{244}Pu/^{238}U)_{whit}$$

where ${}^{U}X_{whit}$ is the fraction of St. Severin's U residing in whitlockite. If ${}^{U}X_{whit} = 0.115$ (Jones and Burnett, 1979) and $(^{244}Pu/^{238}U)$ whit = 0.046 (Burnett et al., 1981), then $(^{244}Pu/^{238}U)$ St. Severin is 0.0053. Thus, if the $^{244}Pu/^{238}U$ ratios of St. Severin is 0.005 from unirradiated samples are correct then all the Pu resided in whitlockite and was uncorrelated with U. If Pu was sited only in whitlockite, the Podosek method cannot easily yield the correct $^{244}Pu/^{238}U$ ratio. If this model is correct, then the 1000-1200°C releases of the irradiated samples should contain most of the whitlockite fission Xe. This is consistent with the step-wise thermal release data of Lewis (1975), who found that 30-75% of the whitlockite Xe was lost in this temperature range. This model also requires that enough U fission Xe is degassed during this temperature interval to lower the $^{244}Pu/^{238}U$ ratio of these releases from 0.046 (pure whitlockite) to 0.015. Plagioclase could possibly supply this U fission-Xe. Plagioclase melts at ~1150°C and should contain fission Xe from grain-boundary U (Jones and Burnett, 1979). Whether or not plagioclase alone is sufficient to lower the $^{244}Pu/^{238}U$ ratio of the 1000-1200°C releases to 0.015 depends on the fraction of whitlockite which degasses in this interval. It is difficult to completely reconcile the model of of uncorrelated U and Pu with the Podosek Xe release data. For U and Pu in different mineralogical sites, the $^{130}Xe/^{132}Xe$ vs. $^{134}Xe/^{132}Xe$ plot for temperature fractions from an irradiated meteorite should be a scatter plot. This was not observed. Specifically a coincidental release of uncorrelated ^{235}U and ^{244}Pu fission Xe is required which gives

the same apparent $^{244}Pu/^{238}U$ for at least two temperature intervals, yielding a linear array having no physical significance.

If most of the Pu resides in whitlockite, Sm (and the other LREE's) may be similarly sited. Table 10 shows a comparison of whole-rock REE concentrations calculated from the whitlockite data of Mason and Graham (1970) and whole-rock concentrations measured by Masuda et al. (1973). The calculated concentrations of the light rare earths agree with the measured concentrations to within 25%, which is reasonable considering sampling differences. Recent analyses by Jacobsen (pers. comm.) on St. Severin whitlockite (Nd ≅ 140 ppm; Sm ≅ 43 ppm) indicate that the analyses of Mason and Graham (1970) may be systematically low by ~ 30-40%. This would make for better agreement between the calculations of Table 10 and the measurements of Masuda et al. (1973). In addition, the calculated Pu/Nd ratio of 12 X 10^{-5} for the St. Severin whitlockite (using the Jacobsen Nd concentration) is in fair agreement with but higher than the Pu/Nd ratios measured by Marti et al. (1977), supportive of the hypothesis that 75% (or more) of the Pu is retained in whitlockite.

Jacobsen and Wasserburg (1980) have reported Sm-Nd data for light and dark portions of the St. Severin meteorite. Although the samples analyzed by Jacobsen and Wasserburg are not aliquots of the light and dark fragments analyzed for xenon by Wasserburg et al. (1969a), they do come from the same cut slab (S.B. Jacobsen and J.C. Huneke, pers. comm.). The light fraction, which has a higher ^{244}Pu concentration, also has higher Sm and Nd contents. If the quantitative retention of Pu and the LREE's in whitlockite is a viable hypothesis, then the Sm-Nd data can be used to calculate the abundance of whitlockite in both lithologies and both light and dark should have the same $^{244}Pu/Nd$ ratio (i.e. that of

Table 10

Comparison of Calculated and Measured REE's in St. Severin

Element	E_{Cwhit} (ppm)[a]	$E_{Cwhole\ rock\ (Model)}$[c]	E_{Cmeas}[b]	Model/meas.
La	64	0.32	0.39	0.82
Ce	130	0.65	0.94	0.69
Nd	100	0.50	0.66	0.76
Sm	34	0.17	0.22	0.77
Eu	2.5	0.012	0.085	0.14
Gd	50	0.25	0.30	0.83
Dy	49	0.24	0.37	0.65
Er	26	0.13	0.25	0.52
Yb	25	0.12	0.25	0.48

a. Mason and Graham (1970)

b. Masuda et al. (1973)

c. $E_{C_{whole\ rock}} = E_{C_{whit}} \cdot Xwhit$;
Xwhit = mass fraction of whitlockite = 0.005

whitlockite). Specifically by this model:

$$(^{244}Pu/Nd)rock = {}^{Nd}Xwhit\ (^{244}Pu/Nd)whit = (^{244}Pu/Nd)whit$$

since $^{Nd}Xwhit$ is the fraction of a sample's Nd that is contained in whitlockite and is assumed to be unity.

Table 11 shows the calculated abundance of whitlockite in the light and dark lithologies. The independent Nd and Sm calculations agree within 10%. The $^{244}Pu/Nd$ ratios, although 20-50% higher than that reported by Marti et al. (1977), agree within error ($\pm$ 20%). Although not a proof, these data are consistent with the hypothesis that most Pu is sited in whitlockite and that the $^{244}Pu/^{238}U$ ratio of St. Severin is 0.005 $\pm$ 2.

5. Other Chondrites

In addition to St. Severin, other equilibrated ordinary chondrite Xe analyses exist in the literature. The data for four of these, Beardsly (H5), Richardton (H5), Holbrook (L6)and Bruderheim (L6), are summarized by Reynolds et al. (1969); a fifth, Olivenza (LL5), is another of the meteorites studied by Alaerts et al. (1979). Figure 24 shows a plot of $^{244}Pu/^{238}U$ vs. $[^{132}Xe]$. The U data for samples other than St. Severin come from Morgan (1971). For Olivenza a U content of 12ppb was assumed. The precision of these data is not good but all calculated $^{244}Pu/^{238}U$ ratios are lower than 0.015. The error in the $^{244}Pu/^{238}U$ ratio increases with increasing trapped Xe, showing the difficulty in measuring small fission effects when most of the Xe is non-fissiogenic. The trapped component is assumed to be AVCC. The light lithology St. Severin analysis of Wasserburg et al. (1969a) is a bit higher than the

Table 11

Sample	Nd(ppm)	Sm(ppm)	Calculated % whit (Nd)	Calculated % whit(Sm)	Measured* $^{244}Pu/Nd$	$^{244}Pu/^{238}U$
Whitlockite	140[1]	43[1]	____	____	$12 \times 10^{-5} \pm 2$[3]	0.046 ± 9[2,3]
St. Severin light	1.286[4]	0.440[4]	0.92	1.0	$11 \times 10^{-5} \pm 2$[3]	0.009 ± 2[5,3]
St. Severin dark	0.560	0.185[4]	0.40	.43	$15 \times 10^{-5} \pm 3$[3]	0.006 ± 1[5,3]

1 Jacobsen (pers. comm.)

2 Burnett et al. (1981)

3 Error bars assigned assuming 20% uncertainty in $^{136}Xe_f$ measurement. Error for last decimal.

4 Jacobsen and Wasserburg (1980)

5 Calculated assuming 12ppb U in total rock samples

*Fission Xe concentrations from Wasserburg et al. (1969a); $^{244}Pu/Nd$ from Marti et al. (1977) is 9×10^{-5}

Figure 24

This figure shows a plot of $^{244}Pu/^{238}U$ vs. ^{132}Xe content for five ordinary chondrites and St. Severin. Trapped composition was taken as AVCC; spallation corrections are small. Constants used are as given in Table 9. All $^{244}Pu/^{238}U$ ratios are less than 0.01 and show no change with the amount of trapped Xe (^{132}Xe), implying that AVCC is a reasonable choice for a trapped Xe component.

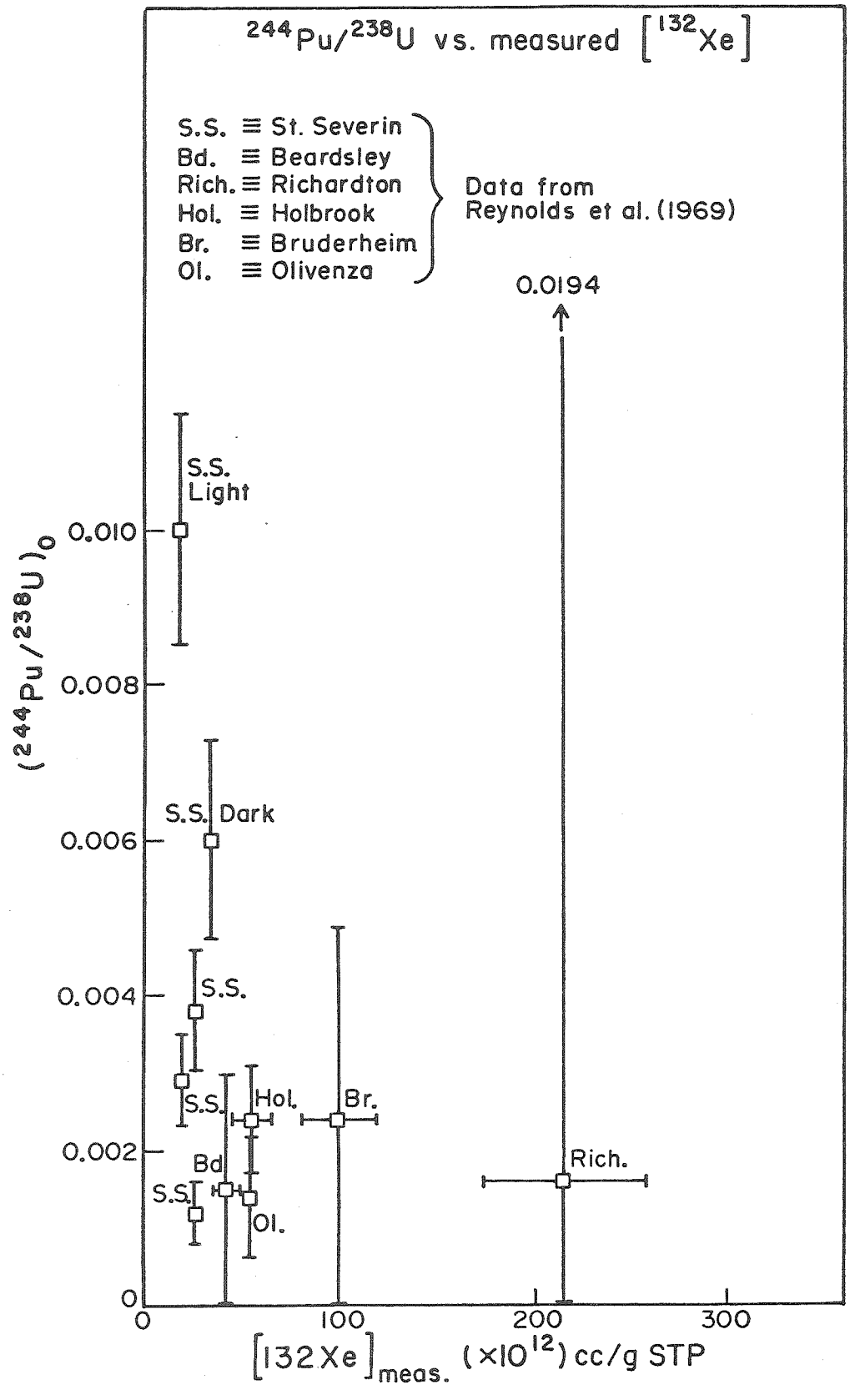
$^{244}Pu/^{238}U$ vs. measured $[^{132}Xe]$
S.S. ≡ St. Severin
Bd. ≡ Beardsley
Rich. ≡ Richardton
Hol. ≡ Holbrook
Br. ≡ Bruderheim
Ol. ≡ Olivenza
Data from Reynolds et al. (1969)
0.0194
S.S. Light
S.S. Dark
S.S.
S.S.
Hol.
Br.
Bd
S.S.
Ol.
Rich.
$(^{244}Pu/^{238}U)_0$
0.010
0.008
0.006
0.004
0.002
0
0
100
200
300
$[132Xe]_{meas.}$ $(\times 10^{12})$ cc/g STP

other $^{244}Pu/^{238}U$ ratios and may indicate phosphate enrichments. The calculated phosphate abundance for this sample in Table 11 is twice the St. Severin average (Jones and Burnett, 1979).

Figure 25 is the same as Figure 24 but the composition of Alaerts et al. (1979) was the assumed trapped component. Here there is a definite correlation of $^{244}Pu/^{238}U$ when compared with Figure 23. Because the data are the same in both figures, this correlation is independent of the error bars of the $^{244}Pu/^{238}U$ analyses and suggests that the Alaerts et al. trapped component undercorrects and yields anomalously high $^{244}Pu/^{238}U$ ratios. Because of this, AVCC is the preferred trapped composition for these data. As with the St. Severin data no $^{244}Pu/^{238}U$ ratios as high as 0.015 are observed. In fact, the only sample in Figure 24 to have a ratio as high as 0.010 was apparently phosphate enriched (see St. Severin discussion, this section). The trapped composition of Hohenberg et al. (1981) is not of consequence in the discussion of unirradiated chondrites. If the Hohenberg et al. trapped composition (or air xenon) were the trapped component, the assumption of AVCC makes the resulting $^{244}Pu/^{238}U$ ratio too high, further increasing the difference in $^{244}Pu/^{238}U$ between irradiated and unirradiated samples.

6. Conclusions

In summary, it is noted that a large discrepancy in $^{244}Pu/^{238}U$ ratios exists. Three analyses (Podosek, 1970a; Drozd et al., 1977; Hohenberg et al. 1981) give ratios of 0.015 ± 1 and five other analyses (Marti et al., 1969; Wasserburg et al., 1969a; Hohenberg et al., 1967; Hohenberg, 1970) give ratios of 0.005 ± 2. Four more indirect determinations (Marti et al. 1977) average between 0.003 and 0.004. Although the case is not

Figure 25

This figure shows $^{244}Pu/^{238}U$ ratios vs. ^{132}Xe concentration for five ordinary chondrites and St. Severin. The only difference between Figures 24 and 25 is the choice of trapped composition. Here the trapped Xe composition is assumed to be that of Alaerts et al. (1979). The increase in $^{244}Pu/^{238}U$ with trapped Xe (^{132}Xe) implies that using the Alaerts et al. composition leads to an undercorrection for trapped Xe.

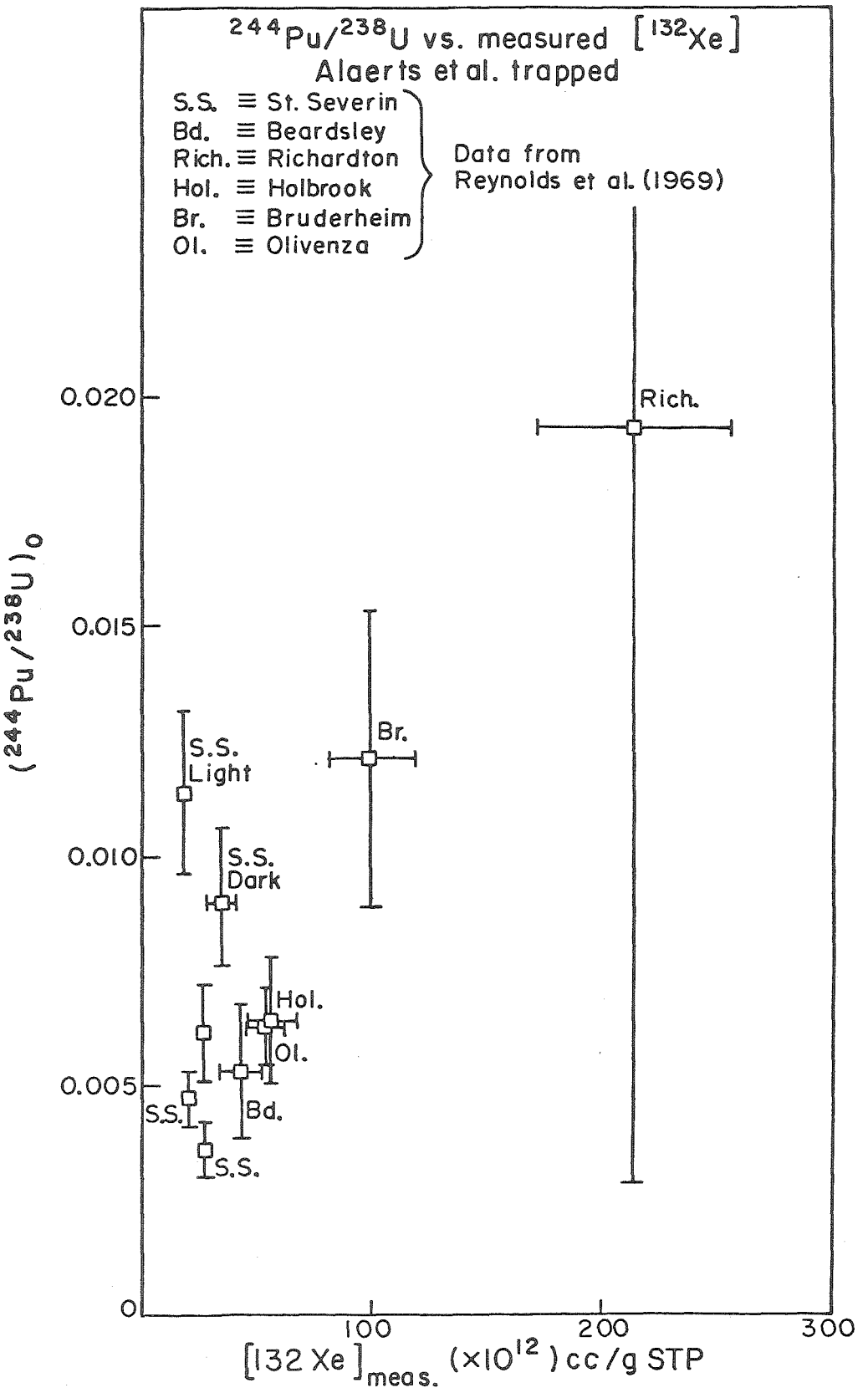
$^{244}Pu/^{238}U$ vs. measured $[^{132}Xe]$
Alaerts et al. trapped
S.S. ≡ St. Severin
Bd. ≡ Beardsley
Rich. ≡ Richardton
Hol. ≡ Holbrook
Br. ≡ Bruderheim
Ol. ≡ Olivenza
Data from
Reynolds et al. (1969)
Rich.
Br.
S.S.
Light
S.S.
Dark
Hol.
Ol.
Bd.
S.S.
S.S.
0.020
0.015
0.010
0.005
0
100
200
300
$(^{244}Pu/^{238}U)_0$
$[^{132}Xe]_{meas.}$ ($\times 10^{12}$) cc/g STP

clearcut, reasons have been presented for suspecting that the higher $^{244}Pu/^{238}U$ is not representative of most early solar system materials. Preference is given to the low $^{244}Pu/^{238}U$ ratios because, although fission Xe concentrations based on total rock analyses are imprecise, it seems difficult for their average to be systematically wrong by a factor of three. Such a systematic error for St. Severin probably requires the existence of a trapped xenon component with a $^{136}Xe/^{132}Xe$ ratio of 0.275-0.300. Such a component has never been measured and is not considered to be a viable choice for a trapped component (Pepin and Phinney, 1981). This interpretation implies that there is, as yet, essentially no measurable difference in ages between chondrites, Allende coarse-grained inclusions, AdoR and some eucrites. As previously discussed, this is consistent with most isotopic dating techniques, and is not inconsistent with the Sm and Pu data presented here. The implications of a $^{244}Pu/^{238}U$ ratio of 0.005 will be discussed further.

C. Pu/U, Supernovae and Isotopic Anomalies

In the preceding sections the controversy concerning the $^{244}Pu/^{238}U$ ratio of our solar system has been discussed. Although uncertainties still exist, a low $^{244}Pu/^{238}U$ ratio (0.005 ± 2) is favored. Since earlier discussions of nucleosynthesis in the galaxy have been primarily concerned with very high Pu/U ratios (~0.03) (Hohenberg, 1969; Wasserburg et al., 1969b), it seems appropriate to discuss the implications of a low Pu/U ratio. The discovery of the decay products of very short-lived nuclides such as ^{26}Al and ^{107}Pd ($t_{1/2}$ = 0.7 m.y. and 6.5 m.y. respectively) complicate such a discussion (Lee et al., 1977; Kelly and Wasserburg, 1978).

(1) Nuclides such as ^{244}Pu, ^{129}I ($t_{1/2}$ = 15.7 m.y.) and perhaps ^{235}U ($t_{1/2}$ = 700 m.y.) give information about the delay time Δ between the isolation of the solar system from nucleosynthetic sources in the galaxy and the formation of meteorites. Because of the large decay interval (Δ) calculated from these longer-lived elements (~10^8 years), the ^{26}Al and ^{107}Pd must be explained either as (a) very small amounts of freshly synthesized material or (b) the result of some solar system process (e.g. a solar proton irradiation). Since $^{26}Al/^{27}Al$, $^{129}I/^{127}I$ and $^{107}Pd/^{110}Pd$ are approximately constant (10^{-4} - 10^{-5}) (Kelly and Wasserburg, 1978), the abundance of all short-lived nuclides may only be indicative of a dilution factor and have little cosmochronological significance.

Table 12 shows the Δ's calculated for two different production models. Δ_1 is the delay after continuous, uniform nucleosynthesis over a time T [YONI model of Wasserburg et al. (1969b)], and Δ_2 is the delay after a period (T) of multiple, discreet production "spikes"

Table 12

Element	Measured Ratio (4.5 AE)	$\Delta 1$(m.y.)	Δ_2(m.y.)
$^{235}U/^{238}U$	0.313	113 $\pm$ 250	144 $\pm$ 320
$^{244}Pu/^{238}U$	0.005	140 $\pm$ 45	222 $\pm$ 70
$^{129}I/^{127}I$	1.09×10^{-4}	99 $\pm$ 20	143 $\pm$ 30
	Average Δ	117 $\pm$ 21	170 $\pm$ 45

Errors to Δ_1 assigned using range of production ratios from Schramm and Wasserburg (1970) and Kelly and Wasserburg (1978). Δ_2 errors are assigned assuming $\sigma(\Delta_1)/\Delta_1 = \sigma(\Delta_2)/\Delta_2$.

of equal intensity [multi-spike model of Trivedi (1977)]. In this model fifty uniform spikes were used. For a T of ~ 7×10^9y, this corresponds to a recurrence interval of about 140 m.y. T is different for each model and is calculated from a Th/U ratio of 3.9 today. Production ratios, decay constants and abundance ratios (except for Pu) are basically those used by Schramm and Wasserburg (1970) and Kelly and Wasserburg (1978). The agreement between the U, I, and Pu data is acceptable. The means $\Delta_1 = 117 \pm 21$ and $\Delta_2 = 170 \pm 45$ are essentially within the precision of the input parameters and the difference between Δ_1 and Δ_2 is not large. Conversely, for the case of uniform production, if T and Δ are taken to be 6.9×10^9y and 1×10^8y, respectively, then at $T + \Delta$ $^{235}U/^{238}U = 0.325$, $^{129}I/^{129}I = 1.19 \times 10^{-4}$ and $^{244}Pu/^{238}U = 0.0086$. The U and I are in good agreement with chondritic measurements but the $^{244}Pu/^{238}U$ is high compared to the assumed value of 0.005. If Δ is changed to make $^{244}Pu/^{138}U = 0.005$, $^{235}U/^{238}U$ remains essentially unchanged but $^{129}I/^{127}I$ is lowered to 6×10^{-6}. For both models Δ_{Pu} is larger than Δ_I. If this discrepancy is not an artifact of inaccurate production ratios or of the model, it may indicate that the last event which added ^{26}Al and ^{107}Pd to the solar nebula also added most of the ^{129}I. If this event added negligible Pu and U (Kelly and Wasserburg, 1978; Chen and Wasserburg, 1980) and $^{244}Pu/^{238}U = 0.005$, then the ^{26}Al "spike" would have to have changed the nebular $^{129}I/^{127}I$ ratio from 6×10^{-6} to 1.09×10^{-4}. If this could be demonstrated, the widespread $^{129}I/^{127}I = 1.09 \times 10^{-4}$ (Hohenberg et al., 1967) might imply that the entire solar system (rather that just Ca-Al-rich inclusions) contained significant ^{26}Al.

D. Dating of Early Solar System Events by ^{244}Pu Xenology

As alluded to earlier, the only meteorite which shows a demonstrably different $^{244}Pu/^{238}U$ or $^{244}Pu/Nd$ ratio is the meteorite Stannern (Marti et al., 1977), whose younger age (as compared to other eucrites) is substantiated by other chronometers (Birck and Allegre, 1978). Still, there exists a factor of two spread in the data (0.005 ± 2) which at the 2σ level could conceal age differences of 160 m.y. (two half-lives). To investigate this possibility in detail will require $^{244}Pu/^{238}U$ measurements to much better precision than $\pm$ 0.001 out of 0.005. Because of the small amount of trapped xenon in eucrites, this precision in $^{244}Pu/^{238}U$ measurements should be attainable. Ordinary chondrite $^{244}Pu/^{238}U$ measurements are more difficult because of the large trapped xenon component. However, if the Pu and Nd are entirely within phosphates, applying the Marti et al. (1977) technique to a phosphate separate should yield a valid $^{244}Pu/^{238}U$ ratio.

REFERENCES

Alaerts L., Lewis R.S. and Anders E. (1979) Isotopic anomalies of noble gases in meteorites and their origins. Geochim. Cosmochim. Acta 43, 1399-1416.

Albarede F. and Bottinga Y. (1972) Kinetic disequilibrium in trace element partitioning between phenocrysts and host lava. Geochim. Cosmochim. Acta 36, 141-156.

Alexander E.C. Jr., Davis P.K. and Reynolds J.H. (1972) Rare gas analyses on neutron irradiated Apollo 12 samples. Proc. Third Lunar Sci. Conf., Geochim. Cosmochim. Acta Suppl. 3, V. 2, pp 1787-1795. M.I.T. Press.

Alexander E.C. Jr., Lewis R.S., Reynolds J.H. and Michel M.C. (1971) Plutonium-244: Confirmation as an extinct radioactivity. Science 172, 837-840.

Benjamin T.M. (1979) Experimental actinide element partitioning between whitlockite, apatite, diopsidic clinopyroxene, and anhydrous melt at one bar and 20 kilobars pressure. Ph.D. thesis, California Institute of Technology, Pasadena.

Benjamin T.M., Arndt N.T. and Holloway J.R. (1977) Instrumental technique for β-track mapping. Carnegie Inst. Wash. Yearbk. 76, 658-660.

Benjamin T., Heuser W.R. and Burnett D.S. (1978) Laboratory studies of partitioning revelant to ^{244}Pu chronometry. Proc. 9th Lunar and Plan. Sci. Conf. Geochim. Cosmochim. Acta Suppl. 10, V. 1, pp 1393-1406. Pergamon.

Benjamin T.M., Heuser W.R., Burnett D.S. and Seitz M.G. (1980) Actinide crystal-liquid partitioning for clinopyroxene and $Ca_3(PO_4)_2$ Geochim. Cosmochim. Acta 44, 1251-1264.

Bhandari N., Bhat S., Lal D., Rajagopalan G., Tamhane A.S. and

Venkatavaradan (1971) Fossil fission tracks in the meteorite Angra dos Reis: A predominantly fission origin. Nature 234, 540-543.

Birck J.L. and Allegre C.J. (1978) Chronology and chemical history of the parent body of basaltic achondrites studied by the ^{87}Rb-^{87}Sr method. Earth Planet. Sci. Lett. 39, 37-51.

Boynton W.V. (1978) Fractionation in the solar nebular, II. Condensation of Th, U, Pu and Cm. Earth. Planet. Sci. Lett. 40, 63-70.

Burnett D.S., Stapanian M.I. and Jones J.H. (1981) Meteorite actinide chemistry and cosmochronology. To appear in: W.A. Fowler birthday volume (ed C.A. Barnes, D.D. Clayton and D.N. Schramm). Cambridge U. Press, New York.

Burton J.A., Prim R.C. and Slichter W.P. (1953) The distribution of solute in crystals grown from the melt. Part I. Theoretical. J. Chem. Phys. 21, 1987-1991.

Cantelaube Y., Maurette M. and Pellas P. (1967) Traces d'ions lourds dans les mineraux de la chondrite de St. Severin. In Radioactive Dating and Methods of Low Level Counting, pp 215-229. International Atomic Energy Agency, Vienna.

Carmichael I.S.E., Turner F.J. and Verhoogen J. (1974) Igneous Petrology. McGraw-Hill, San Francisco.

Champion D.E., Albee A.L. and Chodos A.A.(1975) Reproducibility and operator bias in a computer-controlled system for quantitative electron microprobe analysis. Proc. 10th Nat. Conf. Electron Probe Assn. 55A.

Chen J.H. and Tilton G.R. (1976) Isotopic lead investigations on the Allende carbonaceous chondrite. Geochim. Cosmochim. Acta. 40, 635-643.

Chen J.H. and Wasserburg G.J. (1980) A search for isotopic anomalies in uranium. Geophys. Res. Lett. 7, 275-278.

Chen J.H. and Wasserburg G.J. (1981) The isotopic composition of uranium and lead in Allende inclusions and meteoritic phosphates. Earth. Planet. Sci. Lett. 52, 1-15.

Cotton F.A. and Wilkinson G. (1962) Advanced Inorganic Chemistry. Interscience Publishers, New York.

Crozaz G. (1974) U, Th and extinct ^{244}Pu in the phosphates of the St. Severin meteorite. Earth. Planet. Sci. Lett. 23, 164-169.

Drake M.J. (1972) The distribution of major and trace elements between plagioclase feldspar and magmatic silicate liquid: An experimental study. Ph.D. thesis, University of Oregon, Eugene.

Drake M.J. and Holloway J.R. (1977) Partitioning of samarium between plagioclase, amphibole, and hydrous silicate liquid at high pressures: Preliminary results (Abstract). In Papers Presented to the International Conference on Experimental Trace Element Geochemistry. pp 21-23.

Drozd R.J., Morgan C.J., Podosek F.A., Poupeau G., Shirck J.R. and Taylor G.J. (1977) ^{244}Pu in the early solar system? Ap. J. 212, 567-580.

Evans R.D. (1955) The Atomic Nucleus. McGraw-Hill, San Francisco.

Fleischer R.L., Price P.B. and Walker R.M. (1975) Nuclear Tracks in Solids. University of California Press, Los Angeles.

Ganapathy R. and Grossman L. (1976) The case for an unfractionated $^{244}Pu/^{238}U$ ratio in high-temperature condensates. Earth. Planet. Sci. Lett. 31, 386-392.

Gray C.M., Papanastassiou D.A. and Wasserburg G.J. (1973) The identification of early condensates from the solar nebula. Icarus 20, 213-239.

Grossman L. (1975) Petrology and mineral chemistry of Ca-rich inclusions in

the Allende meteorite. Geochim. Cosmochim. Acta 39, 433-454.

Grossman L. (1980) Refractory inclusions in the Allende meteorite. In Ann. Rev. Earth. Planet. Sci. 8, 559-608.

Grossman L. and Ganapathy R. (1976a) Trace elements in the Allende meteorite-I. Coarse-grained, Ca-rich inclusions. Geochim. Comsmochim. Acta 40, 331-344.

Grossman L. and Ganapathy R. (1976b) Trace elements in the Allende meteorite-II. Fine-grained, Ca-rich inclusions. Geochim. Cosmochim. Acta 40, 967-977.

Grutzeck M., Kreidelbaugh S. and Weill D. (1974) The distribution of Sr and REE between diopside and silicate liquid. Geophys. Res. Lett. 1, 273,275.

Harrison W.J. (1977) An experimental study of the partitioning of samarium between garnet and liquid at high pressures (Abstract). In Papers Presented to the International Conference on Experimental Trace Element Geochemistry. pp 41-42.

Hoffmann A.W. and Magaritz M. (1977) Diffusion of Ca, Sr, Ba and Co in a basalt melt: Implications for the geochemistry of the mantle. J. Geophys. Res. 82, 5432-5440.

Hohenberg C.M. (1969) Radioisotopes and the history of nucleosynthesis in the galaxy. Science 166, 212-215.

Hohenberg C.M. (1970) Xenon from the Angra dos Reis meteorite. Geochim. Cosmochim. Acta 34, 185-191.

Hohenberg C.M., Hudson B., Kennedy B.M. and Podosek (1981) Noble gas retention chronologies for the St. Severin meteorite. Geochim. Cosmochim. Acta (submitted).

Hohenberg C.M., Munk M.N. and Reynolds J.H. (1967) Spallation and fissiogenic xenon and krypton from stepwise heating of the Pasamonte

achondrite; the case for extinct plutonium 244 in meteorites; relative ages of chondrites and achondrites. J. Geophys. Res. 72, 3139-3177.

Holloway J.R. and Drake M.J. (1977) Quantitative microautoradiography by X-ray emission micro-analysis. Geochim. Cosmochim. Acta 41, 1395-1397.

Huebner J.S. (1971) Buffering techniques for hydrostatic systems at elevated pressures. In Research Techniques for High Pressure and High Temperature (ed. G.C. Ulmer), pp 123-177. Springer-Verlag, New York.

Huebner J.S., Ross M. and Hickling N. (1975) Significance of exsolved pyroxenes from lunar breccia 77215. Proc. Lunar Sci. Conf. 6th, Geochim. Cosmochim. Acta Suppl. 6, V. 1, 529-546.

Hyde E.K. (1962) A Revised Version of a Review of Nuclear Fission, Part One - Fission Phenomena at Low Energy. UCRL-9036-Rev. University of California, Berkeley.

Hytönen K. and Yoder H.S. (1961) The plane enstatite-anorthite-diopside and its relation to basalts. Carnegie Inst. of Wash. Yearbook 60, 125-141.

Irving A.J. (1978) A review of experimental studies of crystal/liquid trace element partitioning. Geochim. Cosmochim. Acta 42, 743-770.

Jacobson S.B. and Wasserburg G.J. (1980) Sm-Nd isotopic evolution of chondrites. Earth Planet. Sci. Lett. 50, 139-155.

Jones J.H. and Burnett D.S. (1979) The distribution of U and Pu in the St. Severin chondrite. Geochim. Cosmochim. Acta 43, 1895-1905.

Jones J.H., Benjamin T.M., Heuser R. and Burnett D.S. (1980) Meteoritic actinide chemistry: Laboratory partitioning studies (Abstract). In Lunar and Planetary Science XI. pp 514-516. Lunar and Plane-

tary Institute, Houston.

Katz L. and Penfold A.S. (1952) Range-energy relations for electrons and the determination of beta-ray end-point energies by absorption. Rev. Mod. Phys. 24, 28-44.

Kelly W.R. and Wasserburg G.J. (1978) Evidence for the existence of ^{107}Pd in the early solar system. Geophys. Res. Lett. 5, 1079-1082.

Lee T., Papanastassiou D.A. and Wasserburg G.J. (1977) Aluminum-26 in the early solar system: Fossil or fuel? Ap. J. 211, L107-L110.

Lewis R.S. (1975) Rare gases in separated whitlockite from the St. Severin chondrite: Xenon and krypton from fission of extinct ^{244}Pu. Geochim. Cosmochim. Acta 39, 417-432.

Lindstrom D.J. and Weill D.F. (1978) Partitioning of transition metals between diopside and coexisting silicate liquids-I. nickel, cobalt and manganese. Geochim. Cosmochim. Acta 42, 817-832.

Lugmair G.W., Marti K., Kurtz J.P. and Scheinin N.B. (1976) History and genesis of lunar troctolite 76535 or: How old is old? Proc. Lunar Sci. Conf. 7th., Geochim. Cosmochim. Acta Suppl. 7, V. 2, 2009-2033.

Lugmair G.W. and Marti K. (1977) Sm-Nd-Pu timepieces in the Angra dos Reis meteorite. Earth Planet. Sci. Lett. 35, 273-284.

Ma M.-S., Murali A.V. and Schmitt R.A. (1977) Genesis of the Angra dos Reis and other achondritic meteorites. Earth Planet. Sci. Lett. 35, 331-346.

Manhes G., Minster J.F. and Allegre C.J. (1978) Comparative uranium-thorium-lead and rubidium-strontium study of the St. Severin amphoterite: Consequences for early solar system chronology. Earth Planet. Sci. Lett. 39, 14-24.

Marti K., Lugmair G.W. and Scheinin N.B. (1977) Sm-Nd-Pu systematics in the

early solar system (Abstract). In Lunar Science VIII, pp 619-621. The Lunar Science Institute, Houston.

Marti K., Shedlovsky J.D., Lindstrom R.M., Arnold J.R. and Bhandari N.G. (1969) Cosmic ray produced radionuclides and rare gases near the surface of the St. Severin meteorite. In Meteorite Research (ed. P. Millman), pp 246-266. Springer-Verlag, New York.

Marvin U.B., Wood J.A. and Dickey J.S., Jr. (1970) Ca-Al-rich phases in the Allende meteorite. Earth Planet. Sci. Lett. 7, 346-350.

Mason B. and Graham A.L. (1970) Minor and trace elements in meteoritic minerals. Smithson. Cont. Earth Sci. 3, 1-17.

Mason B. and Martin P.M. (1974) Geochemical differences among components of the Allende meteorite. Smithson. Cont. Earth Sci. 19, 84-95.

Masuda A., Nakamura N. and Tanaka T. (1973) Fine structures of mutally normalized rare-earth patterns of chondrites. Geochim. Cosmochim. Acta 37, 239-248.

McCallister R.H., Brady J.B. and Mysen B.O. (1979) Self-diffusion of Ca in diopside. Carnegie Inst. Wash. Yearbook 78, 574-577.

McKay G.A. (1977) Crystal/liquid equilibration in trace element partitioning experiments (Abstract). In Papers Submitted to the International Conference on Experimental Trace Element Geochemistry, pp.81-82.

Morgan J.W. (1971) Uranium (92). In Handbook of Elemental Abundances in Meteorites (B. Mason, ed.), Gordon and Breach Science Publishers, New York. pp. 529-548.

Morgan J.W. and Lovering J.F. (1973) Uranium and thorium in achondrites. Geochim. Cosmochim. Acta 37, 1697-1707.

Mueller R.F. and Saxena S.K. (1977) Chemical Petrology. Springer-Verlag, New York.

Myers J. and Gunter W.D. (1979) Measurement of the oxygen fugacity of the cobalt-cobalt oxide buffer assemblage. Am. Min. 64, 224-228.

Mysen B.O. (1977) Experimental determination of cerium, samarium and thulium partitioning between hydrous liquid, garnet peridotite minerals and pargasite. Carnegie Inst. Wash. Yearbk. 76, 588-594.

Mysen B.O., Ryerson F.J. and Virgo D. (1981) The structural role of phosphorus in silicate melts. Submitted to Am. Min.

Mysen B.O. and Seitz M.G. (1975) Trace element partitioning determined by beta-track mapping--an experimental study using carbon and samarium as examples. J. Geophys. Res. 80, 2627-2635.

Nagasawa H., Blanchard D.P., Jeffrey W.J., Brannon J.C., Philpotts J.A. and Onuma N. (1977) Trace element distribution in mineral separates of the Allende inclusions and their genetic implications. Geochim. Cosmochim. Acta 41, 1587-1600.

Nagasawa H., Schreiber H.D. and Blanchard D.P. (1976) Partition coefficients of REE and Sc in perovskite, melilite and spinel and their implications for Allende inclusions(Abstract). In Lunar Science VII pp. 588-590. The Lunar Science Institute, Houston.

Nakamura N. (1974) Determination of REE, Ba, Fe, Mg, Na and K in carbonaceous and ordinary chondrites. Geochim. Cosmochim. Acta 38, 757-775.

Nelms A.T. (1956) Energy loss and range of electrons and positrons. National Bureau of Standards Circular 577. U.S. Government Printing Office, Washington, D.C.

Nicholls I.A. and Harris K.L. (1980) Experimental rare earth element partition cofficients for garnet, clinopyroxene and amphibole coexisting with andesitic and basaltic liquids. Geochim. Cosmochim. Acta 44, 287-308.

Northcliffe L.C. and Schilling R.F. (1970) Range and stopping-power tables for heavy ions. Nuclear Data Tables A7, 233-463.

Papanastassiou D.A. and Wasserburg G.J. (1969) Initial strontium isotopic abundances and the resolution of small time differences in the formation of planetary objects. Earth Planet. Sci. Lett. 5, 361-376.

Pepin R.O. and Phinney D. (1981) Components of xenon in the solar system. To appear in: The Moon and Planets.

Podosek F.A. (1970a) The abundance of ^{244}Pu in the early solar system. Earth Planet. Sci. Lett. 8, 183-187.

Podosek F.A. (1970b) Dating of meteorites by the high temperature release of ^{129}Xe. Geochim. Cosmochim. Acta 34, 341-365.

Podosek F.A. (1972) Gas retention chronology of Petersburg and other meteorites. Geochim. Cosmochim. Acta 36, 755-772.

Podosek F.A. and Lewis R.S. (1972) ^{129}I and ^{244}Pu abundances in white inclusions of the Allende meteorite. Earth Planet. Sci. Lett. 15, 101-109.

Powell M.A., Walker D., Grove T.L. and Hays J.F. (1980) Cation diffusion in basaltic melts: measurements from crystal-liquid boundary layers in controlled cooling experiments (Abstract). G.S.A. Abstracts with Programs, 502.

Prinz M., Keil K., Hlava P.F., Berkley J.L., Gomes C.B. and Curvello W.S. (1977) Studies of Brazilian meteorites III. Origin and history of the Angra dos Reis achondrite. Earth Planet. Sci. Lett. 35, 317-330.

Reynolds M.A., Rao M.N., Meason J.L. and Kuroda P.K. (1969) Fissiogenic and radiogenic xenon in the chondrites Beardsley and Holbrook. J. Geophys. Res. 74, 2711-2716.

Robie R.A., Hemingway B.S. and Fisher J.R.(1978) Thermodynamic properties

of minerals and related substances at 298.15 K and 1 bar (10^5 Pascals) pressure and at higher temperatures. Geological Survey Bulletin 1452. U.S. Government Printing Office, Washington, D.C.

Rowe M.W. and Kuroda P.K. (1965) Fissiogenic xenon from the Pasamonte achondrite. J. Geophys. Res. 70, 709-714.

Ryerson F.J. and Hess P.C. (1978) Implications of liquid-liquid distribution cofficients to mineral-liquid partitioning. Geochim. Cosmochim. Acta 42, 921-932.

Sanz H.G. and Wasserburg G.J. (1969) Determination of an internal ^{87}Rb-^{87}Sr isochron for the Olivenza chondrite. Earth Planet. Sci. Lett. 6, 335-345.

Schnetzler C.C. and Philpotts J.A. (1969) Genesis of the calcium-rich achondrites in light of rare-earth and barium concentrations. In Meteorite Research (ed., P. Millman), pp. 206-216. Springer-Verlag, New York.

Schnetzler C.C. and Philpotts J.A. (1970) Partition coefficients of rare-earth elements between igneous matrix material and rock-forming mineral phenocrysts-II. Geochim. Cosmochim. Acta 34, 331-340.

Schramm D.N. and Wasserburg G.J. (1970) Nucleochronologies and the mean age of the elements. Ap. J. 162, 57-69.

Shannnon R.D. (1976) Revised effective ionic radii and systematic studies of interatomic distances in halides and chalcogenides. Acta Cryst. A32, 751-767.

Stapanian M.I. (1980) Induced fission track measurements of carbonaceous chondrite Th/U ratios and Th/U microdistributions in Allende inclusions Ph. D. thesis, California Institute of Technology, Pasadena.

Stolper E.M. (1977) Experimental petrology of eucritic meteorites. Geochim. Cosmochim. Acta 41, 587-611.

Tanaka T. and Nishizawa O. (1975) Partitioning of REE, Ba and Sr between crystal and liquid phases for a natural silicate system at 20kb pressure. Geochem. J. 9, 161-166.

Tatsumoto M., Knight R.J. and Allegre C.J. (1973) Time differences in the formation of meteorites as determined from the ratio of lead-207 and lead-206. Science 180, 1279-1283.

Tatsumoto M., Unruh D.M. and Desborough G.A. (1976) U-Th-Pb and Rb-Sr systematics of Allende and U-Th-Pb systematics of Orgueil. Geochim. Cosmochim. Acta 40, 617-634.

Trivedi B.M.P. (1977) A new approach to nucleocosmochronology. Ap. J. 215, 877-884.

Unruh D.M., Nakamura N. and Tatsumoto M. (1977) History of the Pasamonte achondrite: Relative susceptibility of the Sm-Nd, Rb-Sr, and U-Pb systems to metamorphic events. Earth Planet. Sci. Lett. 37, 1-12.

Wasserburg G.J., Huneke J.C. and Burnett D.S.(1969a) Correlation between fission tracks and fission type xenon in meteoritic whitlockite. J. Geophys. Res. 74, 4221-4232.

Wasserburg G.J., MacDonald G.J.F., Hoyle F. and Fowler W.A. (1964) Relative contributions of uranium, thorium and potassium to heat production in the earth. Science 143, 465-467.

Wasserburg G.J., Schramm D.N. and Huneke J.C. (1969b) Nuclear chronologies for the galaxy. Ap. J. 157, L91-L96.

Wasserburg G.J., Tera F., Papanastassiou D.A. and Huneke J.C. (1977) Isotopic and chemical investigations on Angra dos Reis. Earth Planet. Sci. Lett. 35, 294-316.

Zaikowski A. (1980) I-Xe dating of Allende inclusions: Antiquity and fine structure. Earth Planet. Sci. Lett. 47, 211-222.

APPENDIX I

Quantitative Radiography Using Ag X-rays

John H. Jones and Donald S. Burnett

Division of Geological and Planetary Sciences
California Institute of Technology
Pasadena, CA 91125

To appear in: Nuclear Instruments and Methods

Caltech Contribution Number 3488

ABSTRACT

We have used an electron microprobe or scanning electron microscope to analyze the Ag produced by exposure of Ilford nuclear emulsions to ^{151}Sm beta particles. The low beam currents of the SEM yielded satisfactory results while the higher current density of the microprobe produced variable amounts of volatilization. Nonlinearities in Ag counting rate vs. exposure time curves were found at both high and low Ag concentrations. Two different types (mechanisms?) of emulsion fading were observed, one operating on a hour, the other on a day, time scale. The low-Ag nonlinearities are perhaps explained by either dose-dependent short time scale fading or by the requirement of multiple hits to render some AgBr grains developable.

INTRODUCTION

Dosimetry measurements of ionizing radiation requiring high resolution (1-10μ) are important for both the physical and biological sciences. Accurate measurements of relative concentrations of radioactive tracers are often needed in diffusion studies[1], biological experiments using ^{14}C or ^{3}H labeled compounds[2], and trace element studies of geological systems[3]. Based on the original work of Holloway and Drake[4] and Benjamin et al.[5], we have systematically investigated the quantitative aspects of measuring Ag concentrations in nuclear emulsions exposed to radioactivity using a scanning electron microscope (SEM) or an electron microprobe. Such instruments are widely available. The Ag-L x-rays are produced by a highly focussed electron beam and detected by a Si(Li) semiconductor detector. The counting rates are proportional to the amount of developed Ag in surface layers of the nuclear emulsion which, in turn, is approximately proportional to radiation dose, within a limited range of exposure. This technique is an alternative to optical micro-densitometry. The techniques reported here were developed to measure partition coefficients (D) of an element, e. g., Sm, between mineral crystals and the silicate liquids from which they were grown. These partition coefficients will be used later to illustrate our results and are defined as:

$$Sm_D = \frac{\text{concentration of Sm in crystal}}{\text{concentration of Sm in liquid}}$$

EXPERIMENTAL

The sources we have studied are thick samples of synthetic silicate glasses and minerals, typically containing about 50 ppm ^{151}Sm ($T_{1/2}$=93y, Emax=76 Kev), a nearly pure β-emitter (one 20 Kev gamma per hundred betas). The silicate materials, mm in total size, are encapsulated in epoxy and polished to yield a flat surface for exposure. Ilford K5 and L4 emulsion plates (usually 25 microns thickness) were developed typically for seven minutes in Ilford ID-19 developer with constant agitation. Room temperature was monitored during exposure and development, but was not strictly controlled. Temperatures ranged from 21°C to 26°C over a several month period, but with the range during an exposure being less than 1°C. Since we are only interested in relative measurements on a given emulsion plate, this temperature variability is thought to be acceptable. Typical exposure times were 5-10 hrs. Relative humidity was not controlled but has been monitored during our more recent exposures.

The analyses were made with either the electron microprobe or the SEM. Both systems have solid-state Si(Li) detectors with associated multichannel analyzers. All microprobe (MAC-5-SA3) analyses were made with a regulated electron beam current (5nA sample current on brass). The current remained stable to within 1%. Beam sizes used were 20-40μ. Our SEM (ISI Super II) does not have a beam regulation mode, but we find that the beam becomes stable after ~2 hr. warm-up time. The typical current used is 0.15nA on brass. After warm-up, the beam is stable to $1x10^{-3}$nA over several hours. Measurements are done at about 2650X with a scanned area of 23x23 microns. All measurements on both the microprobe and SEM were made at 15 Kev accelerating voltage. 15

Kev corresponds to a 3μ penetration depth which seemed a reasonable choice in light of the low energy of the ^{151}Sm beta and the shrinkage and collapse of the emulsion after developing, which can reduce the emulsion thickness as much as 60%. All emulsion plates were carbon coated to assure electrical conduction. For day-to-day and inter-sample counting rate comparisons, we calculate all counting rates for an exposed emulsion as a fraction of the counting rate measured from Ag metal[5]. This method of expressing counting rates should facilitate interlaboratory comparison of data.

BACKGROUND CORRECTION

Figure 1 shows a representative x-ray spectrum for an exposed emulsion. With our detector resolution (about 160 eV, FWHM) the Ag Lα and Lβ lines are only partially resolved. Other x-ray lines result from inorganic contaminants in the emulsion and by secondary fluorescence from the glass which serves as the emulsion substrate.

In the normal working range of 1-10% Ag metal counting rate, bremsstrahlung from the organics of the developed emulsion contributes significantly (~10%) to the counts in the Ag L x-ray region. Thus, a detector with an energy window centered about the Ag L peaks (2.8-3.2 Kev) would accumulate x-rays from three distinct sources: (1) Ag line x-rays, (2) bremsstrahlung from the organics of the emulsion and (3) bremsstrahlung from the Ag. The relative proportions of these components will vary with the Ag to gel ratio of the developed emulsion (i.e. the amount of exposure), but for the typical range of Ag concentrations the relative importance is in the order given. Figure 2 demonstrates the relative importance of the Ag and organic bremsstrahlung contributions for two energy intervals where the observed counting rate can be confidently ascribed to the continuous radiation. Increasing exposure to a ^{151}Sm source will increase the relative amounts of Ag to gel in the developed emulsion; thus it is not clear that the resulting variation of Ag counting rate with exposure time should be linear, although an approximately linear trend is observed (Figure 2). Nevertheless, the intercept in Figure 2 gives a maximum value to the contribution of organic bremsstrahlung and the increase in counting rate for any exposure time, relative to an exposed emulsion is a lower limit to the Ag bremsstrahlung contribution. The relative Ag to organic bremsstrahlung

contribution appears to increase with increasing energy; and we estimate that in the region of the Ag L line x-rays the contribution of Ag bremsstrahlung is about comparable to that of the organic constituents for our typical sample exposures.

Spectra taken on developed, but unexposed, low background emulsions show that the background spectrum in the region of the Ag L lines is relatively flat. However, because of the presence of Ca and, occasionally, K and Cl K x-ray lines, it is not possible to find a clear energy range near to the Ag L region to use for a reliable background subtraction. Background correction by simple subtraction of an off-sample (unexposed) area of the emulsion may not be accurate because of differing Ag/gel ratio and, hence, the organic bremsstrahlung contribution will differ from the exposed area of the emulsion. We have utilized a background subtraction procedure which, although approximate, appears to be sufficiently accurate for our purposes, but which is simpler than the use of least-squares spectral fitting routines. As illustrated in Figure 3, a spectral window of width 2Δ is selected such that some Ag L line counts are exluded. "Background" counts, C_b, are calculated:

$$C_b = \Delta \, (\overline{C}(E_l) + \overline{C}(E_u))$$

where E_l and E_u are the lower and upper energies of the spectral window and $\overline{C}$ is the average counts per channel of 3 channels centered about E_l and E_u. Graphically, C_b corresponds to the area illustrated in Figure 3. A "corrected" Ag count, C_{corr}, is calculated: $C_{corr} = C_m - C_b$, where C_m is the total measured number of counts within the window. This difference method throws away many counts that are due to Ag; however to the extent

that the shape of the total Ag x-ray spectrum (line + bremsstrahlung) is independent of peak height and that the organic bremsstrahlung contribution can be approximated as linear in the selected spectral window, the resultant C_{corr} is proportional to the Ag content of the emulsion. This same procedure may be used in unexposed areas of the emulsion to correct for background Ag. For our typical exposure conditions this correction is small.

As a test of this method, we have generated synthetic spectra by adding a Ag metal x-ray spectrum to an idealized background spectrum (linear with a negative slope with respect to energy) in various proportions. The synthetic spectra were then corrected for background using our standard technique. The resulting Ccorr scaled exactly with the proportion of the Ag metal component over a two order of magnitude range in Ag/background ratio.

Statistical Errors

Our typical exposures correspond to $C_{corr} \simeq 5$-10% Ag metal with $C_{corr}/C_b \sim 0.5$. Absolute counting rates are about 100 cps for the 34 channel window. With typical counting times of 100-300 sec, the expected error in C_{corr}, based on equation (1) due to background correction is about 3-4% (standard deviation).

However, a larger source of statistical error arises because the Ag analyzed is not a uniform surface layer but, instead, is clumped into discrete tracks. Thus, the measured point-to-point variance of the Ag counting rate for a set of analyses will not depend on the duration of the analysis, (i.e., on the total number of counts per point analyzed). If a minimum number of counts are accumulated, the variance will depend instead on Ag counting rate, which is approximately propor-

tional to the number of beta particles/cm^2 that interacted with the emulsion during its exposure. For example, if an emulsion is exposed to a beta fluence of $1.6 \times 10^6/cm^2$ and areas of $(25\mu)^2$ are analyzed, each of these analyses will be made on ~10 beta tracks. Thus, a point to point precision of 30% should be expected, almost independent of the total number of counts per point, even if other sources of error could be reduced to zero. Figure 4 shows the relation between exposure time and the percentage standard deviation (σ) of sets of five replicate analyses. Error bars of the percent σ were calculated[6]:

$$(\text{Error})^2 = \frac{\sigma^2}{2(N-1)}$$

where N is the number of replicate analyses (5). The data are in reasonable agreement with a $(1/\tau)^{1/2}$ relationship -- as is expected since

$$(\%\sigma)^2 = (\sigma_R/R)^2 = \frac{1}{M} = \frac{1}{K\tau} ,$$

where M is the number of particles that registered in the area analyzed and K is a constant. In theory, empirical curves like Figure 4 could be used to provide <u>a priori</u> estimates of the expected precision for any exposure. A complication is that we have observed a total spread of a factor of two in the Ag counting rates of different emulsion plates which were exposed and developed for the same amount of time, although exposures on the same plate appear to be reproducible. However, because of the $(1/\tau)^{1/2}$ dependence, a factor of two in the total range would still yield error estimates accurate to ±20%, which should be precise enough to indicate other sources of variability (e.g. variability in the distribution of radioactivity in the source, chemical or physical

developing of the emulsion, etc.). The data plotted in Figure 4 correspond to an effective beta track production rate of roughly $4x10^6$/ cm^2-hr-ppm ^{151}Sm. This is an effective number because it only has significance for the calculation of the variability of the Ag counting rate (proportional to track density) and to the area analyzed. In these terms the data of Figure 4 correspond to (% σ) $\cong 400/(RA)^{1/2}$ where R is the counting rate expressed as a percentage of Ag metal and A is the beam area in $(microns)^2$. Replicate analyses of the same emulsion on different days have shown agreement well within these errors. Comparison of the above track production rates with optical microscope counts is difficult because of the low energy of the ^{151}Sm betas; however, optical counts indicate a track production rate about ten times higher than the $4x10^6$ value given above. The exact origin of this difference is unknown, but, at least in part, reflects a tendency to count grains developed from a single beta as separate tracks.

Electron Beam Damage

Figure 5 shows the effects of repetitive counting on a single spot on the emulsion using the SEM. It is always possible to observe a "burn" mark on the emulsion following our analysis and for the L-type emulsion, a definite pit is observed, even for the low current density of the SEM. For this reason analysis with a K-type emulsion seems preferrable. However, as shown in Figure 5, the actual effects on the Ag counting rate, due to volatilization of the organic constituent, are not large, a maximum of ~0.5% per min for the total counting rate of the L-type emulsions and even this vanishes, as expected when the background subtraction is made. Repetitive 15 second counts on the same spot using the microprobe also showed no variation.

As a further test, a series of exposures of the same source on a K5 emulsion (5 min - 3 hr) were analyzed on both the microprobe and SEM. The background corrected counts were normalized to the Ag metal counting rate of each instrument. Ideally, the Ag metal-normalized counting rate for each instrument should be the same, or at least the ratio of the Ag-normalized counting rates should be constant, independent of exposure time. Figure 6 shows that in actuality the SEM/microprobe counting rate ratio increases from 0.43 to 0.66 with increasing exposure. These results suggest that the microprobe volatilizes organic material, essentially instantaneously (much less than 15 seconds), concentrating the Ag in a residue, which gives an anomalously high counting rate. The approach to unity with increasing exposure (fig. 6) presumably reflects the ability of the Ag to conduct away heat, thereby minimizing volatilization of organic material. The cores of the pits left by the microprobe beam were anlayzed with the SEM and normalized to a second

analysis on nearby virgin emulsion. Counting rate ratios, (pit core)/(virgin emulsion), were 0.67 and 0.81 for the 10 min and 1 hour exposures, respectively, qualitatively supporting the above interpretation.

Dependence of Ag counting rate on exposure time

Figure 7 shows the dependence of Ag counting rate for exposures of different areas on a single emulsion plate to the same ^{151}Sm source for varying lengths of time. The response curve shows deviations from linearity at both high and low doses, although, in the 1-2 hour exposure time range (10-20% Ag metal), the measured counting rates are proportional to exposure time. The deviations from linearity at long exposure times are expected because of depletion of Ag in the emulsion. The deviations from linearity at short exposure times are not easily explained. The short-time deviations shown in Figure 7 are not large (3-4 standard deviations); but qualitatively similar deviations have been consistently observed in three series of exposures. The magnitudes of the low exposure deviations appear to vary with different emulsion slides, and in some cases, within errors, a completely linear response is found. The deviations cannot be correlated with exposure or developing conditions such as temperature and humidity. Because our uncorrected counting rates also show low exposure non-linearity, it does not appear possible to ascribe the deviations in C_{corr} shown on Figure 4 to errors in our background correction procedures.

It may be possible to eliminate the effect by using a stronger source. A weaker source (11 ppm as opposed to the normal 177 ppm ^{151}Sm) shows the low-Ag nonlinearities in two out of three exposures, but linear behavior was observed with a 1000 ppm ^{151}Sm source exposed to two emulsions.

It appears possible to minimize the nonlinearity by using longer development times. Two series of exposures (on 2 different plates) showed no low-Ag nonlinearities when developed for 11 minutes instead of our standard 7 minutes, although a single set of exposures with a weak (11 ppm) source, also developed for 11 minutes, showed nonlinear response. In general, therefore, the use of strong sources (~20 mCi/g) and longer development may give more linear responses, although more documentation would be required.

Latent Image Fading

We have observed two types (mechanisms?) of fading in Ilford K5; 25μ emulsions: (a) long term fading - time scale on the order of days and (b) short term fading - time scale on the order of hours. (a) Figure 8 shows a series of 12 hour exposures made with an 11 ppm ^{151}Sm standard on a single emulsion plate. The observed fading rate is 6%/day, although the exact rate probably varies from plate to plate. (b) Figure 9 shows the results of two series of 15 minute exposures, each series on a single plate, using a 177 ppm ^{151}Sm source. The short exposure-development time differences for both series indicates a fading rate of ~14%/hr. Figure 9 shows that this fading mechanism becomes unimportant within 2 hours of exposure, presumably either because a population of AgBr grains which are susceptible to rapid fading becomes depleted or because a fading agent (oxidant?) becomes exhausted.

Figure 11 suggests (with much scatter) that there may be a correlation between the percentage of fading and the amount of exposure. If fading was more important for lower exposure, this would provide a means of understanding the nonlinearities in the dependence of Ag

counting rate on time (Fig. 7).

A similar nonlinear response to what we have observed is well known for low energy photons, and can be understood in terms of the necessity for "multiple hits" to produce a developable grain[7]. Conceivably, a similar multiple hit requirement is required by our observations. However, the correlation suggested by Figure 10 is difficult to understand simply in terms of multiple hits. What seems to be required is a relatively small population of grains that have a high probability of being rendered developable and are depleted by relatively low doses (≤10% Ag) compared to the more stable grains, but this population is required to also be more prone to fading. Perhaps the outermost surface layer of the AgBr grains would have these properties, and it may be that the observed fading and nonlinear response that we have observed is accentuated by the use of infinitely thick sources which maximize the relative number of low energy electrons.

Applications

As indicated in the Introduction, we are utilizing the beta radiography technique described in previous sections to measure the relative amounts of ^{151}Sm in synthetic minerals compared to the silicate melts from which they were grown.

Overall we have obtained relatively consistent crystal-liquid partition coefficients (D), as long as we stay with one emulsion type. However, we have seen consistent differences between K and L type emulsions. For example, for ^{151}Sm partitioning between the silicate mineral clinopyroxene and the quenched liquid, K emulsions consistently give us D = 0.35±.02, whereas measurements on the same crystal with L type emulsions give D = 0.45-0.50. The values obtained with K

emulsions seem preferable because the L emulsions are observed to be more easily damaged by the electron beam and, because of the smaller AgBr grain size, should be more susceptible to latent image fading[8].

Figure 12 shows a point by point display of our ^{Sm}D(cpx) data with a horizontal row of points representing independent analyses of a given ^{151}Sm-bearing clinopyroxene crystal. The data points in a given row represent both different areas on the same crystal or the same area on different emulsion slides. No systematic differences can be seen in either case. Results for different synthesis runs are also distinguished. The predicted standard deviation for the distribution of individual analyses, calculated by methods described above, is shown above the figure. The observed spread matches well with the calculated standard deviation, indicating that the observed spread is due to counting statistics and that we have obtained a relatively precise D value of 0.35±0.02 (error of mean).

D values have been measured in two different ways: A) directly, in a single exposure, by measuring the ratio of the Ag counting rate on the portion of the emulsion exposed to a crystal to the counting rate of a portion exposed to the glass, and B) indirectly, by making two exposures on a single slide, adjusting the time so that the Ag counting for the crystal was about equal to that for the glass in the other exposure. For method A) we have simply calculated D values as the ratio of the background corrected counting rates for the crystal and glass without trying to correct for the type of nonlinear response indicated by Figure 8. However, most of our exposures have resulted in Ag counting rate near the linear region of Figure 8. For method B) a D value is calculated as the ratio of the measured counting rates

divided by exposure time for the crystal and glass. Method B) has the advantage that even if the emulsion response to varying radiation dose is nonlinear, e.g. as shown in Figure 7, correct D values are obtained if the exposure times are adjusted to give the same Ag counting rate and if the relationship between Ag counting rate and dose (^{151}Sm concentration times exposure time for our samples) is independent of source strength. Table 1 shows that consistent values are obtained for both methods. This gives us confidence that our measured D values are reliable.

Our results may also have application to investigators who optically count β tracks. Because of the low number of tracks/cm^2 required for optical counting (≤1% Ag metal counting rate), exposures must of necessity be in the Ag content range where we observe nonlinearities, and these effects may need to be considered for quantitative measurement. This is especially true for thin emulsions (<30μ) such as ours where fading effects (based on track counting) have already been demonstrated[8].

References

[1] A.W. Hofmann and M. Magaritz, J. Geophys. Res. 82 (1977) 5432-5440.

[2] A.W. Rogers, Techniques of Autoradiography, 2nd ed. (Elsevier, 1973).

[3] B.O. Mysen and M.G. Seitz, J. Geophys. Res. 80 (1975) 2627-2635.

[4] J.R. Holloway and M.J. Drake, Geochim. Cosmochim. Acta 41 (1977) 1395-1397.

[5] T.M. Benjamin, N.T. Arnt and J.R. Holloway, Carnegie Inst. Wash. Yearbook 76 (1977) 658-660.

[6] A. Hald, Statistical Theory With Engineering Applications (John Wiley and Sons, New York, 1952) 299-300.

[7] R.C. Valentine, in Advances in Optical and Electron Microscopy, R. Barer and V.E. Cosslett, eds. (Academic Press, New York) 180-203.

[8] G. Leide, Arkiv Fysik 22 (1962) 147-173.

Table 1

Comparison of 1-Exposure (a) and 2-Exposure (b) Methods

Sample		Sm_D 2-Exposure	Sm_D 1-Exposure
Clinopyroxene #1	(a)	0.425±0.021	0.425±0.005
Clinopyroxene #2	(a)	0.437±0.045	0.425±0.040
Clinopyroxene #3	(b)	0.365±0.050	0.353±0.035

(a) L4;25μ emulsion

(b) K5;25μ emulsion

Figure Captions

Figure 1

X-ray spectrum of an Ilford K5;25μ emulsion. The three large peaks are Si K, S K and Ag L (X-rays from left to right). The two small peaks at low and high energy are Br L and Ca K X-rays respectively. Note the approximate linearity of the bremsstrahlung continuum in the Ag L region, even though it is not linear overall. This spectrum is atypical in that the Si peak is much larger than normal. See Figure 3 for a more detailed representation of the Ag peaks.

Figure 2

(a) Bremsstrahlung in the 2.52-2.59 Kev region as a function of exposure time. Note approximate linearity at short exposure times and saturation at long exposure times. Intercept value at $\tau=0$ gives contribution from organics; values at other times reflect the contribution of Ag bremsstrahlung.

(b) Same as (a) but for the 1.88-2.06 Kev region. The same dependence on Ag is shown, but the initial slope is 2-3 times steeper, even though the percentage contribution of the Ag is smaller in this region.

Figure 3

Detailed blowup of the Ag L line region. The window A B spans the energies E_l to E_u, where $E_u - E_l = 2\Delta$. The background subtraction C_b is made by averaging the counts in the windows C D and E F which are centered about E_l and E_u. Average counts for these two windows are shown as I and I'. Counts above the line I I' are retained and correspond to C_{corr} (see text).

Figure 4

Variation of percent standard deviation as a function of exposure time. Each point represents the stndard deviation of five analyses. Error bars are assigned following Hald[6] (see text). Dashed line is constrained to pass through the 15 minute point. The points show a reasonable fit to the $(1/\tau)^{1/2}$ dependence as expected (see text).

Figure 5

Effect of electron beam damage on Ilford L4 and K5 emulsions. Top of figure shows uncorrected data from replicate analyses of the same spot on an L4 emulsion, illustrating volatile loss. Center of figure shows same data after background correction; no change in Ag content with time is seen. Bottom of figure shows uncorrected K5 data (notice change of scale) which show little or no change, even after 20 minutes. All points represent 200 sec. counts. Note suppressed zero.

Figure 6

Analyses of a series of exposures for different times on a single K5; 25μ emulsion with a ^{151}Sm standard (177 ppm) were made using both the electron microprobe and the SEM. The data from each instrument were normalized to that instrument's Ag metal count rate. The SEM and microprobe data were then ratioed. Instead of showing a flat pattern the SEM/microprobe ratios show a regular increase with exposure time. This presumably reflects volatilization of organics and concentration of Ag by the microprobe, which has a factor of 40 higher current density.

Figure 7

Ag concentration as a function of exposure time on a single emulsion. Data are expressed as percentages of Ag metal counting rate. The data show approximate linearity at short exposure times but with some deviation (see inset; see text) for the very shortest exposures. As was seen in Figure 2, the data saturate at long exposure times, following the expected $[1-\exp(-\lambda \tau)]$ relationship. Errors are standard deviations of five analyses.

Figure 8

Ag counting rate of a series of 12 hour exposures of ^{151}Sm standard (11 ppm) (made on the same emulsion) as a function of delay between exposure and development. Points are plotted at the midpoint of the exposure time internal. "Day" exposures ranged from 9:00 A.M. to 9:00 P.M. while for "night" exposures the reverse was true. Observed slope corresponds to a fading of 6%/day.

Figure 9

Ag content of 15 minute exposures of ^{151}Sm standard (177 ppm) on two K5;25μ emulsions plotted vs. time lapsed between exposure and development. x's and o's delineate the two series of exposures. After ~1 hour of fading the Ag content has dropped by ~14% and remains essentially constant, even after 11 hours. Error bars are errors of the mean (1σ).

Figure 10

Percent fading between two exposures on the same emulsion vs. percent Ag in the unfaded exposure. One exposure was made and allowed to fade for $\geq$1.5 hr. A second identical exposure was made and the slide was then developed immediately. The data shown were taken on seven

different K5;25μ emulsions, using a strong (1000 ppm ^{151}Sm) source. Different symbols indicate different exposure times. The data are consistent with an inverse relation between percent fading and percent Ag.

Figure 11

Individual analyses of D_{Sm}(cpx) show a spread consistent with independently calculated error estimates (σ = 0.05, see text; σ mean = 0.02).

Figure 1

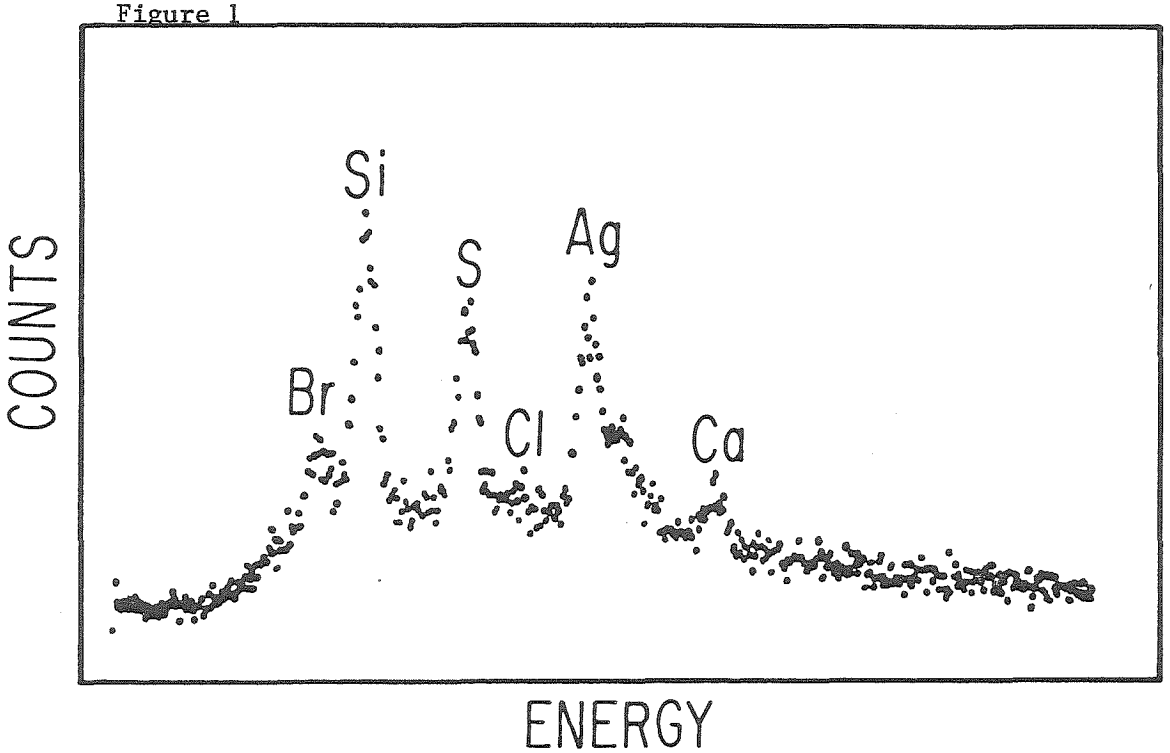

Figure 2

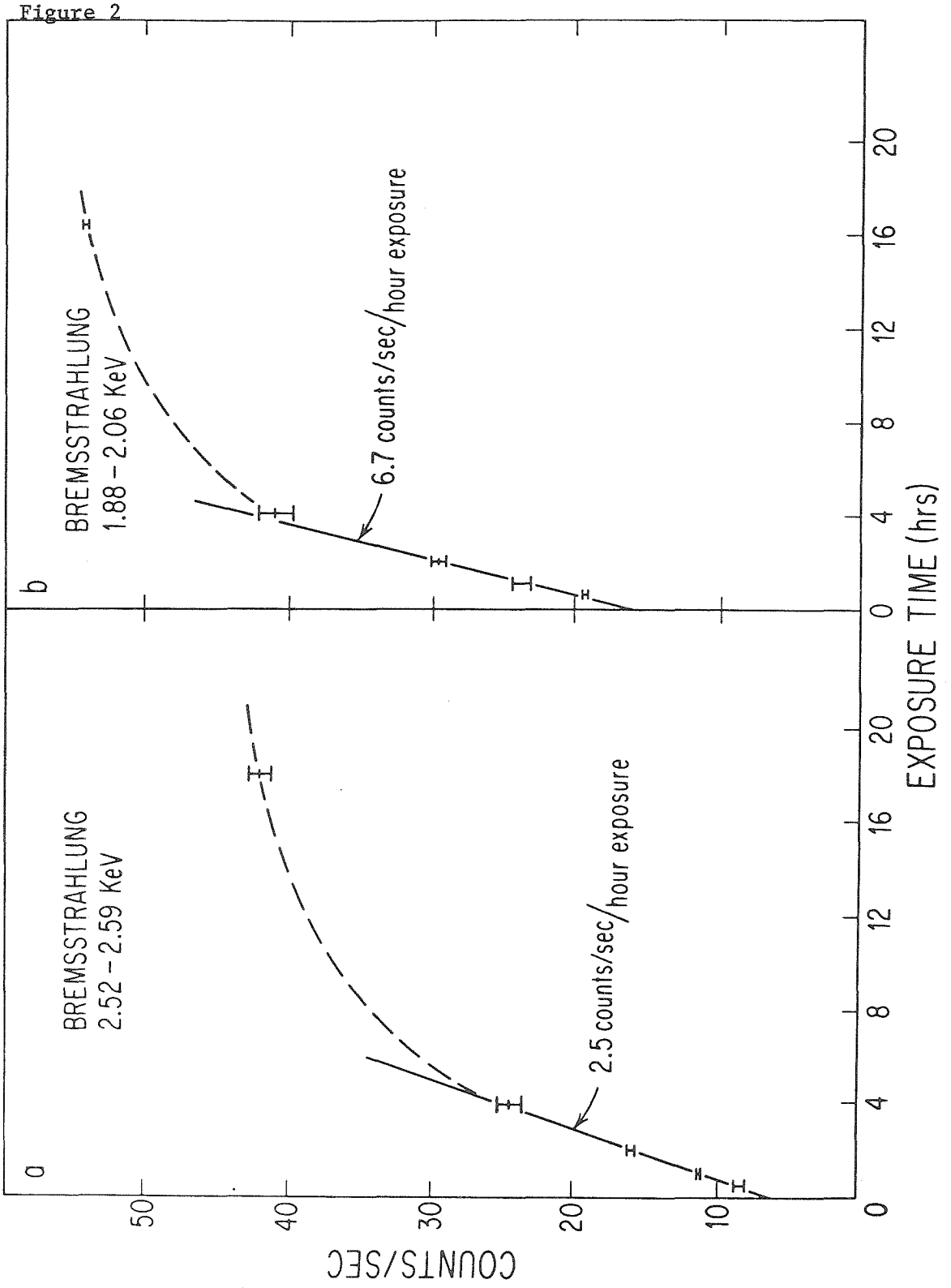
a
BREMSSTRAHLUNG
2.52 - 2.59 KeV
2.5 counts/sec/hour exposure
b
BREMSSTRAHLUNG
1.88 - 2.06 KeV
6.7 counts/sec/hour exposure
COUNTS/SEC
EXPOSURE TIME (hrs)
0
4
8
12
16
20
10
20
30
40
50

Figure 3

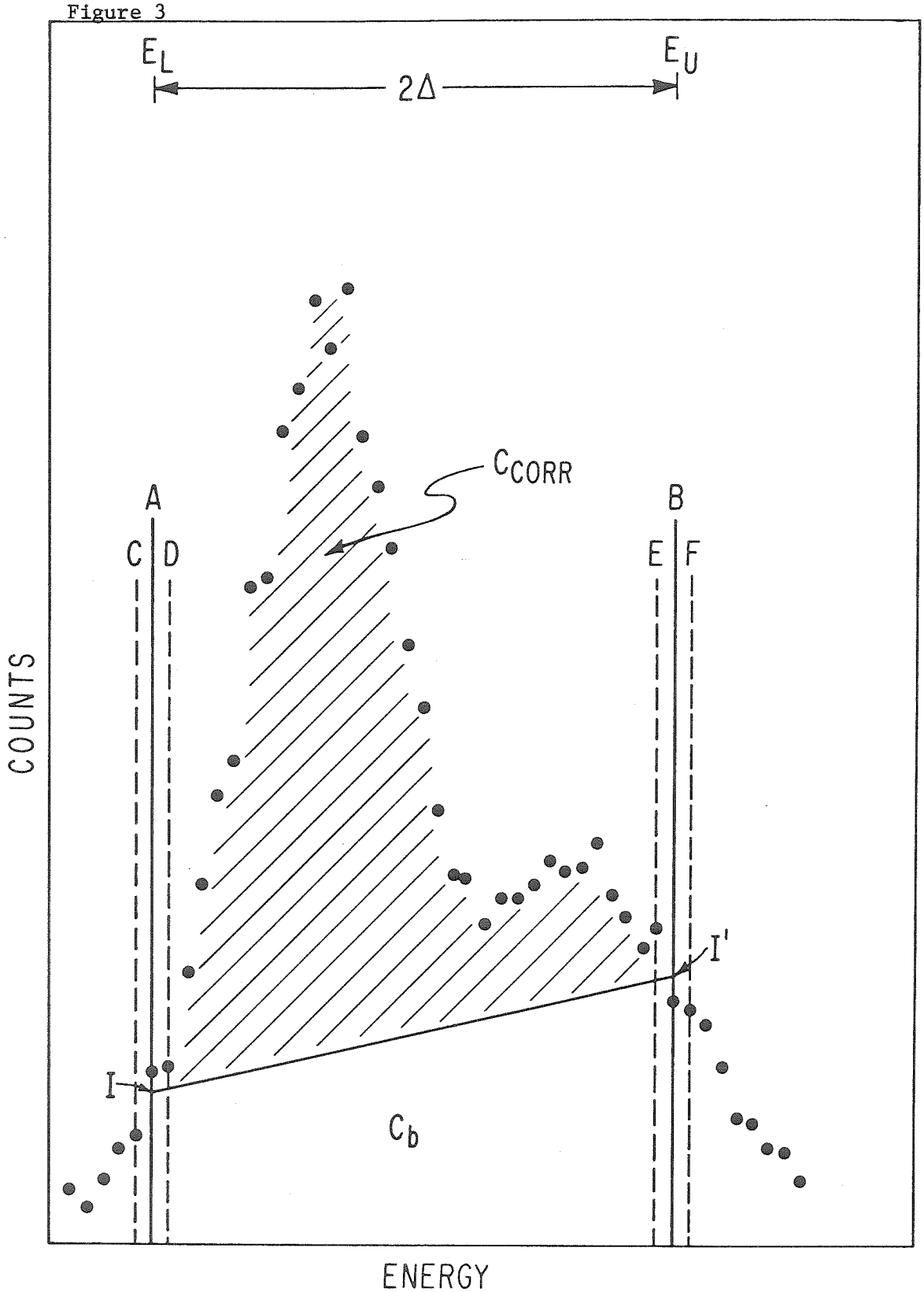

Figure 4

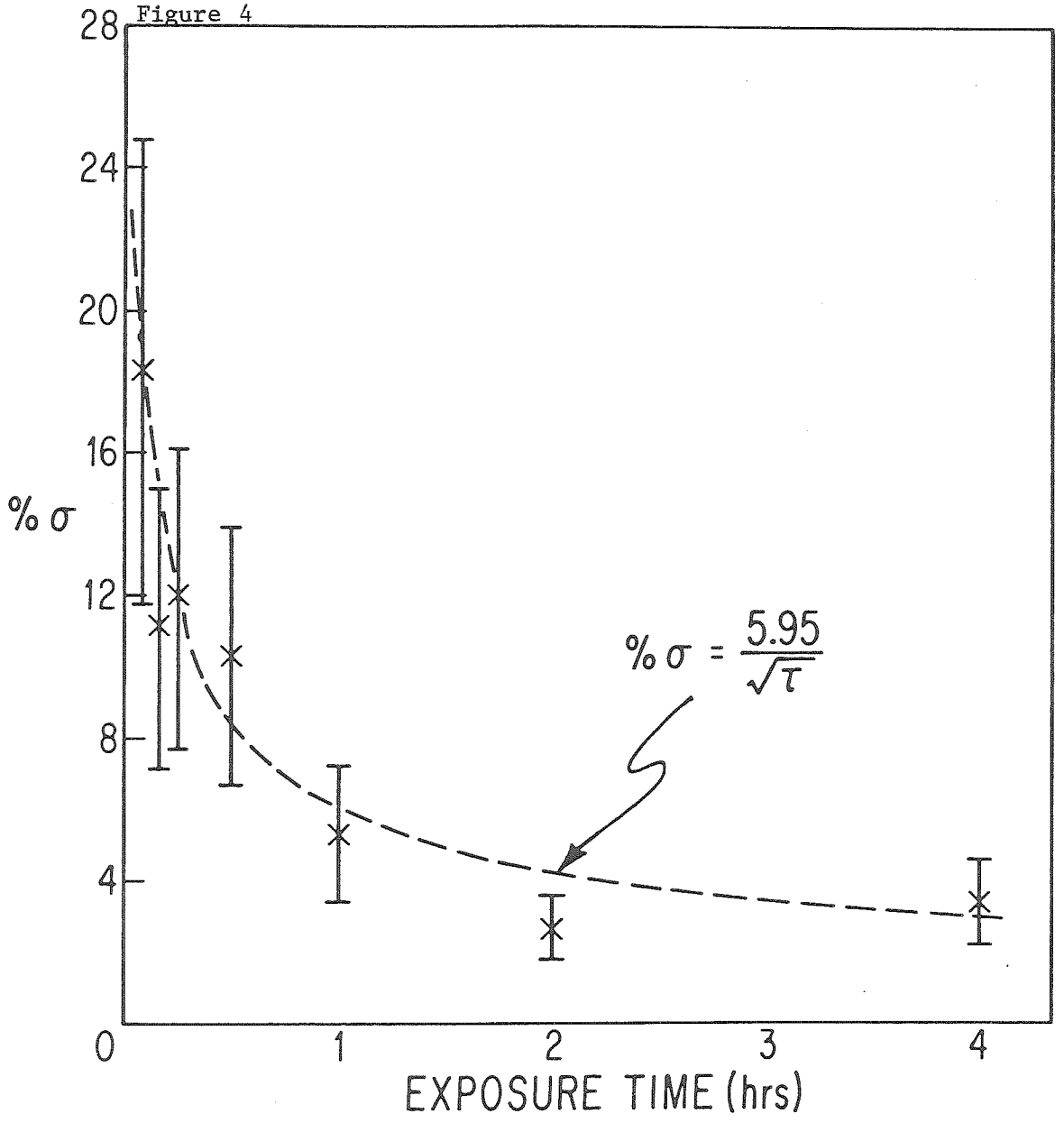

Figure 5

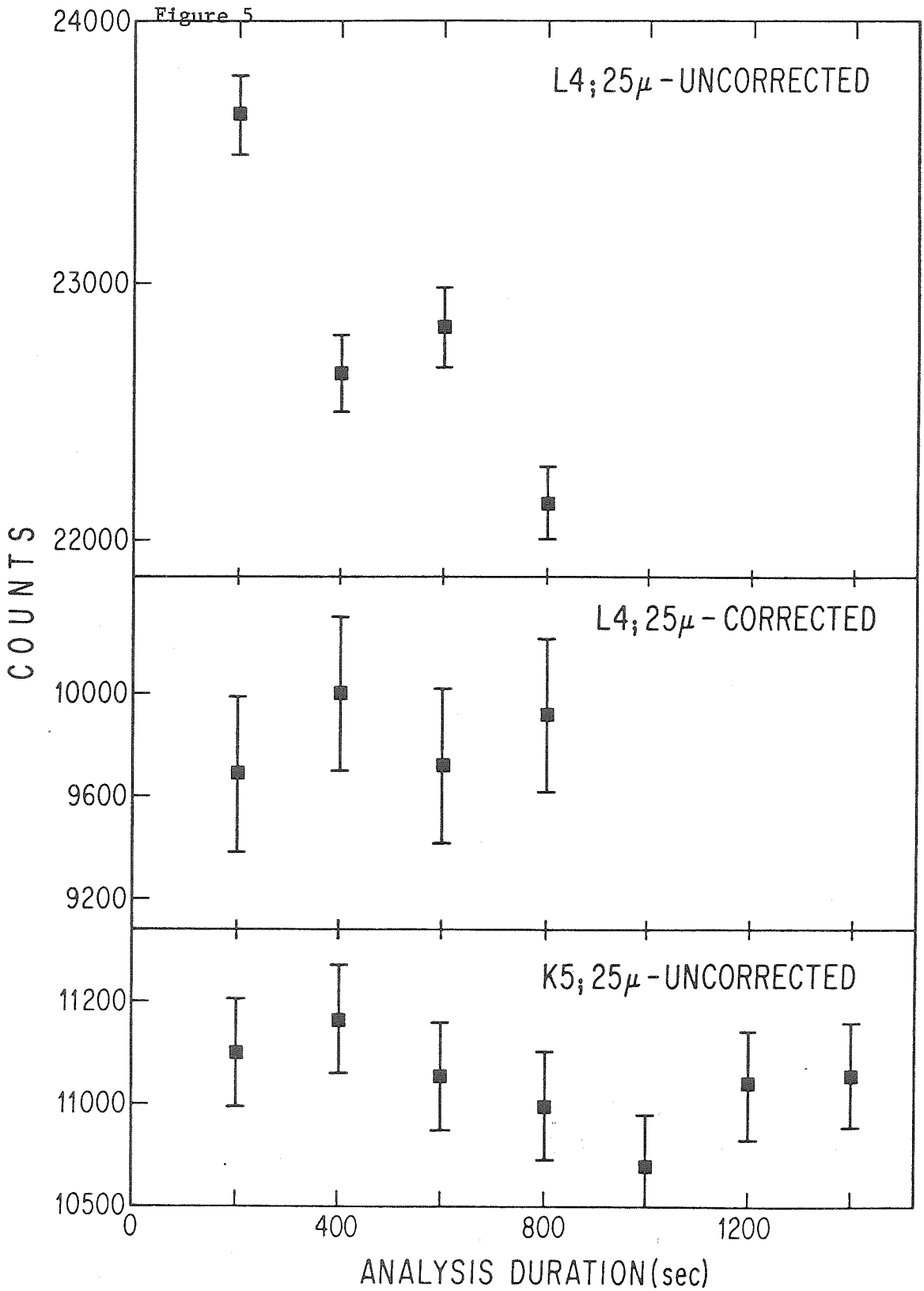
24000
23000
22000
L4; 25μ - UNCORRECTED
COUNTS
10000
9600
9200
L4; 25μ - CORRECTED
11200
11000
10500
K5; 25μ - UNCORRECTED
0
400
800
1200
ANALYSIS DURATION (sec)

Figure 6

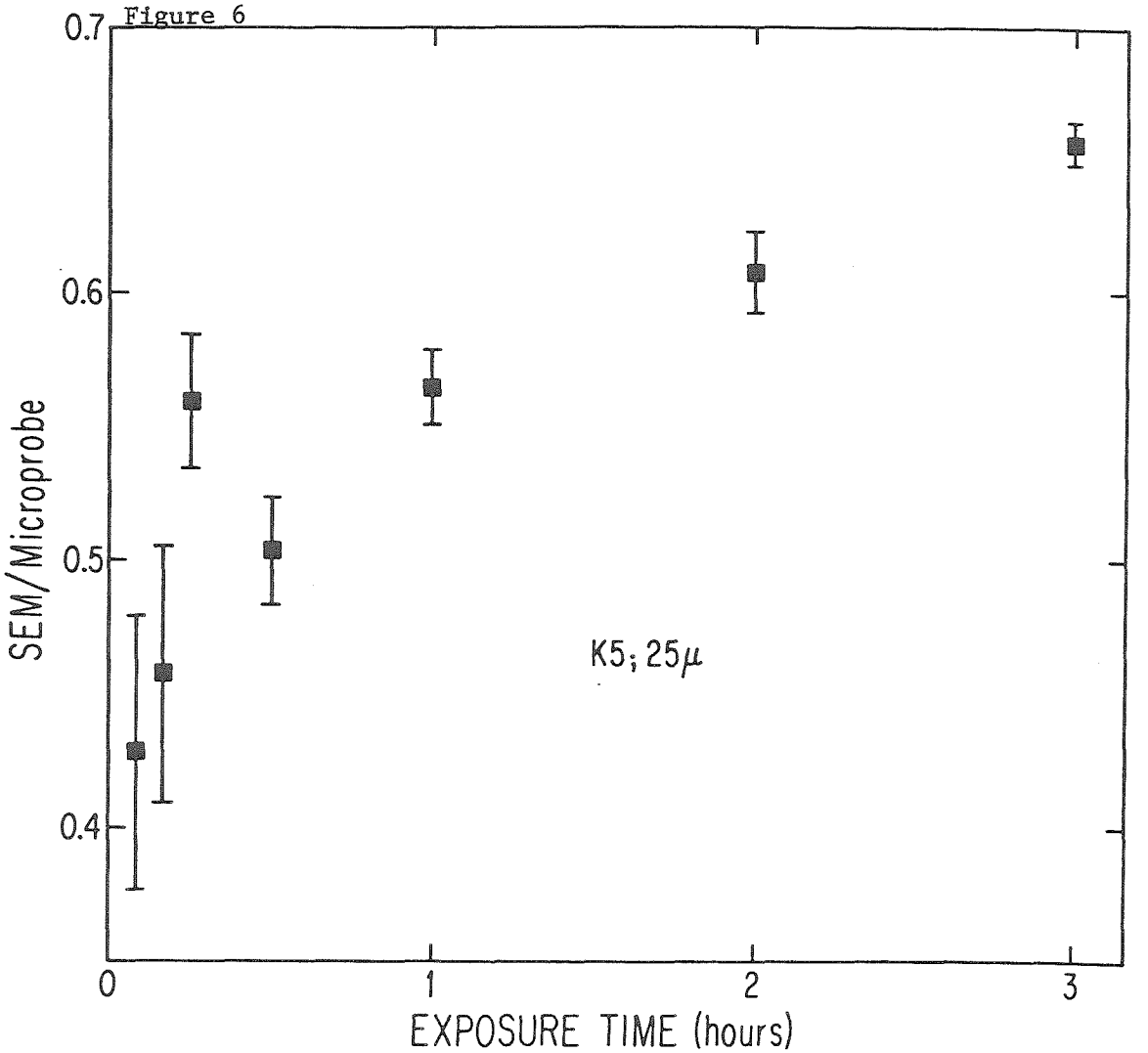

Figure 7

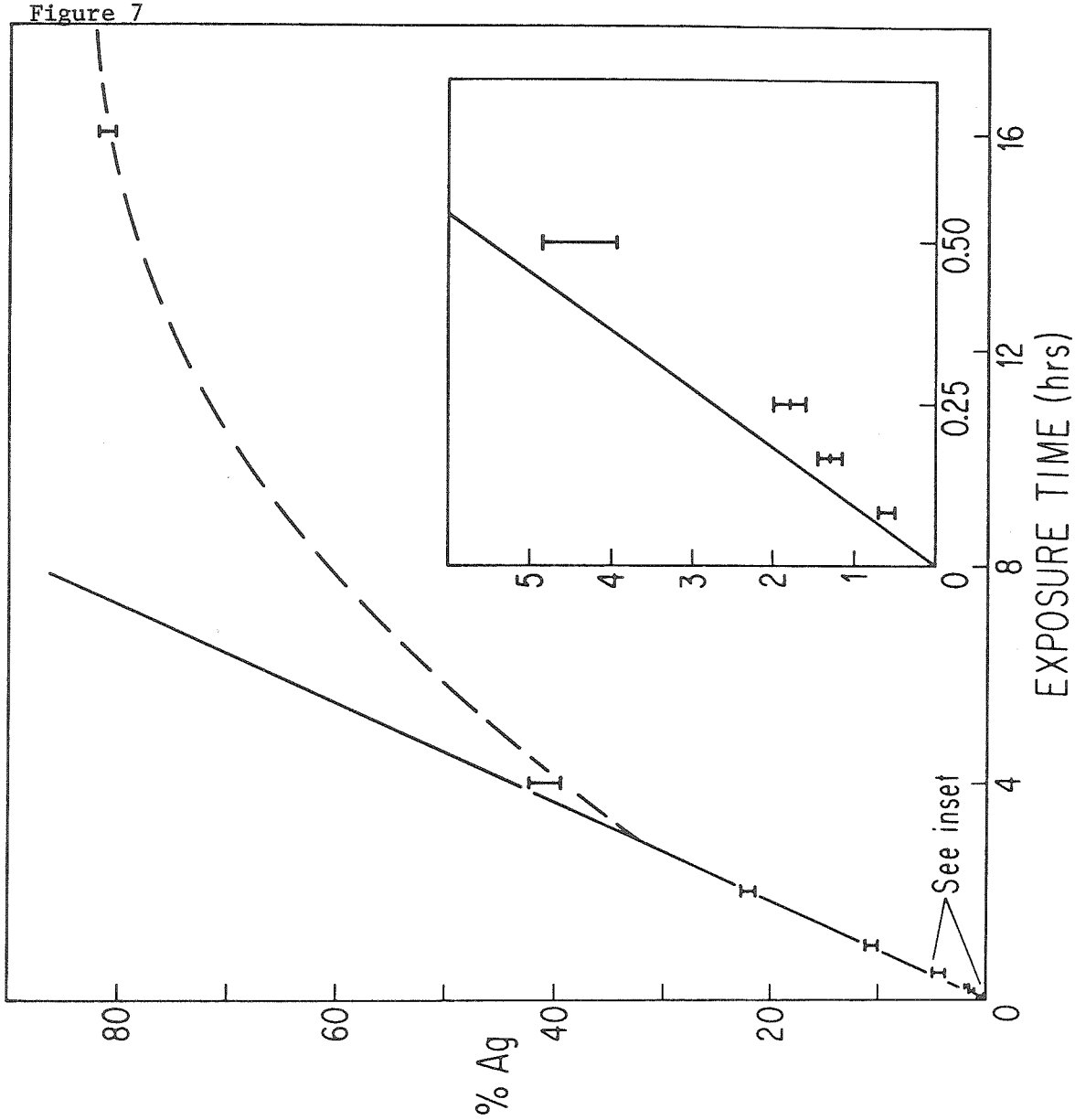
% Ag
0
20
40
60
80
0
4
8
12
16
EXPOSURE TIME (hrs)
See inset
0
0.25
0.50
1
2
3
4
5

Figure 8

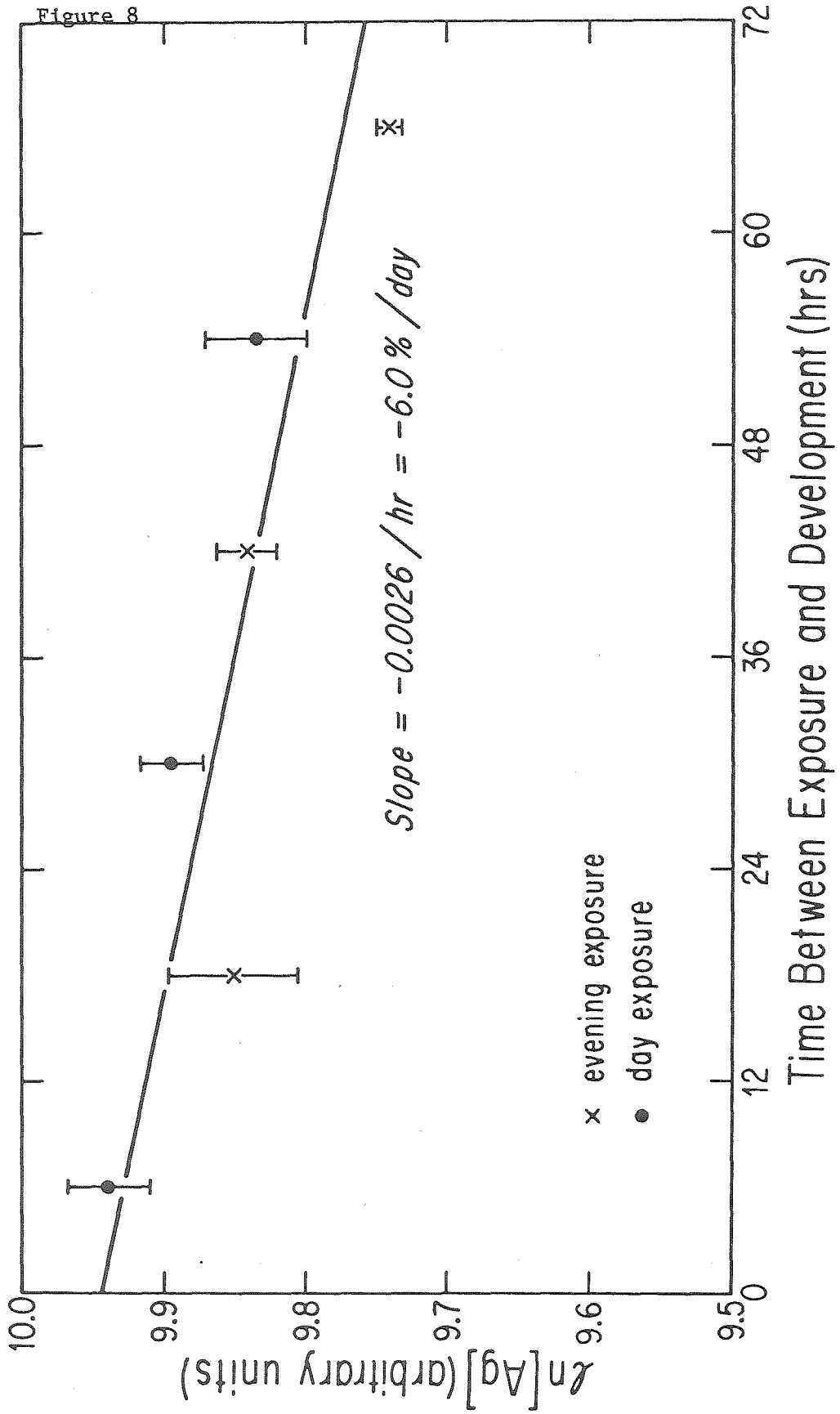
10.0
9.9
9.8
9.7
9.6
9.5
0
12
24
36
48
60
72
ℓn[Ag] (arbitrary units)
Time Between Exposure and Development (hrs)
Slope = -0.0026 / hr = -6.0 % / day
× evening exposure
• day exposure

Figure 9

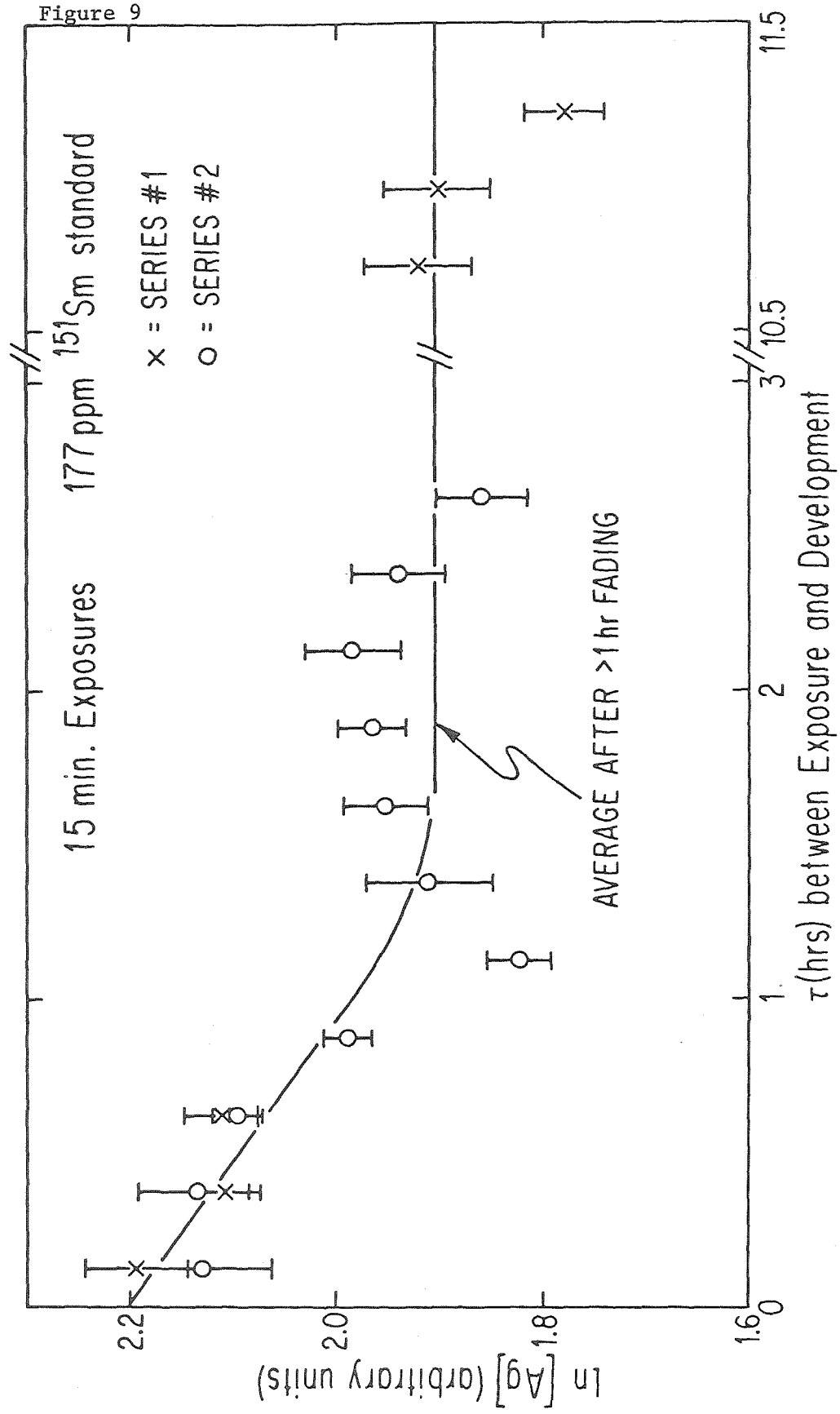
15 min. Exposures 177 ppm ^{151}Sm standard
x = SERIES #1
o = SERIES #2
AVERAGE AFTER >1 hr FADING
ln [Ag] (arbitrary units)
τ(hrs) between Exposure and Development
2.2
2.0
1.8
1.6
0
1
2
3
10.5
11.5

Figure 10

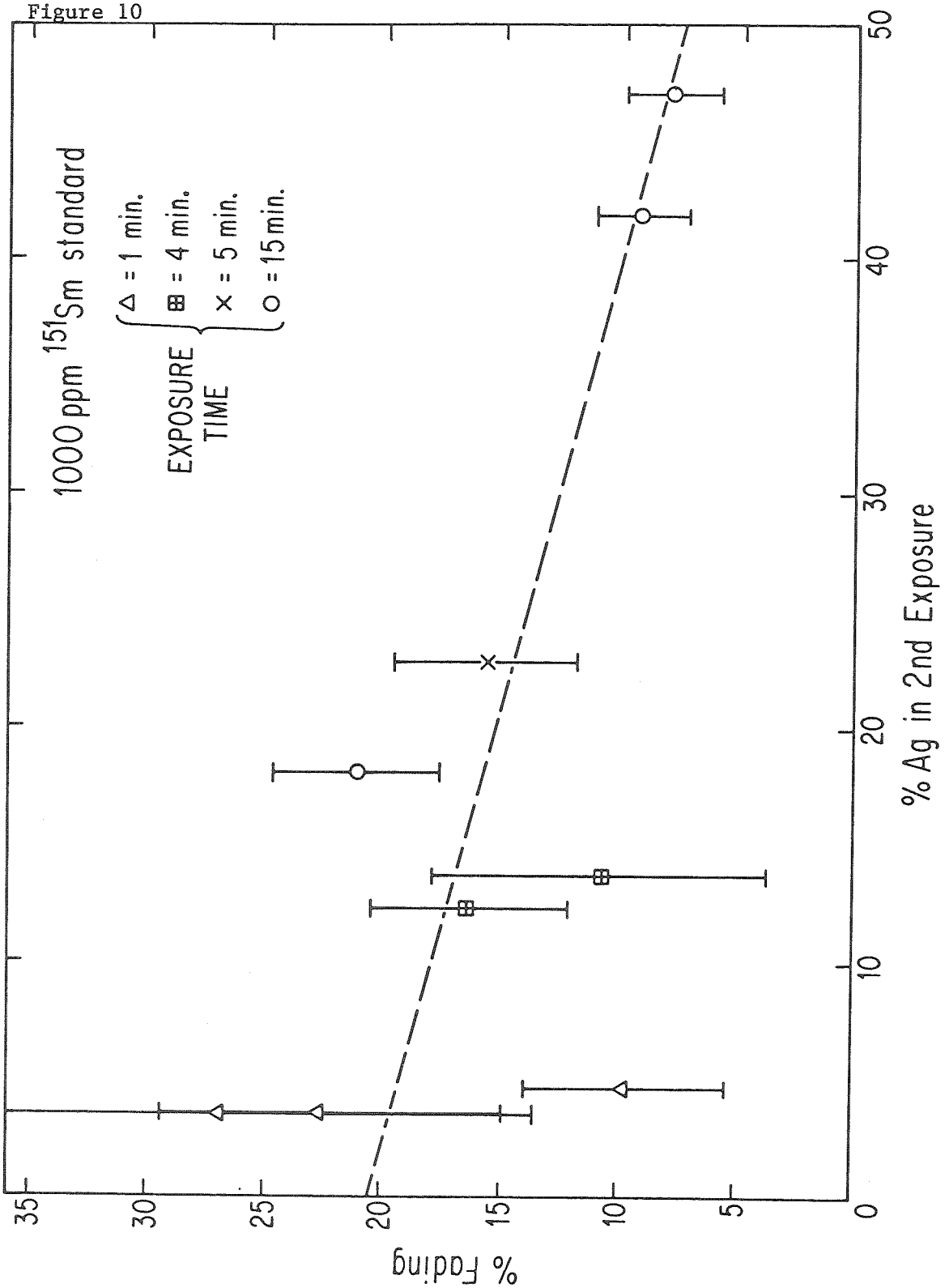
1000 ppm ^{151}Sm standard
EXPOSURE TIME
Δ = 1 min.
⊞ = 4 min.
× = 5 min.
○ = 15 min.
% Fading
% Ag in 2nd Exposure
0
5
10
15
20
25
30
35
10
20
30
40
50

Figure 11

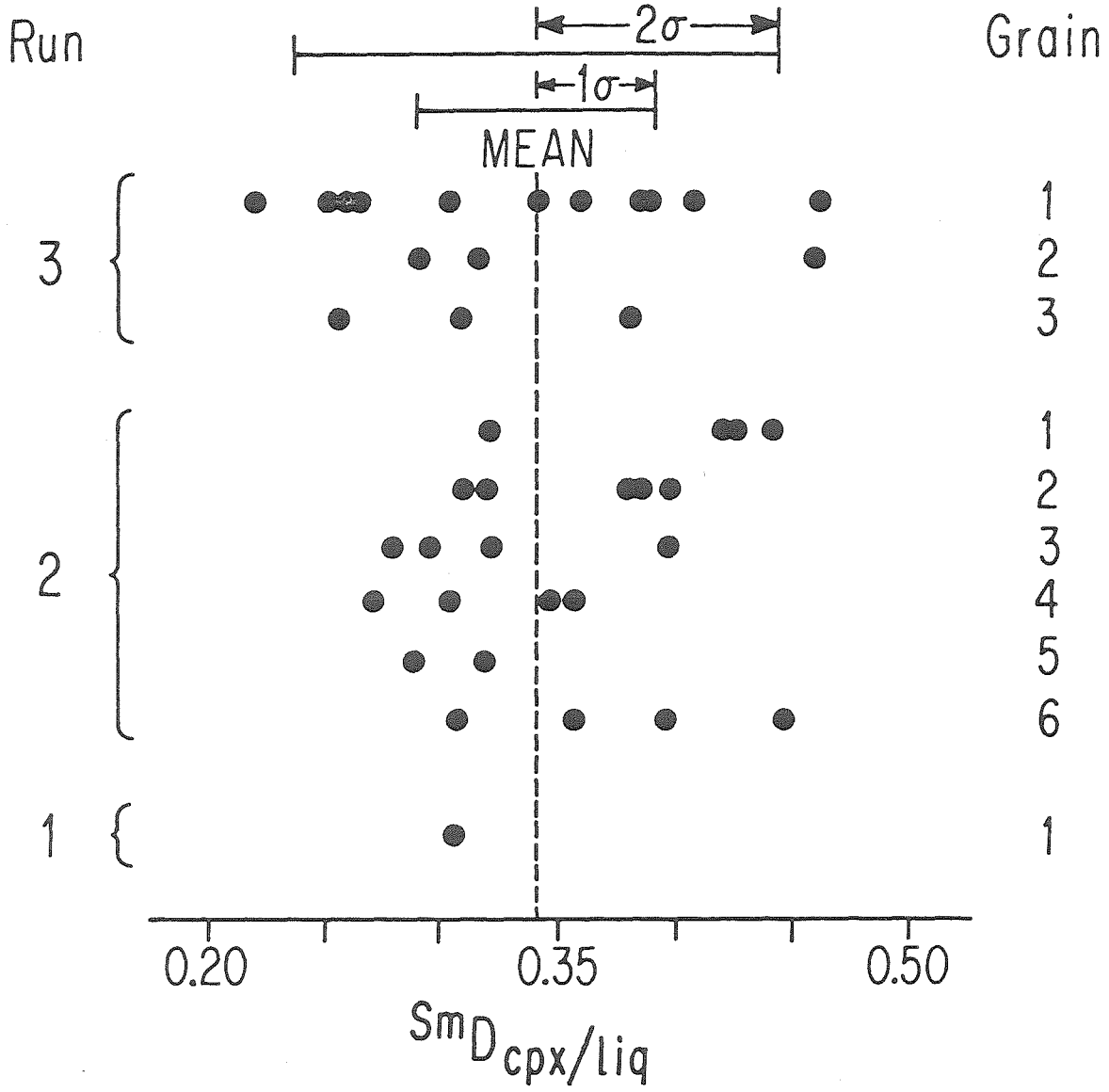

APPENDIX II

LABORATORY STUDIES OF ACTINIDE METAL-SILICATE FRACTIONATION

Proc. Lunar Planet. Sci. Conf. 11th (1980), p. 995–1001.
Printed in the United States of America

Laboratory studies of actinide metal-silicate fractionation

J. H. Jones and D. S. Burnett

Division of Geological and Planetary Sciences, California Institute of Technology, Pasadena, California 91125

Abstract—Actinide and Sm partition coefficients between silicate melt and several metallic phases have been measured. Under reducing conditions Si, Th, U and Pu can be reduced to metals from silicate melts and alloyed with a platinum-gold alloy ($Pt_{95}Au_5$). U and Pu enter a molten Pt-Si alloy with roughly equal affinity but U strongly partitions into the solid Pt. Th behaves qualitatively the same as Pu but is much less readily reduced than U, and Sm appears to remain unreduced. Experiments with Fe metal have shown that the partition coefficients of the actinides between Fe and silicate liquid are extremely low, suggesting a very low actinide concentration in planetary cores. Our experiments show that platinum metals can efficiently fractionate actinides and fractionate actinides from lanthanides and this process may be relevant to the condensation behavior of these elements from the solar nebula. Pt-metal grains in Allende Ca-Al-rich inclusions appear to be U-poor, although we predict that the sub-class of Zr-bearing Pt metals may have high U contents.

INTRODUCTION

The actinide elements have special importance because (a) they provide insight into the history of r-process nucleosynthesis in the galaxy, (b) they yield chronological information about events in our solar system, and (c) they act as heat sources for planets. It is our aim to understand the chemistries of the actinides in order to predict their behavior in solar system processes. As a part of this ongoing program, we have investigated the partitioning of the actinides into various metallic phases. The data which are presented here are meant to be indicative of actinide behavior rather than quantitative simulations of specific processes, nevertheless the data do provide new insights into actinide chemistry in natural systems.

Our previous studies of actinide and Sm partitioning between a silicate melt and diopsidic clinopyroxene or Ca-phosphate (Benjamin *et al.*, 1978; Benjamin, 1979; Benjamin *et al.*, 1980; Jones *et al.*, 1980) have documented the importance of redox conditions (see also Boynton, 1978a). Crystal-liquid partition coefficients for Pu and U show large (order of magnitude) increases with decreases in oxygen fugacity (from 0.2 to 10^{-9} atm), reflecting the formation of reduced species (Pu^{+3} and U^{+4}) at the expense of higher valence states (Pu^{+4}, U^{+5} and U^{+6}). Conversely Th and Sm partition coefficients do not change because these elements have only one stable valence state. Studies by Calas (1979) and Schreiber and Andrews (1980) indicate that U should be primarily tetravalent at $f_{O_2} = 10^{-9}$

atm; however, the presence of significant amounts of Pu^{+4} in our $f_{O_2} = 10^{-9}$ atm experiments could not be ruled out (see Benjamin *et al.*, 1978 for limits). Because meteorites and lunar rocks are believed to have formed under more reducing conditions, experiments at lower f_{O_2} were required before applications of our data (e.g., D_{Pu}/D_{Nd}) could be made. Experiments at lower f_{O_2} could also test for the presence of trivalent U (Boynton, 1978a) or divalent Pu (Benjamin, 1979).

EXPERIMENTS AND RESULTS

I. Actinide partitioning into Pt metal systems

Experiments were performed in graphite crucibles, sealed in evacuated SiO_2 glass, containing about 10 mg of actinide-spiked silicate glass powder (Di_2AnAb). Actinides and Sm were present in trace amounts (<50 ppm) and microanalyses were made by particle track radiography. We utilized our standard thermal history: 4–6 hours at 1280°C, slow cooling at 2–5°/hr. to grow crystals and quenching at 1200–1210°C (Benjamin *et al.*, 1978; Jones *et al.*, 1980). In contrast to our previous experiments using Co-CoO buffers and sealed Pt capsules, the experiments in graphite crucibles did not grow clinopyroxene crystals even though temperatures were 65° below the liquidus. It appears that the Pt played an important role as a site of crystal nucleation in our previous experiments. Consequently, we inserted a $Pt_{95}Au_5$ sheet as a floor to the graphite crucible to promote crystal growth and in many, but not all, subsequent experiments crystals were obtained. However, we were surprised to find that the Pt sheet was now spherical, as if molten, although the experiments were performed ~400° below the melting point of $Pt_{95}Au_5$. Metallographic examination and X-ray spectra showed the existence of two phases in the metal sphere: unreacted Pt metal grains embedded in a Pt-Si liquid (Si = 2.5 wt. %). Except for gold no other element was present at levels ≥0.1%. As noted previously by Chen and Presnall (1975), Si loss to Pt containers by reduction can occur at low f_{O_2} and the presence of Pt-Si-liquids in our experiments is reasonable given the low eutectic temperature (~800°C) in the Pt-Si binary metal system (Hansen, 1958).

The important result from these experiments is that we observe significant reduction of the actinide elements and alloying with the Pt metal phases. Qualitatively, we observe this for all three actinide elements but not for Sm.

Subsequent to our initial discovery of this effect, simpler metal-silicate liquid partitioning experiments were carried out by holding samples at 1280 ± 5°C for 12 hours, followed by rapid quenching. The results of such experiments, expressed as metal/silicate-liquid partition coefficients (D), are given in Table 1. Corrections have been applied to the observed actinide track densities for the difference in ranges between metal and silicate. The results given in Table 1 should be regarded as qualitative indicators of chemical behavior rather than quantitative measurements of partition coefficients because we probably have not completely attained equilibrium in these experiments. In particular the corroded edges of the Pt metal grains within the liquid Pt-Si metal are best interpreted as due to incomplete dissolution. Nevertheless, because of the lack of zoning in the

Pt-Si liquid, it should be possible to regard the partition coefficients in Table 1 as qualitative indicators of the *relative* ease of reduction/alloying for the different elements and phases investigated. This is particularly true for the element pairs (Pu-Sm and U-Th) which are measured in the same experiment. However, it is possible that our f_{O_2} might vary from experiment to experiment by up to an order of magnitude and in this case D should be very sensitive to f_{O_2}. Thus, it may only be possible to compare the order of magnitude of D between experiments (e.g., D_{Pu} and D_{Th} or D_U) even though the experimental conditions were nominally identical.

As shown in Table 1, Pu and U are partitioned into both the Pt metal and the Pt-Si liquid, however, to different degrees. Pu partitions preferentially into the Pt-Si liquid, whereas U partitions preferentially into the solid Pt metal. Relative to the silicate liquid, Pu and U are approximately equally partitioned into the Pt-Si liquid. There are no obvious actinide concentration gradients in the Pt-Si liquids; consequently, the D for Pt-Si, particularly the relative values, may represent equilibrium values. However the U in the Pt metal is highly zoned, increasing strongly towards the rims of the grains, demonstrating relatively slow diffusion of U in the Pt metal. In contrast Pu and Th show no obvious gradients in the Pt metal. The D_U for Pt is given as a lower limit because the high track density at the rim of the grains could not be quantitatively measured. Nevertheless, a large difference in the ability of U to partition into Pt metal compared to Pu and Th is clearly indicated. The effect of other noble metals (e.g., the 5% Au in our experiments) upon the actinide partitioning is not known and could change the magnitude of the D's somewhat relative to pure Pt. Although the partition coefficient for Th into PtSi is low and only an upper limit can be set for Pt, any reduction of Th is very remarkable in that the equilibrium f_{O_2} for Th-ThO_2 is about 10^{-33} (Benjamin, 1979). None of our samples show evidence of Sm reduction.

II. Actinide partitioning into Fe metal systems

Because of the reduction of actinides and alloying with Pt metal, and because of the possible role of the actinides as heat sources for planetary cores, we performed partitioning experiments between Fe liquid metals and silicate melts. Because of the success with Pt-Si liquid melts, and the presence of FeSi alloys in meteorites, we set out to investigate partitioning into Fe-Si liquids. Quench

Table 1. Metal/silicate partitioning.

	D (metal/silicate)			
Metal	Pu	U	Th	Sm
Pt	0.05	>1.5	$\leq 2 \times 10^{-3}$	≤0.02
Pt-Si	0.6	0.5	0.06	≤0.02
Fe-Si	$<2 \times 10^{-4}$	$<2 \times 10^{-3}$	—	≤0.02
Fe-C	$\leq 4 \times 10^{-4}$	$<1 \times 10^{-5}$	—	—

experiments from 1280°C were performed with shavings of high purity Fe and our spiked silicate glasses enclosed in graphite capsules and sealed in evacuated SiO_2 glass tubes. Rounded blobs of apparently molten Fe metal were obtained but, except for some Pt contamination in our U-spiked compositions, these contained no Si or other elements detectable with standard electron-induced X-ray techniques; however, analysis with an electron microprobe capable of light element analysis showed ~1 wt. % C (T. Bunch, pers. comm.). The Fe-C liquid contains small, more-reflective crystals of higher Fe content. It was possible to form FeSi liquid metals by removing graphite from the system and repeating the above experiments in an SiO_2 glass crucible in the presence of Ti metal. Microprobe analyses of the alloys formed indicated a Si content of 8.5–11% Si (T. Bunch, pers. comm.). These Fe liquid metal alloys contained no detectable Pu or U, and rather low upper limits on D values can be set, as shown in Table 1.

The oxygen fugacities for both the experiments containing graphite and Ti are not well known. At a total pressure of 1 atm and 1500° K the nominal C-CO-CO_2 and Ti-TiO_2 oxygen fugacities are $\sim 10^{-17}$ (French and Eugster, 1965) and $\sim 10^{-24}$ atm respectively. Although $f_{CO} \gg f_{CO_2}$ for our experiments, there is no direct control of f_{CO}. CO is produced from residual H_2O from our samples and containers and from residual O_2 from the forepump vacuum during the sealing of the silica glass tubes. Our starting materials have <0.01% H_2O by infrared spectroscopy and all materials are baked and dessicated prior to loading and the whole assembly flamed until the graphite glows red during the sealing process. Taking 0.01% H_2O from our starting materials gives a reasonable estimate of the maximum f_{CO} of 10^{-1} atm or f_{O_2} $\sim 10^{-19}$ atm. If no H_2O is present, then the residual vacuum O_2 in our samples would set a final f_{O_2} $\sim 10^{-25}$ atm. Thus, we estimate $f_{O_2} = 10^{-22\pm3}$ atm. In our experiments in the presence of Ti metal, the nominal oxygen fugacity of 10^{-24} atm was probably never reached, since the Si-SiO_2 buffer lies at a slightly higher fugacity ($\sim 10^{-22}$ atm) and we do observe some Si alloying with the Ti metal. If the activity coefficient of Si in Fe metal is $\sim 10^{-4}$ (Grossman *et al.*, 1979) the Si concentrations in our FeSi liquid indicate f_{O_2} $\sim 10^{-18}$ atm. Our oxygen fugacity estimate for the Ti-bearing experiments is thus $10^{-21\pm3}$ atm.

DISCUSSION

The basic observation is that Pu, U and Th can be reduced to metals and alloyed with Pt or Pt-Si liquid at comparatively high oxygen fugacities. At 1500° K Si^{+4}, Th^{+4}, U^{+4} and Pu^{+3} oxides are reduced to pure metals at oxygen fugacities of 5×10^{-23}, $\sim 10^{-33}$, 3×10^{-29} and 5×10^{-30} respectively; thus the activity coefficients of these elements in Pt solution must be very small. (For Th we calculate that the activity coefficient in metal must be $\sim 10^{-10}$ smaller than the activity coefficient in the silicate liquid).

In contrast, the Fe systems studied failed to take up significant actinides. Thus, the actinides were never reduced from the silicate melt, even at oxygen fugacities sufficiently low to reduce silicate to silicon. Th, U and Pu are known to form metallic compounds with Fe (Dwight, 1969); however, the activity coefficients must be much larger than for Pt metal solution.

Naturally-occurring Fe metals are U-poor. Reed and Turkevich (1955) found less than 0.5 ppb U in iron meteorites. The partitioning of U into Fe metal relative to Ca-phosphate is $<10^{-2}$ for the St. Severin LL6 chondrite (Jones and Burnett, 1979). More significantly, Stapanian *et al.* (1980) found essentially no U in the Si-rich metal of enstatite chondrites even though, for the very reducing conditions under which these objects formed, U deviates from its usual lithophile character and concentrates in CaS. It is probably also significant that of all the lithophile elements present in our experimental systems, including Sm, only Si and the actinides were reduced. However, unless pressure plays a very important role, the U partition coefficients for Fe metals in Table 1 are sufficiently low that significant actinide incorporation in planetary cores seems unlikely. Overall, Th is less easily reduced and, although data are not available, based on the Pt results it seems unlikely that Th would partition significantly into Fe metals, when U does not. Our data and that of Stapanian *et al.* (1980) indicate that if K is significantly incorporated into planetary cores, the relative chemical behavior of K and actinides must reverse from what is observed at low pressure. One can always appeal to hypothetical and, perhaps, untestable pressure effects but it should also be noted that there are alternative heat sources for planetary cores apart from dissolved radioactive elements [see for example, Ruff and Anderson (1980) and references cited].

The reduction and solution of the actinides into noble metals with the formation of intermetallic compounds, e.g., $PuPt_5$, has been studied (see, e.g., Keller and Erdmann, 1976). Indeed, this method, coupled with a subsequent high temperature sublimation of the actinide from the alloy, has become a standard technique for producing extremely pure transuranic metals. This has been termed "coupled reduction" since both a relatively low f_{O_2} and a noble metal (Pt, Ir, Pd, Rh) are necessary for reduction to occur, implying very low activity coefficients for the reduced metal in Pt solution. Similar lanthanide-noble metal intermetallic compounds are known, but we know of no reference to these having been synthesized by coupled reduction, in agreement with our observation of no Sm reduction.

Taken at face value our data show that, at the f_{O_2} and temperature of these experiments, both Pu and U are reduced and similarly partitioned into a Pt-Si liquid ($D \simeq 0.5$). However, U is strongly partitioned into solid Pt while Pu is strongly excluded. Some reduction of Th is observed but to a much lower degree than U or Pu. Thus, coupled reductions could efficiently fractionate U from the other actinides although more experiments would be necessary to work out the exact nature of these fractionations. If this is not due to the presence of Au, the preference for U could be a reflection of a stabilization of the Pt $5d^9$ shell by a delocalization of the lone U 6d electron (Brewer and Wengert, 1972). This is speculative, but similar arguments also predict lower partitioning of Th into Pt metal, assuming a ground state electron configuration of $7s^22p^2$ for Th metal.

Pt-rich complexes (Fremdlinge) and nuggets in Allende coarse-grained inclusions have been described and studied in some detail (Wark and Lovering, 1978; El Goresy *et al.*, 1978; Blander *et al.*, 1980); however, there is no question that many of these Pt metal grains are U-poor (<10 ppm by fission track analysis) relative to the average solar system U/Pt ratio (Wark, pers. comm., 1980). If

these Pt-rich phases represent condensates from the solar nebula, this lack of association may be difficult to understand. This U deficiency of Pt phases implies one of the following: (1) U was too volatile (Boynton, 1978a) to alloy with Pt, (2) U partitioned preferentially into a co-condensing phase, e.g., perovskite, (3) the redox conditions at the time of Pt-metal condensation were too oxidizing for U to alloy with Pt or (4) U did alloy with Pt but later, at a lower temperature or higher f_{O_2}, exsolved and redistributed, possibly into perovskite or into the Th-U-rich phases described by Wark and Lovering (1978). The solar nebula could have been reducing enough for U to be reduced and alloyed ($f_{O_2} \sim 10^{17}$ atm) (Larimer, 1968), although formation of some Ca-Al-rich inclusions, and especially the fremdlinge (El Goresy *et al.*, 1978), under relatively oxidizing conditions has been proposed (Boynton, 1978b; Grossman *et al.*, 1979).

Whether coupled reduction was an important process for most Allende Pt metal grains is uncertain, but it probably can explain the subclass of Zr-bearing fremdlinge reported by El Goresy *et al.* (1978). Grossman (1980) has emphasized the difficulty in understanding the formation of Zr metal given the high stability of ZrO_2. Brewer (1967) reports coupled reduction of ZrO_2 by H_2 in the presence of Pt, and Brewer and Wengert (1973) report the formation of very stable Zr-Pt intermetallic compounds and estimate dilute-solution Zr activity coefficients in Pt of $<10^{-12}$. We consider it highly likely that these Zr-rich Pt metal grains will also be rich in U. In general, actinide incorporation into Pt-metals must be considered as a possible source of actinide-lanthanide and intra-actinide fractionation. These are complications to both Pu-Nd and Pu-U-Th chronologies for Ca-Al-rich inclusions.

Acknowledgments—We wish to thank T. Benjamin, W. Boynton, L. Brewer, E. Stolper and D. Wark for discussions and T. Bunch and A. Chodos for analyses. Lou Ann Cordell Lexitroned our manuscript. This is Caltech Contribution No. 3444. This research was supported by NASA Grant NSG-7202.

REFERENCES

Benjamin T. M. (1979) Experimental actinide element partitioning between whitlockite, apatite, diopsidic pyroxene, and anhydrous melt at one bar and 20 kilobars pressure. Ph.D. thesis, Calif. Inst. Technol., Pasadena.

Benjamin T., Heuser W. R., and Burnett D. S. (1978) Laboratory studies of actinide partitioning relevant to ^{244}Pu chronometry. *Proc. Lunar Planet. Sci. Conf. 9th*, p. 1393–1406.

Benjamin T., Heuser W. R., Burnett D. S., and Seitz M. G. (1980) Actinide crystal-liquid partitioning for clinopyroxene and $Ca_3(PO_4)_2$. *Geochim. Cosmochim. Acta*. In press.

Blander M., Fuchs L. H., Horowitz C., and Land R. (1980) Primordial refractory metal particles in the Allende meteorite. *Geochim. Cosmochim. Acta* **44**, 217–223.

Boynton W. V. (1978a) Fractionation in the solar nebula, II. Condensation of Th, U, Pu and Cm. *Earth Planet. Sci. Lett.* **40**, 63–70.

Boynton W. V. (1978b) Rare-earth elements as indicators of supernova condensation (abstract). In *Lunar and Planetary Science IX*, p. 120–122. Lunar and Planetary Institute, Houston.

Brewer L. (1967) A most striking confirmation of the Engel metallic correlation. *Acta Met.* **15**, 553–556.

Brewer L. and Wengert P. R. (1973) Transition metal alloys of extraordinary stability; an example of generalized lewis-acid-base interactions in metallic systems. *Metal. Trans.* **4**, 83–104.

Calas G. (1979) Etude experimentale du comportement de l'luranium dans les magmas: Etats d'oxydation et coordinance. *Geochim. Cosmochim. Acta* **43**, 1521–1531.

Chen C. and Presnall D. C. (1975) The system Mg_2SiO_4-SiO_2 at pressures up to 25 kilobars. *Amer. Mineral.* **60**, 398–406.

Dwight A. E. (1969) Alloy chemistry of thorium, uranium, and plutonium compounds. In *Developments in the Structural Chemistry of Alloy Phases* (B. C. Giessen, ed.), p. 181–226. Plenum, N.Y.

El Goresy A., Nagel K., and Ramdohr P. (1978) Fremdlinge and their noble relatives. *Proc. Lunar Planet. Sci. Conf. 9th*, p. 1279–1303.

French B. M. and Eugster H. P. (1965) Experimental control of oxygen fugacities by graphite-gas equilibriums. *J. Geophys. Res.*, **70**, 1529–1539.

Grossman L. (1980) Refractory inclusions in the Allende meteorite. *Ann. Rev. Earth Planet. Sci.* In press.

Grossman L., Olsen E. and Lattimer J. M. (1979) Silicon in carbonaceous chondrite metal: Relic of high-temperature condensation. *Science* **206**, 449–451.

Hensen M. (1958) *Constitution of Binary Alloys*. 2nd ed., p. 1305. McGraw-Hill, N.Y.

Jones J. H. and Burnett D. S. (1979) The distribution of U and Pu in the St. Severin chondrite. *Geochim. Cosmochim. Acta* **43**, 1895–1905.

Jones J. H., Benjamin T. M., Heuser W. R., and Burnett D. S. (1980) Meteoritic actinide chemistry: Laboratory partitioning studies (abstract). In *Lunar and Planetary Science XI*, p. 514–516. Lunar and Planetary Institute, Houston.

Keller C. and Erdmann B. (1976) Preparation and properties of transuranium element-noble metal alloy phases. In *Transuranium Elements Products of Modern Alchemy* (G. T. Seaborg, ed.), p. 306–309. Dowden, Hutchinson and Ross, Stroudsburg, Penn.

Larimer J. W. (1968) Experimental studies on the system Fe-MgO-SiO_2-O_2 and their bearing on the petrology of chondritic meteorites. *Geochim. Cosmochim. Acta* **32**, 1187–1207.

Reed G. W. and Turkevich A. (1955) Uranium content of two iron meteorites. *Nature* **176**, 794–795.

Ruff L. and Anderson D. L. (1980) Core formation, evolution, and convection: A geophysical model. *Phys. Earth Planet. Inter.* **21**, 181–201.

Schreiber H. D. and Andrews S. M. (1980) The redox states of uranium in synthetic basaltic magmas (abstract). In *Lunar and Planetary Science XI*, p. 1000–1002. Lunar and Planetary Institute, Houston.

Stapanian M. I., Burnett D. S., and Furst M. J. (1980) Meteorite actinide chemistry: Th-U microdistributions (abstract). In *Lunar and Planetary Science XI*, p. 1082–1084. Lunar and Planetary Institute, Houston.

Wark D. A. and Lovering J. F. (1978) Refractory/platinum metals and other opaque phases in Allende Ca-Al-rich inclusions (CAI's) (abstract). In *Lunar and Planetary Science IX*, p. 1214–1216. Lunar and Planetary Institute, Houston.

APPENDIX III

THE DISTRIBUTION OF U AND PU IN THE ST. SEVERIN CHONDRITE

Geochimica et Cosmochimica Acta Vol. 43, pp. 1895 to 1905
© Pergamon Press Ltd. 1979. Printed in Great Britain

0016-7037/79/1201-1895$02.00/0

The distribution of U and Pu in the St. Severin chondrite*

J. H. JONES and D. S. BURNETT
Division of Geological and Planetary Sciences, California Institute of Technology, Pasadena, CA 91125, U.S.A.

(*Received 5 February* 1979; *accepted in revised form* 31 *July* 1979)

Abstract—A detailed study of the U distribution of the St. Severin chondrite has been made by fission track radiography in order to clarify the interpretation of fission Xe thermal release data in terms of the mineralogical location of the fission Xe within the meteorite. This is of importance because the $^{244}Pu/^{238}U$ ratio for St. Severin has been widely adopted as the average solar system value. The U contents of the constituent minerals cannot account for the total rock U which, instead, appears to be primarily localized on grain boundaries. The greatest localizations of U are in olivine-poor, orthopyroxene-rich 'clasts'. Our data coupled with those of PODOSEK (1970a) show that ^{244}Pu in St. Severin was also located on grain boundaries and that the bulk of Pu and U are unfractionated within this meteorite. Due to recoil, the ^{244}Pu fission Xe is found in 10 micron surface layers on major phases. Assuming that the grain boundaries (on which the Pu was located) was formed during metamorphism, the $^{244}Pu/^{238}U$ ratio for St. Severin applies to a time subsequent to the textural recrystallization of the meteorite. Our data support the interpretation of Podosek and our best estimate of the solar system $^{244}Pu/^{238}U$ is 0.015.

INTRODUCTION

Inspired by the measurement of a relatively high (0.03) $^{244}Pu/^{238}U$ ratio in a separate of whitlockite $[Ca_3(PO_4)_2]$ from the St. Severin chondrite (WASSERBURG *et al.*, 1969a), many calculations on the time scale for galactic nucleosynthesis have been published (see, e.g., HOHENBERG, 1969; WASSERBURG *et al.*, 1969b; SCHRAMM and WASSERBURG, 1970; FOWLER, 1971), showing that the 0.03 value required a relatively late injection of r-process elements immediately prior to the formation of the solar system. However, interpreting 0.03 as the solar system abundance ratio for $^{244}Pu/^{238}U$ involved the assumption that Pu and U are not geochemically fractionated. The well known constancy of Th/U at 3.8 (MORGAN and LOVERING, 1968; TOKSÖZ and JOHNSTON, 1977) supports this assumption; however, assuming no fractionation is particularly suspect when the Pu/U ratio is obtained from the analysis of a specific mineral. Based on a stepwise heating measurement of the heavy Xe isotopes in a neutron-irradiated St. Severin sample, PODOSEK (1970a, b, 1972) reported a $^{244}Pu/^{238}U$ ratio for a total rock sample of St. Severin of 0.015, which was interpreted as indicating that Pu was enhanced relative to U in whitlockite and that 0.015 should be used for the solar system $^{244}Pu/^{238}U$ ratio.

GANAPATHY and GROSSMAN (1976) questioned this interpretation, arguing that the whitlockite Pu/U ratio was difficult to understand relative to the other minerals in St. Severin and, thus, that St. Severin was probably a disequilibrium assemblage, formed from materials of fractionated Pu/U ratio. CROZAZ (1974) reported a high Th/U = 10 for whitlockite from St. Severin, which challenges the whitlockite Pu/U ratio as the solar system abundance ratio. Laboratory partitioning measurements (BENJAMIN *et al.*, 1978) indicate, at least for the experimental conditions under which the samples were synthesized, that Pu is preferentially incorporated into whitlockite over both Th and U, demonstrating that the whitlockite Pu/U is probably too high. However, Crozaz found no other significant U-bearing phases other than phosphates in St. Severin. She concluded [as had WASSERBURG *et al.* (1969a) previously] that phosphates accounted for a small proportion (5–10%) of the U in the meteorite. Thus, the sources of the fission Xe on which the 0.015 value of Podosek was based were still unknown.

LUGMAIR and MARTI (1977) and WASSERBURG *et al.* (1977) have shown that the Pu/Nd ratio is constant for whitlockite and clinopyroxene in Angra dos Reis and have proposed that this ratio be used for ^{244}Pu chronology rather than $^{244}Pu/^{238}U$. MARTI *et al.* (1977) point out that the Pu/Nd ratio of Angra dos Reis is also found in Juvinas and in melilite from an Allende coarse-grained inclusion and further propose that a solar system $^{244}Pu/^{238}U$ ratio of 0.004 be adopted where this value is calculated as the product of the Angra dos Reis (Pu/Nd) ratio and a chondritic (Nd/U) ratio. The relationship of this result to the 0.015 value from Podosek for St. Severin is unclear.

It appeared to us that a detailed study of the distribution of U in St. Severin would help in understanding the Podosek data in a petrographic context. The basic issue is the interpretation of the fission Xe data in terms of the mineralogical sites of ^{244}Pu in the meteorite. Knowing these sites should provide an improved basis for the evaluation of the $^{244}Pu/^{238}U = 0.015$ value as the solar system average.

* Caltech Contribution No. 3211.

EXPERIMENTAL

Six polished sections of ~45 mm² each were prepared, covered with mica fission track detectors, and irradiated with neutrons to a fluence of ~1–2 × 10^{18} n/cm². Prior to irradiation all samples were ultrasonically cleaned in 100% ethanol with a final cleaning stage of spectro-quality methanol. Standards were 368 ppb U glass, as determined by isotopic dilution. The amount of contamination on the sections was assessed from the background track density on those portions of the mica exposed to the epoxy in which the sections were mounted. The section with the lowest background track density (equivalent to about 2 ppb U, similar to the range, 1.2–1.9 ppb, observed on blank epoxy discs) was selected for detailed mapping. The other sections were only scanned for high track density phases (≳50 ppb U). However, since any localized area can be influenced by contamination, we have measured the U concentrations of the major, but U-poor, minerals, olivine and orthopyroxene, by direct etching of irradiated grains. Prior to irradiation these grains were sealed in quartz vials while under vacuum and then annealed at 800°C for 1 hr. For olivine and orthopyroxene, this annealing should remove all cosmic ray and fossil fission tracks (FLEISCHER *et al.*, 1975; CARVER and ANDERS, 1976).

To assure proper etching conditions, test grains of St. Severin olivine and orthopyroxene were irradiated with ^{252}Cf fission fragments. Etchants and etching times reported by LAL *et al.* (1968) were found to be suitable. All grains on which tracks were counted were identified using the electron microprobe. The irradiated grains were mounted in epoxy and polished such that at least 10 microns of material was removed; thus, any U surface contamination on the grains cannot contribute to the observed track density. We assume that the track density on the interior surfaces of our irradiated grains is twice that which would have been observed on a polished surface in contact with our external mica detector. This factor of 2 is not exactly correct (REIMER *et al.*, 1970) but is sufficiently accurate for our purposes. For phosphates, U concentrations are based on the central track densities from SEM photographs from lightly-etched (8 min) mica detectors.

RESULTS

In order to calculate the fraction of the total rock U which is accounted for by any given mineral, it is necessary to know the modal abundances of the various phases. We have utilized modes obtained in two ways: (1) calculated from bulk chemical and mineral compositions; and (2) observed by direct measurement over ~25 mm² on our best section. Our mineral analyses (Table 1) are consistent with representative LL chondrite data, as given by VAN SCHMUS (1969). For method (1) we used the bulk analysis of JAROSEWICH and MASON (1969), but analyses reported by MÜLLER (1968) or by ORCEL *et al.* (1967) are in good agreement and would have given essentially the same mode. The directly measured modes [method (2)] were obtained with an automated microprobe point-count procedure (ALBEE *et al.*, 1977). St. Severin is known to have a light–dark structure (WASSERBURG *et al.*, 1969a) which is presumably the result of impact brecciation. The specimen from which our sections were made is primarily dark material, but we have also measured a mode for the light material for comparison. Measurements were made of 1800 and 1500 points respectively for the whole rock and light sections. The various modes given in Table 2 show distinct differences. Although our section appears to be metal and sulfide deficient compared to abundances expected from bulk chemical data, the light material is especially deficient in metal and sulfide, and it appears to be depleted in orthopyroxene as well. The mode for the dark material is closer to the mode from the bulk chemical analysis but is still deficient in opaques and orthopyroxene compared to olivine and plagioclase. For our purposes we adopt the mode for the 'best' section in Table 2, for which most of our U data apply; however, our conclusions would be unchanged if the mode from the bulk analyses were adopted instead.

Table 3 gives a summary of our U analyses for the various phases in St. Severin. Olivine systematically excludes large-ion lithophile elements; consequently, it is observed to be essentially devoid of U. This also shows up clearly in sections where large, relict olivine chondrules define essentially track-free regions.

Because U has no known siderophile or chalcophile character, well located sulfide and metal grains in our irradiated section yield very low U contents. The limits given in Table 3 correspond to only a few grains; much lower limits could be obtained, but this does not seem worthwhile. Our results are consistent with those of REED and TURKEVICH (1955) for iron meteorites (<0.5 ppb) and those of TATSUMOTO *et al.* (1973) or REED *et al.* (1960) for troilite from iron meteorites (0.1–1 ppb). These results are given as limits because we have no way to correct for the effects of contamination on localized areas on sections at these concentrations. In general no contamination corrections have been applied to Table 3. Because of small grains the chromite value may be high, but given its low modal abundance,

Table 1. Representative electron microprobe analyses of St. Severin minerals (wt%)

	Olivine	Orthopyroxene	Clinopyroxene	Plagioclase	Chromite	Whitlockite	Chlorapatite
Na_2O	NA	0.01	0.78	9.60	—	2.83	0.31
MgO	36.67	28.10	16.27	—	1.91	3.43	0.03
Al_2O_3	—	0.11	0.93	21.56	5.43	—	—
SiO_2	37.93	55.68	53.66	66.68	—	0.04	0.08
CaO	0.05	0.82	21.08	2.25	—	46.92	53.78
TiO_2	0.01	0.17	0.36	—	4.19	NA	NA
Cr_2O_3	0.15	0.24	0.64	NA	52.69	NA	NA
MnO	0.48	0.45	0.33	NA	1.11	NA	NA
FeO	27.81	16.49	5.90	0.68	33.11	0.48	0.12
NiO	0.04	NA	NA	NA	NA	NA	NA
K_2O	NA	NA	NA	0.91	—	NA	NA
P_2O_5						46.14	41.21
F						NA	0.90
Cl						NA	3.45[a]
Total	103.14	102.02	99.94	101.78	98.46	99.83	98.99

NA = not analyzed.

[a] the measured halogen abundances would fill only about 3/4 of the halogen site in stoichiometric apatite. This may reflect site vacancies, systematic errors in microprobe F analyses or, conceivably, some hydroxyl substitution.

Table 2. Modal abundance of St. Severin minerals[a]

Mineral	From chemical analysis[b]	Point-count 'best' section	Point-count light structure	Dark structure calculated[c]
Olivine	54	62	79	55
Orthopyroxene	19	19	3.7	25
Clinopyroxene	6.2	5.1	6.8	4.5
Plagioclase	10.3	10.3	9.9	10.5
Troilite	5.8	1.7	0.2	2.4
Metal	3.2	1.0	0.1	1.4
Chromite	0.82	0.6	0.5	0.6
Whitlockite	0.48[d]	0.47	0.01	0.73
Chlorapatite	—	0.024		

[a] modal data in wt%.
[b] using bulk analysis of JAROSEWICH and MASON (1969) and mineral analyses from Table 1.
[c] calculated assuming 'Best' Section = 70% dark + 30% light.
[d] assumes all P in whitlockite; if 121 ppm Cl (QUIJANO-RICO and WÄNKE, 1969) assumed to be in chlorapatite, 0.35% chlorapatite and 0.15% whitlockite is calculated. See text.

it makes an insignificant contribution to the whole-rock uranium content. Our whitlockite analyses are in agreement with others from the literature (CANTELAUBE *et al.*, 1967; CROZAZ, 1974; PELLAS and STORZER, 1975; MANHES *et al.*, 1978). Crozaz reported one chlorapatite grain in her St. Severin sections; in contrast, we observed two large (100–200 micron) and seven small (≤ 50 micron) chlorapatites. Our apatite U concentration agrees with Crozaz, but is somewhat higher than values of 3.7 and 4.8 ppm reported for two grains by PELLAS and STORZER (1975). Our adopted modal abundance is an area-weighted average of the grains seen in our sections and those of Crozaz. Despite the greater abundance of chlorapatite in our sections, the phase still makes only a small contribution to the whole rock U. However, it should be noted that if all the chlorine in St. Severin (121 ppm; QUIJANO-RICO and WÄNKE, 1969) is assumed to be in chlorapatite, then all of the U in the meteorite could be accounted for by this phase. Given the relatively high U concentration, chlorapatite grains greater than ~1–3 microns in size would be readily spotted. Therefore, if only grains greater than this size are considered, there is a material balance problem for chlorine as well as U. We cannot rule out that submicron chlorapatite grains contain all the U in St. Severin, but this does not change any subsequent conclusions.

Table 3. U concentrations of St. Severin minerals

Mineral	U (ppb)	Whole rock contribution (ppb)[a,b]
Olivine	0.3 ± 0.1	0.18
Orthopyroxene	2.9 ± 0.2	0.54
Clinopyroxene	5.3 ± 1.4	0.28
Plagioclase	3.2 ± 0.5	0.33
Troilite	<1.3	<0.02
Metal	<1.8	<0.02
Chromite	4.7 ± 0.7	0.03
Whitlockite	276 ± 16	1.30
Chlorapatite	6775 ± 360	1.63
	Total = 4.3 ± 0.5	

Whole rock value: 14 ppb—PELLAS (personal communication). 16 ppb—FISHER (1972). 11 ppb—This work.

[a] Utilizing mode from 'best section', Table 2. Except for apatite where 0.024% was used. See text.
[b] Correction for fission fragment range differences in minerals relative to glass standards has been applied based on ranges calculated by NORTHCLIFFE and SCHILLING (1970). Except for metal and sulfide corrections are less than 9%.

We were not able to etch tracks in St. Severin plagioclase because the grains are highly fractured (shock?) and dissolved before tracks were revealed. Consequently, the plagioclase U content in Table 2 is based on plagioclase grains mapped in our 'best' section. Our plagioclase U content is based on only a few grains; however, track densities over small plagioclase grains in the sections conclusively show that U is not concentrated in this mineral. Given the low plagioclase abundance, 160 ppb would be required to account for the total U and this can unequivocally be ruled out. For comparison, anorthitic feldspars from lunar rocks (CROZAZ *et al.*, 1970) and achondrites (CARVER and ANDERS, 1976) have low (<1 ppb) U contents. If there is a significant amount of surface contamination, even on our best section, the plagioclase U content will be somewhat high.

Figure 1 shows a grain by grain breakdown of our orthopyroxene concentrations, plotted against the area of the grain which was scanned. Some studies have shown that U content is a decreasing function of grain size for igneous rocks (see, for example, BURNETT *et al.*, 1971). There is no obvious correlation but large errors for individual grains prohibit strong conclusions. Secondly, such a correlation would only exist statistically because the grains were extracted from a crushed sample. Thirdly, the area scanned is smaller than the actual grain area because of the presence of opaque inclusions and of badly corroded regions from etching. These prevent tracks from being counted on all portions of the grains, and this difference in area scanned and grain area will also put scatter into Fig. 1. Nevertheless, the results are consistent with a uniform (equilibrated) orthopyroxene U content as shown by the inset in Fig. 1. The inset shows that all but 3 of 30 grains lie within ±2 standard deviations from the mean. Many of the grains counted have fractures which may be natural cleavages. Any U in these fractures could produce fission tracks leading to high apparent U concentrations for the orthopyroxene. U localizations in clinopyroxene cleavages have been documented by BHANDARI *et al.* (1971). In one grain, excluded from Fig. 1, we saw tracks arising from such cleavages. According to Pellas (private communication, 1977) the U concentration for St. Severin orthopyroxene is given incorrectly in LAL *et al.* (1969), with the actual value being 7 ppb. This is about a factor of 2 higher than our concentration of 3 ppb. The 7 ppb figure was based on a measured neutron flux rather than by direct comparison with a U standard, and this may be a source of some of the discrepancy. However, even at 7 ppb, orthopyroxene would only account for ~10% of the total rock U. Our orthopyr-

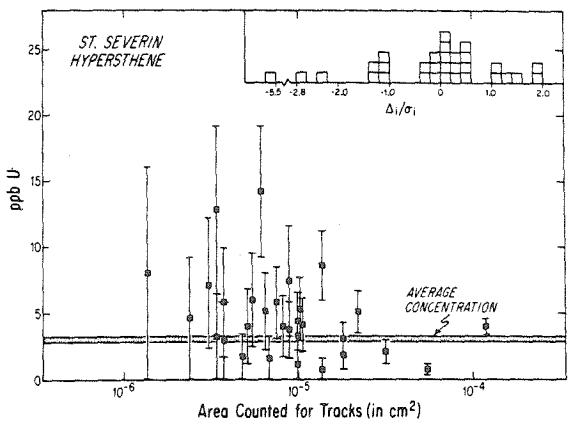

Fig. 1. U concentration in orthopyroxene (in ppb) vs area scanned for tracks. Inset in upper right shows the distribution of the deviation (Δ_i) of each point from the average divided by its standard deviation (σ_i) based on counting statistics. Most points are within $\Delta/\sigma = \pm 2$.

oxene U contents are much higher than those for large orthopyroxene grains from achondrites (CARVER and ANDERS, 1976), even though the achondrite total rock U contents are much higher. This difference is somewhat surprising, and it suggests that our apparent orthopyroxene U contents are high because of tracks originating from fractures or from grain boundaries. It is possibly significant that the lowest U concentration was observed on our most perfect crystal (plotted at -5.5 on the inset to Fig. 1).

A priori, clinopyroxene was the most likely mineral to be a major source of U. In fact, some discussions of the Pu/U fractionation for St. Severin have already assumed that this was determined by partitioning between clinopyroxene and whitlockite (SEITZ *et al.*, 1974; GANAPATHY and GROSSMAN, 1976). Large clinopyroxene grains in St. Severin are very rare, as indicated by the fact that this mineral was not reported in two previous petrographic descriptions (ORCEL *et al.*, 1967; JAROSEWICH and MASON, 1969). Our identification of this mineral as clinopyroxene is based on microprobe analyses (Table 1) and the fact that diopsidic clinopyroxene is a well-known constituent of ordinary chondrites. Based on four, approximately 100 micron, grains in our best section, the average U concentration is 5.7 ppb, with a total range in concentration from 4.4 to 7.7 ppb. Again, this value may be slightly high if there is significant contamination for this section. Most importantly, clinopyroxene grains greater than 20 μ with 80 ppb U (the amount required to dominate the total rock U) would produce distinctive clusters of tracks (stars) in our irradiated sections, and these are definitely not present.

Table 3 combines the measured U mineral contents and the modal abundances to calculate the fraction of the total rock U which can be accounted for by each phase. Table 3 shows that the total rock U content of St. Severin cannot be accounted for by the U contents of the principal minerals, at least for larger ($\gtrsim 20$ micron) grains. The preceding discussion indicates that the uncertainties in the mineral analyses tend to lead to high U contents; thus, this conclusion is quite firm.

The whole-rock U concentration of FISHER (1972) (16 ppb, with $\pm 10\%$ agreement among four duplicate analyses) appears reasonable compared to other literature chondrite U concentrations. Random scanning over our best section gave 11 ppb; by the same method, CROZAZ (1974) found 9–14 ppb, and Storzer and Pellas (private communication) found 13.8 ± 1.4 ppb. The radiogenic ^{4}He data of MARTI *et al.* (1969) correspond to a 4.5×10^9 yr. U–He age if 11 ppb U and Th/U = 3.8 is assumed. All of these measurements are reasonably consistent. We shall adopt 11 ppb as measured for our section. Thus, the rock sections have the U, but our analyzed mineral grains do not.

In order to obtain a more detailed view of the actual U distribution, the mica detector for our best section was given a long (30 min) etch to make the ^{235}U fission tracks readily visible at low magnification. The fission tracks are not randomly distributed but are concentrated in broad (hundreds of microns), comparatively fine-grained (20–30 microns) regions that are rich in orthopyroxene, clinopyroxene and plagioclase and are nearly devoid of olivine. The U content in these regions is ~ 40 ppb. It may be profitable to think of St. Severin as a breccia with these fine-grained, olivine-poor areas as 'clasts'. These 'clasts' appear to be contained within the dark breccia fragments, consistent with our observation of low orthopyroxene contents in the light material. Not all fine-grained areas have high U contents, however.

In light of the foregoing discussion, we conclude that the U in St. Severin is concentrated on grain boundaries or interstitial phases in the fine-grained olivine-poor clasts, with the amounts of interstitial U varying from clast to clast.

We have attempted to observe directly a correlation between track patterns and grain boundary locations in the track rich areas. This comparison is difficult because: (a) there are too few tracks to delineate clearly an image of the grain boundary distribution, (b) the fission fragment range (~ 10 microns) is comparable to many grain radii making

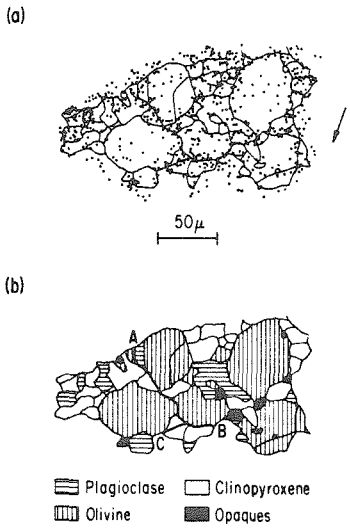

Fig. 2. Detailed view of U fission tracks for a St. Severin section irradiated to $\sim 10^{19}$n/cm^2. Part (a) is a superposition of the grain boundaries and the fission tracks (dots) on the mica detector affixed to the meteorite during the irradiation. Part (b) is a map identifying the minerals corresponding to the grains in (a). The nominal track locations have been shifted relative to the meteorite section by an amount given by the arrow in (a) to get a better fit of the "holes" in the track distribution to the large olivine grains. The average U concentration of the area drawn is 11 ppb. Given the 10 micron range of fission fragments, a grain boundary distribution is hard to observe directly, but the data shown are consistent with this hypothesis, particularly the boundaries illustrated by the path ABC.

a grain boundary correlation difficult to recognize, (c) there are uncertainties ($\sim$ 15 microns) in relating positions on the mica detectors to the corresponding sample locations and (d) a small gap between the sample and mica detector will blur any small scale track pattern. The problems involved in trying to demonstrate the grain boundary-U correlation are illustrated in Fig. 2. Polished (cm-sized) slabs of St. Severin were covered with mica detectors and irradiated with a thermal neutron fluence of $\sim 10^{19}$/cm^2 (slabs were used because epoxy cannot survive this fluence). Several relatively coarse-grained areas (80–100 micron grains) were selected prior to irradiation. Fig. 2a shows the detailed track-grain boundary comparison for the area selected for detailed analysis. Figure 2b (based on microprobe data) identifies the minerals in Fig. 2a. Each dot in 2a represents the point of exit of a single fission fragment from the sample, but it should be emphasized that the location of the fissioning U atom may be as much as 10 microns removed from the point of exit and larger if there is a gap between sample and detector. Figure 2a is a 'best fit' in the sense that the large 'holes' in the track map were matched to the large olivine grains by a small translation ($\approx$ 20 microns, indicated by arrow in 2a) relative to the 'absolute' locations of the tracks determined by matching large phosphate grains (elsewhere in the section) and corresponding localizations of tracks (stars) on the mica detector. This amount of translation is acceptable within the errors of locating the absolute position of a given fission track on a section. The area pre-selected for analysis turned out to be rich in clinopyroxene and free of orthopyroxene. The average U content defined by the tracks shown in Fig. 2a is 11 ppb indicating lack of significant contamination. Interpretation of the track patterns is complicated by the presence of the fine-grained phases; nevertheless, the features of the track patterns, particularly the concentrations along the boundaries ABC (Fig. 2b), are best accounted for by a grain boundary U distribution. The overall track patterns in our sections are not well matched by postulating that the U is concentrated in small clinopyroxene grains, although that model could not completely be ruled out for the area shown in Fig. 2.

Our assignment of U to grain boundary locations is thus primarily indirect, but it is required by the mineral results and not ruled out by the actual observed track distributions.

DISCUSSION

Based on the data of Table 3 and the actual fission track distribution over polished sections of St. Severin, we find that at least 50% of the U resides on grain boundaries, preferentially in fine-grained, olivine-poor 'clasts'. Fission fragments from fission events along these grain boundaries—both ^{244}Pu spontaneous fission, 4.6 $\times$ 10^9 yr ago and the ^{235}U neutron induced fission produced by reactor irradiation during the analysis by PODOSEK (1972)—will recoil into the surrounding mineral grains. If our observation of U localization in orthopyroxene-rich clasts is generally valid, more fission Xe will be found in orthopyroxene, but there will still be significant recoil into olivine, feldspar and clinopyroxene. We conclude that the fission Xe measured by Podosek arose from the outer 10 micron layers of major phases.

Podosek found a linear array of stepwise-heating Xe isotopic data (for a reactor-irradiated St. Severin sample) when plotted on a ^{130}Xe/^{132}Xe vs ^{134}Xe/^{132}Xe correlation diagram. Taken at face value this linear array indicates that the heavy Xe isotopes in St. Severin could be regarded as a two-component mixture of fission Xe (from both ^{244}Pu and neutron-induced ^{235}U fission) with an ambient 'trapped' Xe component similar to that found in carbonaceous chondrites (AVCC). The fact that different temperature fractions showed variations in these isotopic ratios indicated that the fission and trapped Xe components were located at different sites in the meteorite; otherwise no isotopic variations would have been observed. Extrapolation of the correlation line to the ^{130}Xe/^{132}Xe = 0 axis yielded the ^{134}Xe/^{132}Xe ratio in the fission component, and from this a ^{244}Pu/^{238}U ratio was calculated. The fact that only one fission component was observed (i.e., the data formed a linear array) suggested that Pu and U were unfractionated. In relating our work to the stepwise heating data, it is useful to consider two (perhaps oversimplified) scenarios:

I. When the amounts of fission Xe released in the various temperature fractions are considered, most ($\sim$ 60%) of the fission Xe is found in the 1300–1500°C

temperature fractions. However, the spread in the isotope ratios which permits the calculation of a $^{244}Pu/^{238}U$ ratio is obtained from the 1100 and 1200°C temperature fractions. The 1300, 1400 and 1500°C data points plot comparatively close to AVCC, and the errors on Pu/U derived from these data points by themselves correspond to a wide range of Pu/U ratios (0–0.02), although the actual values tend to be lower than 0.015. Extrapolation of the correlation line thus might give only the Pu/U ratio of a specific phase(s) which releases Xe at 1100–1200°C. This phase could contain as little as 30% of the fission Xe and might have a Pu/U ratio which is chemically fractionated from the actual total rock value. Assuming that this hypothetical phase is also required to have about 30% of the U, it could be identified in our experiment. For example, a major mineral with relatively low U content ($\lesssim 50$ ppb) could account for an appreciable fraction of the total U but still have been missed in previous studies.

In summary, scenario I essentially postulates that the Podosek correlation line does not actually yield the total rock Pu/U but that of some specific phase.

II. Here we take the Podosek correlation line at face value to indicate that, except for minor phases such as phosphates, Pu and U are not fractionated. In this scenario, the distribution of U gives directly the distribution of Pu, which was the original experimental objective.

Our data appear to rule out scenario I, for which the extrapolation of the correlation line was determined by the release of a single phase accounting for about 30% of the fission Xe. No phase accounting for 30% of the U was found. In particular, clinopyroxene, which *a priori* was the most plausible candidate, accounts for less than 10% of the U.

However, a variation on scenario I must be considered in which the 1100/1200°C fission Xe represents the combined release of the two phosphates: whitlockite plus apatite. From Table 3 the combined phosphates account for 2.9 ppb or 26% of the total rock U (assuming 11 ppb). The amount of ^{235}U fission Xe in the 1100 and 1200°C temperature fractions is equivalent to 25% of the U fission Xe (equivalent to ~3 ppb) (PODOSEK, 1970a), in good agreement with that obtained from our track data and modal abundances. Furthermore, combining our relative phosphate U contents and modal abundances with the Pu (whitlockite)/Pu (apatite) = 2 ratio from adjacent grain fossil track measurements by PELLAS and STORZER (1977 and private communication) gives a weighted average Pu/U ratio for the two phosphates of 0.017, in agreement with the Podosek value! If this 'phosphate model' is correct, the Pu/U = 0.015 ratio of Podosek cannot be immediately equated to the total rock ratio, following the general discussion in 'scenario I'.

Similarly, using the data of CROZAZ (1974) and our modal abundances, an average St. Severin phosphate Th/U ratio of 6 is obtained indicating fractionation of Th and U in the combined phosphates compared to our assumed total rock Th/U of 3.8. Since Th and U are fractionated, the probability of Pu-U fractionation is also high. Parenthetically, there is no direct measurement of Th/U in the same whole rock St. Severin specimen. Combining the total rock Th concentration of MATSUDA *et al.* (1972) with a range of total rock U contents from 11–16 ppb—gives low Th/U ratios, 2.0–3.6, but we tentatively ascribe this to sampling differences. A Th/U measurement on the same specimen is required. However, there are serious difficulties with this 'two-phosphate model' which probably make it incorrect: (1) It is probable that our samples are anomalously apatite-rich. Shirck reports two apatites out of 200 phosphate grains (as quoted in CROZAZ, 1974), 5 times less than our modal abundances. Morover, WASSERBURG *et al.* (1969a) found no apatites in microprobe analyses of hundreds of phosphate grains from their mineral separates. (2) LEWIS (1975) reports Xe analyses for both neutron-irradiated and unirradiated samples of phosphate separates from a large, 1.3 kg, sample of St. Severin. His mineral characterization procedures did not distinguish apatite from whitlockite; however, on the assumption that the separation procedures did not bias between the two phosphates, the data for his irradiated samples provide a direct measurement of the Pu/U for a mixture of St. Severin phosphates. Stepwise temperature measurements on the irradiated samples indicated variations in the Pu/U ratio within the separate. This variation can be explained by the presence of both apatite and whitlockite with very different Pu/U ratios or, following Lewis, by variations in Pu/U among different whitlockite grains. The data of PELLAS and STORZER (1975) support the latter interpretation. In any case, however, the average Pu/U ratios of the phosphate separates can be calculated from the Xe data, yielding 0.040 and 0.034 for the coarse and fine size fractions respectively. These ratios are higher than calculated above (0.017) for an apatite-whitlockite mixture. The discrepancy probably indicates that either the adopted Pu(whitlockite)/Pu(apatite) ratio or the relative modal abundance of whitlockite and apatite is incorrect. It appears much more reasonable that the apatite abundance in our sample is high. (3) Plagioclase of the St. Severin composition (An_{10-15}) begins to melt at 1130–1150°C and the recoil fission Xe on the surface of this mineral should be released by 1100°C or certainly in the 1200°C fraction (allowing for temperature calibration uncertainties). The modal plagioclase abundance is 10% so at least this much of the fission Xe should be accounted for by recoils into plagioclase. Further, because plagioclase grains are systematically smaller (thus having more surface area) and/or if our observation of a concentration of U in olivine-free clasts (which have 20–30% feldspar) is generally valid, the plagioclase surface fission Xe might account for most of the fission Xe observed in the 1100/1200°C fractions.

Summarizing, we feel that arguments (1–3) are quite strong and rule out the 'two-phosphate' model as an interpretation of the 1100/1200°C fission Xe release of Podosek. The agreement between the Pu/U measured in the stepwise-heating experiments of Podosek and that calculated from this model is probably coincidental, due to an anomalously high apatite abundance in our sections. However, it should also be emphasized that there are features of the PODOSEK (1970a) data that are not easily understood and/or require further study: (1) The PODOSEK (1970) data yield a U content of 6 ppb which does not agree well with other total rock U data. (2) The neutron fluences, required to calculate Pu/U, were obtained from the amount of ^{128}Xe produced in KI, assuming only thermal neutron capture on ^{127}I; effects of resonance neutron capture were not considered. The effect of this assumption will be to overestimate (Pu/U) and to underestimate the U content. The magnitude of the error is difficult to estimate; ALEXANDER *et al.* (1972) obtain reasonable U values for Apollo 12 samples by the same assumption. Consequently, it appears that systematic neutron fluence errors are not serious, and that the U concentration discrepancies indicated in (1) and (2) must be ascribed to other sources of error, e.g., absolute Xe concentration measurements. It should be emphasized that only the neutron fluence and Xe isotope ratios enter

the calculation of Pu/U, consequently there is no strong basis for questioning the 0.015 value on analytical grounds, although additional data are clearly needed.

We conclude that scenario II given in the introduction is probably correct; thus, the interpretation of the Podosek correlation line can be taken at face value, indicating $^{244}Pu/^{238}U = 0.015$ as the actual total rock ratio and implying that, overall, U and Pu have the same distribution within the meteorite. There are two ways in which this conclusion could be invalid: (a) The Pu/U ratio varies systematically for different grain boundaries, and (b) Podosek also analyzed a specimen which is anomalously apatite-rich. There is no evidence for either of these alternatives. One can then equate the grain-boundary distribution of U we observe today to the distribution of ^{244}Pu in the meteorite 4.6×10^9 yr ago. We can now pursue the implications of that distribution.

Given the superficial distribution of ^{244}Pu fission Xe on grain surfaces, the question arises whether the inferred $^{244}Pu/^{238}U$ ratio of 0.015 could be low because of diffusion loss of ^{244}Pu fission Xe. The high release temperature of the reactor-produced ^{235}U fission Xe which, as our data show, will also recoil into grain surfaces, suggests that this is unlikely. The recoil of the fission Xe into major mineral phases has probably stabilized it against diffusion loss. Similarly, assuming Th is also concentrated on grain boundaries, the alpha particles in the U-Th decay series will be implanted to 15–30 micron depths and the resulting ^4He also stabilized against diffusion loss. The relatively high U-He age of St. Severin (MARTI *et al.*, 1969; FISHER, 1972) and the qualitatively similar siting of the ^4He and fission Xe is a strong argument against diffusion loss of fission Xe. However, the recoil effects in the radiogenic Pb are much smaller; consequently, disturbances of the Pb-U-Th isotopic relationships in St. Severin and other equilibrated chondrites may be rather likely, given the superficial location of the U, Th and radiogenic Pb. No disturbance is evident in the St. Severin Pb data of MANHES *et al.* (1978), but the measurements made were not particularly sensitive to anything except very large disturbances.

The above arguments against significant ^{244}Pu fission Xe loss are qualitative; it would be desirable to be able to treat the problem of fission Xe retention quantitatively. Given the knowledge of the location of the ^{244}Pu fission Xe in St. Severin and the fact that the distribution (surface layer) is relatively simple, it would appear possible to define more precisely the concept of a 'time (or temperature) of Xe retention' which is important for all chronology calculations based on $^{244}Pu/^{238}U$ or $^{244}Pu/Nd$. Estimates of the diffusion coefficients as a function of temperature in principle can be obtained from thermal release data; however, even for an initial surface layer distribution the diffusive loss for spherical grains of the size found in St. Severin still depends on grain size. More importantly, essentially all fission Xe was observed at temperatures above 1100°C where partial melting has occurred. This prohibits interpretation of the release data in terms of diffusion. However careful stepwise heating measurements below partial melting temperatures yield fission Xe diffusion coefficients which then could be used to calculate reliable amounts of gas loss for an assumed thermal history.

St. Severin is a complex and evolved object. It has suffered brecciation and metamorphic recrystallization, probably in that order. The metamorphic time scale was probably not negligible compared to the ^{244}Pu half-life, as indicated by the ^{244}Pu fission track studies of PELLAS and STORZER (1977) or by evolved $^{87}Sr/^{86}Sr$ measured in some whitlockites (PAPANASTASSIOU and WASSERBURG, 1969; MANHES *et al.*, 1978). It is perhaps unreasonable that such an evolved object be used for the solar system $^{244}Pu/^{238}U$ ratio; this is essentially the basis of GANAPATHY and GROSSMAN's (1976) arguments. One might then expect other meteorites, theoretically more 'primitive', to show higher $^{244}Pu/^{238}U$ ratios. But the high Pu/U ratio for a mixed set of Allende white inclusions (PODOSEK and LEWIS, 1972) undoubtedly reflects Pu/U chemical fractionation as judged by the high Th/U ratios in some inclusions (CHEN and TILTON, 1976; TATSUMOTO *et al.*, 1976). The $^{244}Pu/^{238}U$ ratio for a coarse-grained Allende inclusion matches the St. Severin ratio well (DROZD *et al.*, 1977). The only known candidate for such a primitive sample is Nadiabondi (H5) whose whitlockite has a $^{244}Pu/^{238}U$ ratio ~ 5 times that of St. Severin's whitlockite (KIRSTEN *et al.*, 1977). However, another H5 chondrite, Allegan, appears to have a lower Pu/U ratio than St. Severin (PODOSEK, 1970b). The question then arises as to whether the ^{244}Pu fission Xe data for St. Severin define a $^{244}Pu/^{238}U$ ratio which predates metamorphism.

PAPANASTASSIOU and WASSERBURG (1969) found significant evolution in initial ($^{87}Sr/^{86}Sr$) for St. Severin whitlockite, (0.6998), suggesting metamorphic re-equilibration over a time scale of ~300 Myr. MANHES *et al.* (1978) using the whitlockite separates of LEWIS (1975), report a much lower (0.6990) initial $^{87}Sr/^{86}Sr$; however they also found that a hand-picked separate of large whitlockite grains gave a high (0.6996) value. They ascribed this evolved ratio to inherited radiogenic ^{87}Sr from adjacent troilite because the hand-picked whitlockites were binary grains with troilite and because troilite exhibited high Rb/Sr and a low model age, suggestive of Sr loss. It is not clear that the MANHES *et al.* explanation can account for the Papanastassiou and Wasserburg result which was based on a separate from about 100 g of meteorite (WASSERBURG *et al.*, 1969a), although our sections indicate that a relatively high (~35%) fraction of whitlockites ($\gtrsim$100 microns) show a grain boundary with troilite. The low initial $^{87}Sr/^{86}Sr$ of MANHES *et al.* suggests that either the metamorphic interval of St. Severin was rather short or that a significant fraction of the Sr in St. Severin was not isotopically re-equilibrated during metamorphism. The slow cooling rates

inferred by PELLAS and STORZER (1977) argue against a short metamorphic interval. Thus, our interpretation is that Sr isotopic re-equilibration was not complete during metamorphism. Could the ^{244}Pu fission Xe data also relate to an older time, i.e., was fission Xe retained during the metamorphic interval? Results by HUNEKE *et al.* (1977) for basaltic clasts in the Kapoeta achondrite indicate that Sr re-equilibration occurred in these without ^{244}Pu fission Xe loss. Our data put some constraints on the discussion of this problem. From the simplest point of view the grain boundaries on which the U resides today and from which the measured fission Xe evolves were probably formed during the metamorphism. These boundaries did not exist during older times; consequently, it would be concluded that the measured ^{244}Pu/^{238}U ratio does not apply to a time prior to metamorphism, but instead corresponds to some time during metamorphism. Specifically, the measured ratio applies to a time after the textural re-equilibration of the meteorite.

Our conclusions raise (or at least reemphasize) some serious chronology problems. If the ^{244}Pu/^{238}U = 0.015 ratio applies to the end of a period of metamorphism lasting more than 10^8 years, then one should find meteorites with ^{244}Pu/^{238}U ratios at least 2–3 times that measured for St. Severin. However, the ^{128}Xe-^{129}I age for St. Severin is not significantly lower (8 Myr younger than Bjurböle) than most other meteorites (PODOSEK, 1970a). Since the distribution of I is not known, it is possible that the time of radiogenic ^{129}Xe retention was pre-metamorphism and therefore much earlier than the time of ^{244}Pu fission Xe retention. There is not a good correlation between radiogenic ^{129}Xe and fission Xe in St. Severin, supporting this possibility. Alternatively, since textural re-equilibration and fission Xe retention may have occurred relatively early in the metamorphic period, it is also possible that there is no significant difference between one effective time of retention for radiogenic ^{129}Xe and fission Xe and that significantly higher Pu/U ratios will not be found in other meteorites. In general, we have no solutions for the difficulties in understanding the results of various methods of measuring meteorite age differences which have been noted by several authors (see, e.g., GRAY *et al.*, 1973).

In summary, we feel that our data (1) strongly support the validity of the ^{244}Pu/^{238}U value of 0.015 for St. Severin as a true whole rock result and (2) support the assumption that this ratio is unaffected by fission Xe diffusion loss. Thus, ^{244}Pu/^{238}U = 0.015 would be our best estimate for the solar system value although additional direct measurements on equilibrated chondrites are required. The arguments of Grossman and Ganapathy for the use of Allende coarse-grained inclusions as the source of the solar system ^{244}Pu/^{238}U appear equally valid to us; however more data to check the constancy of Th/U in Allende coarse-grained inclusions are needed (BOYNTON, 1978; CHEN and TILTON, 1976). It is probably significant that DROZD *et al.* (1977) found 0.017 = ^{244}Pu/^{238}U in one such inclusion.

Our data of course say nothing about the possibility that Pu and U were fractionated on a whole rock basis during the formation and metamorphism of St. Severin. However, this possibility can be tested by exactly the same method as used by Grossman and Ganapathy for the Allende coarse-grained inclusions. Figure 3 shows the ratio of the concentrations of 'refractory' trace elements in St. Severin to those in Cl chondrites. These elements (plus others for which St.

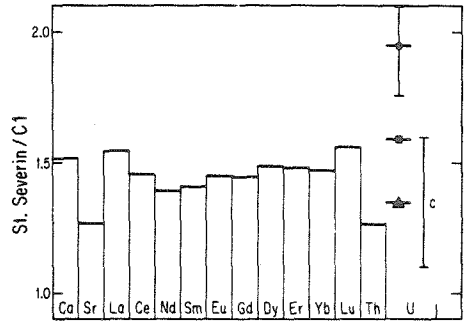

Fig. 3. Enrichment factors for refractory elements in St. Severin relative to Cl chondrites are shown to be uniform. Factors given are weight concentration ratios. Data sources for St. Severin and Cl's respectively are as follows: Ca—JAROSEWICH and MASON (1969), GROSSMAN and GANAPATHY (1976); Sr—GOPALAN and WETHERILL (1969), TATSUMOTO *et al.* (1976); REE—MASUDA *et al.* (1973), NAKAMURA (1974); Th—MATSUDA *et al.* (1972), TATSUMOTO *et al.* (1976); U: solid points—FISHER (1972), solid square—PELLAS (personal communication), solid triangle—(this paper), the range of values labeled *C* is from CROZAZ (1974), all are normalized to the U data of TATSUMOTO *et al.* (1976) for Cl chondrites.

Severin data are unavailable) are uniformly enriched in coarse-grained Allende inclusions. The figure also shows that there is no consistent evidence for strong fractionations of these refractory elements in St. Severin. (Note the supressed zero in Fig. 3). Much of the observed scatter may represent sample variations in absolute abundances rather than in relative abundance variations. It would seem worthwhile to have an analysis of these elements on a single sample, particularly the Th/U ratio, which is the best clue to Pu/U fractionation.

MARTI *et al.* (1977) have proposed 0.004 as the solar system $^{244}Pu/^{238}U$ ratio, where this value was calculated as $(^{244}Pu/Nd)_{ADOR} \times (Nd/^{238}U)_{ch}$ where ADOR refers to Angra dos Reis and ch to chondritic. Figure 3 shows that Nd/U in St. Severin is equal to the Cl chondrite value; consequently, the Pu/Nd is about 4 times higher for St. Severin than ADOR, if we adopt 0.015 as the $^{244}Pu/^{235}U$ ratio for St. Severin. [It is also possible to calculate (Pu/U) or (Pu/Nd) for St. Severin based on Pu concentrations obtained from absolute fission ^{136}Xe concentrations for unirradiated whole rock St. Severin samples. However, we consider these less reliable because of sampling problems and errors in the decomposition of the Xe mass spectrum whereas the Podosek Pu/U comes from the same sample and is independent of any absolute rare gas concentration measurements. Thus, using Xe data from MARTI *et al.* (1969) and WASSERBURG *et al.* (1969) and 12 ppb U, Pu/U ratios for St. Severin ranging from 0.005 to 0.013 are obtained. These tend to be lower than 0.015, but do not clarify the situation, although it is worth noting that the uncertainties in the 0.015 ratio are such as to make it high]. The studies on ADOR (MARTI and LUGMAIR, 1977, WASSERBURG *et al.*, 1977) support the Pu/Nd hypothesis although recent work (BENJAMIN *et al.*, 1979) shows that Nd and Pu do not have equal crystal-liquid partition coefficients. This means that fractionation can occur in some igneous processes, although in many cases the fractionation will be small. It is also possible that the lack of fractionation is only valid for igneous processes and that Pu and Nd were fractionated (e.g., by nebular processes) in the formation of the ADOR parent planet. Another possibility is that the lower Pu/Nd ratio may represent a 160 Myr younger age for ADOR than St. Severin. ADOR has a slightly lower initial $^{87}Sr/^{86}Sr$ (WASSERBURG *et al.*, 1977) relative to 0.6990 as quoted by Manhes *et al.* for St. Severin; however, the extremely low alkali contents and K/U ratio of ADOR (TERA *et al.*, 1970) suggest a very refractory parent planet for ADOR (perhaps one formed from Allende-coarse-grained-inclusion type material). If so, then the low $^{87}Sr/^{86}Sr$ reflects an early time of formation for the ADOR parent planet but the lower Pu/Nd (or Pu/U) in ADOR reflects a later magmatic event 160 Myr after the textural re-equilibration of St. Severin. This is speculative, but in any case we feel that the directly measured chondritic Pu/U from St. Severin is preferable for the solar system ratio to the one inferred indirectly by Marti *et al.* The closer coherence of Pu to Nd than U is a fact for ADOR, and we agree that relative meteorite ages may be more accurately calculated from Pu/Nd. This hypothesis can be independently evaluated, but relative meteorite ages should be recognized as a distinct application of the presence of ^{244}Pu in the early solar system from the use of $^{244}Pu/^{238}U$ for cosmochronological purposes.

Acknowledgements—The St. Severin samples were obtained through the co-operation of P. PELLAS, J. REYNOLDS and G. J. WASSERBURG. We thank F. OBERLI and G. J. WASSERBURG for isotopic dilution measurements of our glass standards. We acknowledge profitable discussions with T. BENJAMIN and P. PELLAS and very thorough reviews by G. CROZAZ and G. LUGMAIR. We also thank LOU ANN CORDELL and BETTY ROBINSON for their skill and patience. This research was supported by NSF grant EAR76-84402.

REFERENCES

ALBEE A. L., BEATY D. W., CHODOS A. A. and QUICK J. E. (1978) Quantitative analysis of petrographic properties and of mineral compositions with a computer-controlled energy-dispersive system. *Proc. Natl. Conf. on Electron Probe Anal. 12th*, in press.

ALEXANDER E. C. JR., DAVIS P. K. and REYNOLDS J. H. (1972) Rare gas analyses on neutron irradiated Apollo 12 samples. *Proc. Third Lunar Sci. Conf., Geochim. Cosmochim. Acta Suppl.* **3**, Vol. 2, pp. 1787–1795. M.I.T. Press.

BENJAMIN T., HEUSER W. R. and BURNETT D. S. (1978) Laboratory studies of actinide partitioning relevant to ^{244}Pu chronometry. *Proc. 9th Lunar and Plan. Sci. Conf., Geochim. Cosmochim. Acta Suppl.* **10**, Vol. 1, pp. 1393–1406. Pergamon.

BENJAMIN T. B., JONES J. H. and BURNETT D. S. (1979) Laboratory partitioning studies testing the validity of ^{244}Pu—rare earth chronology (Abstract). In *Lunar and Planetary Science X*, 98–100, The Lunar and Planetary Institute, Houston.

BHANDARI N., BHAT S., LAL D., RAJAGOPALAN G., TAMHANE A. S. and VENICATAVARDAN V. S. (1971) Fossil tracks in the meteorite Angra Dos Reis: A predominantly fission origin. *Nature* **234**, 540–543.

BOYNTON W. V. (1978) Fractionation in the solar nebula. II. Condensation of Th, U, Pu and Cm. *Earth Planet. Sci. Lett.* **40**, 63–70.

BURNETT D., MONNIN M., SEITZ M., WALKER R. and YUHAS D. (1971) Lunar astrology—U-Th distributions and fission-track dating of lunar samples. *Proc. Second Lunar Sci. Conf., Geochim. Cosmochim. Acta Suppl.* 2, Vol. 2, pp. 1503–1519. M.I.T. Press.

CANTELAUBE Y., MAURETTE M. and PELLAS P. (1967) Traces d'ions lourds dans les Mineraux de la Chondrite de St. Severin. In *Radioactive Dating and Methods of Low Level Counting*, pp. 215–229. International Atomic Energy Agency, Vienna.

CARVER E. A. and ANDERS E. (1976) Fission track ages of four meteorites. *Geochim. Cosmochim. Acta* **40**, 467–477.

CHEN J. H. and TILTON G. R. (1976) Isotopic lead investigations on the Allende carbonaceous chondrite. *Geochim. Cosmochim. Acta* **40**, 635–643.

CROZAZ G. (1974) U, Th and extinct ^{244}Pu in the phosphates of the St. Severin meteorite. *Earth Planet. Sci. Lett.* **23**, 164–169.

CROZAZ G., HAACK U., HAIR M., MAURETTE M., WALKER R. and WOOLUM D. (1970) Nuclear track studies of ancient solar radiations and dynamic lunar surface processes. *Proceedings of the Apollo 11 Lunar Science Con-*

ference, Geochim. Cosmochim. Acta, Suppl. 1, Vol. 3, pp. 2051–2080. Pergamon.

DROZD R. J., MORGAN C. J., PODOSEK F. A., POUPEAU G., SHIRCK J. R. and TAYLOR G. J. (1977) Plutonium 244 in the early solar system? *Astrophys. J.* **212**, 567–580.

FISHER D. (1972) Uranium content and radiogenic ages of hypersthene, bronzite, amphoterite and carbonaceous chondrites. *Geochim. Cosmochim. Acta* **36**, 15–33.

FLEISHER R. L., PRICE P. B. and WALKER R. M. (1975) *Nuclear Tracks in Solids, Principles and Applications.* University of California Press, Berkeley.

FOWLER W. A. (1971) New observations and old nucleocosmochronologies. In *Cosmology, Fusion and Other Matters*: A memorial to George Gamow (ed. F. Reines), Colorado Associated University Press, Boulder.

GANAPATHY R. and GROSSMAN L. (1976) The case for an unfractionated $^{244}Pu/^{238}U$ ratio in high-temperature condensates. *Earth Planet. Sci. Lett.* **31**, 386–392.

GOPALAN K. and WETHERILL G. W. (1969) Rubidium-strontium age of amphoterite (LL) chondrites. *J. Geophys. Res.* **74**, 4349–4358.

GRAY C. M., PAPANASTASSIOU D. A. and WASSERBURG G. J. (1973) The identification of early condensates from the solar nebula. *Icarus* **20**, 213–239.

GROSSMAN L. and GANAPATHY R. (1976) Trace elements in the Allende meteorite—I. Coarse-grained, Ca-rich inclusions. *Geochim. Cosmochim. Acta* **40**, 331–344.

HOHENBERG C. M. (1969) Radioisotopes and the history of nucleosynthesis in the galaxy. *Science* **166**, 212–215.

HUNEKE J. C., SMITH S. P., RAJAN R. S., PAPANASTASSIOU D. A. and WASSERBURG G. J. (1977) Comparison of the chronology of the Kapoeta parent planet and the moon. (Abstract) In *Lunar Science* **VIII**, pp. 484–486. The Lunar Science Institute, Houston.

JAROSEWICH E. and MASON B. (1969) Chemical analyses with notes on one mesosiderite and seven chondrites. *Geochim. Cosmochim. Acta* **33**, 411–416.

KIRSTEN T., JORDAN J., RICHTER H., PELLAS P. and STORZER D. (1977) Plutonium in phosphates from ordinary chondrites inferred from xenon and track data (Abstract). *Meteoritics* **12**, 279–281.

LAL D., MURALLI A., RAJAN R. S., TAMHANE A., LORIN J. and PELLAS P. (1968) Techniques for proper revelation and viewing of etch tracks in meteoritic and terrestrial minerals. *Earth Planet. Sci. Lett.* **5**, 111–119.

LAL D., LORIN J., PELLAS P., RAJAN R. and TAMHANE A. (1969) On the energy spectrum of iron-group nuclei: As deduced from fossil-track studies in meteoritic minerals. In *Meteorite Research* (ed. P. Millman), pp. 275–285. Springer-Verlag.

LEWIS R. S. (1975) Rare gases in separated whitlockite from the St. Severin chondrite: Xenon and krypton from fission of extinct ^{244}Pu. *Geochim. Cosmochim. Acta* **39**, 417–432.

LUGMAIR G. W. and MARTI K. (1977) Sm-Nd-Pu timepieces in the Angra Dos Reis meteorite. *Earth Planet. Sci. Lett.* **35**, 273–284.

MANHES G., MINSTER J. F. and ALLEGRE C. J. (1978) Comparative uranium–thorium–lead and rubidium–strontium study of the St. Severin amphoterite. Consequences for early solar system chronology. *Earth Planet. Sci. Lett.* **39**, 14–24.

MARTI K., LUGMAIR G. W. and SCHEININ N. B. (1977) Sm-Nd-Pu systematics in the early solar system (Abstract). In *Lunar Science* **VIII**, pp. 619–621. The Lunar Science Institute, Houston.

MARTI K., SHEDLOVSKY J. D., LINDSTROM R. M., ARNOLD J. R. and BHANDARI N. G. (1969) Cosmic ray produced radionuclides and rare gases near the surface of Saint Severin meteorite. In *Meteorite Research* (ed. P. Millman), pp. 246–266. Springer-Verlag.

MASUDA A., NAKAMURA N. and TANAKA T. (1973) Fine structures of mutually normalized rare-earth patterns of chondrites. *Geochim. Cosmochim. Acta* **37**, 239–248.

MATSUDA H., SHIMA M. and HONDA M. (1972) Distribution of uranium and thorium among components of some chondrites. *Geochem. J.* **6**, 37–42.

MORGAN J. W. and LOVERING J. F. (1968) Uranium and thorium abundances in chondritic meteorites. *Talanta* **15**, 1079–1095.

MÜELLER O. (1968) Die chemische Zusammersetzung des Steinmeteoriten St. Severin. *Z. Naturforsch.* **23a**, 48–51.

NAKAMURA N. (1974) Determination of REE, Ba, Fe, Mg, Na and K in carbonaceous and ordinary chondrites. *Geochim. Cosmochim. Acta* **38**, 757–775.

NORTHCLIFFE L. C. and SCHILLING R. F. (1970) Range and stopping-power tables for heavy ions. *Nuclear Data Tables* **A7**, 233–463.

ORCEL J., DAVID B., KRAUT T., NORDEMANN D. and TOBAILEM J. (1967) Sur la meteorite de Saint Severin (charente): Chute du 27 juin 1966. *Compt. Rend.* **D264**, 1556–1560.

PAPANASTASSIOU D. A. and WASSERBURG G. J. (1969) Initial strontium isotopic abundances and the resolution of small time differences in the formation of planetary objects. *Earth Planet. Sci. Lett.* **5**, 361–376.

PELLAS P. and STORZER D. (1975) Uranium and plutonium in chondritic phosphates (Abstract). *Meteoritics* **10**, 471–473.

PELLAS P. and STORZER D. (1977) Cooling histories of stony meteorites (Abstract). In *Lunar Science* **VIII**, pp. 762–765. Lunar Science Institute, Houston.

PODOSEK F. A. (1970a) The abundance of ^{244}Pu in the early solar system. *Earth Planet. Sci. Lett.* **8**, 183–187.

PODOSEK F. A. (1970b) Dating of meteorites by the high temperature release of Xe^{129}. *Geochim. Cosmochim. Acta* **34**, 341–365.

PODOSEK F. A. (1972) Gas retention chronology of Petersburg and other meteorites. *Geochim. Cosmochim. Acta* **36**, 755–772.

PODOSEK F. A. and LEWIS R. S. (1972) ^{129}I and ^{244}Pu abundances in white inclusions of the Allende meteorite. *Earth Planet. Sci. Lett.* **15**, 101–109.

QUIJANO-RICO M. and WÄNKE H. (1969) Determination of boron, lithium and chlorine in meteorites. In *Meteorite Research* (ed. P. Millman), pp. 132–145. Springer-Verlag.

REED G. W. and TURKEVICH A. (1955) Uranium content of two iron meteorites. *Nature* **176**, 794–795.

REED G. W., KIGOSHI K. and TURKEVICH A. (1960) Determinations of concentrations of heavy elements in meteorites by activation analysis. *Geochim. Cosmochim. Acta* **20**, 122–140.

REIMER G., STORZER D. and WAGNER G. (1970) Geometry factor in fission track counting. *Earth Planet. Sci. Lett.* **9**, 401–404.

SCHRAMM D. M. and WASSERBURG G. J. (1970) Nucleochronologies and the mean age of the elements. *Ap. J.* **162**, 57–69.

SEITZ M. G., BURNETT D. S. and BELL P. M. (1974) U, Th, Pu fractionation in geologic systems: Early Pu/U abundance in meteorites. *Carnegie Inst. Washington Yearbook* **73**, 547–548.

TATSUMOTO M., KNIGHT R. J. and ALLEGRE C. J. (1973) Time differences in the formation of meteorites as determined by $^{207}Pb/^{206}Pb$. *Science* **180**, 1279–1283.

TATSUMOTO M., UNRUH D. M. and DESBOROUGH G. A. (1976) U–Th–Pb and Rb–Sr systematics of Allende and U–Th–Pb systematics of Orgueil. *Geochim. Cosmochim. Acta* **40**, 617–634.

TERA F., EUGSTER O., BURNETT D. S. and WASSERBURG G. J. (1970) Comparative study of Li, Na, K, Rb, Cs, Ca, Sr and Ba abundances in achondrites and in Apollo 11 lunar samples. *Proceedings of the Apollo 11 Lunar Science Conference, Geochim. Cosmochim. Acta Suppl.* **1**, Vol. 2, pp. 1637–1657. Pergamon.

TÖKSOZ M. N. and JOHNSTON D. H. (1977) The evolution of the moon and the terrestrial planets. In *The Soviet–American Conference on Cosmochemistry of the Moon and Planets*, (eds J. Pomeroy and N. Hubbard), pp. 295–328. NASA, Washington, District of Columbia.

VAN SCHMUS W. R. (1969) The mineralogy and petrology of chondritic meteorites. *Earth Sci. Rev.* **5**, 145–184.

WASSERBURG G. J., HUNEKE J. C. and BURNETT D. S. (1969a) Correlation between fission tracks and fission type xenon in meteoritic whitlockite. *J. Geophys. Res.* **74**, 4221–4232.

WASSERBURG G. J., SCHRAMM D. M. and HUNEKE J. C. (1969b) Nuclear chronologies for the galaxy. *Ap. J.* **157**, L91–L96.

WASSERBURG G. J., TERA F., PAPANASTASSIOU D. A. and HUNEKE J. C. (1977) Isotopic and chemical investigations on Angra Dos Reis. *Earth Planet. Sci. Lett.* **35**, 294–316.

Appendix IV

Beta Radiography of Finite Samples

The following examples are used to illustrate the dependence of ^{Sm}D values on grain size. Because individual beta particles do not have definite, well-defined ranges, beta ranges must be treated collectively. Empirically, betas are exponentially absorbed by a thick absorber (thickness, r) such that the flux I is given by

$$I = I_o\, e^{-ur}$$

where I_o is the unattenuated flux and u is the coefficient of absorbtion. The absorber thickness necessary to attenuate the beta flux by 0.5 ($d_{1/2}$) is given by

$$d_{1/2} = \ln 2 \cdot \rho / u$$

where ρ is the density of the absorber (Evans, 1955). For a ^{151}Sm source of $\rho = 3 g/cm^3$ and $d_{1/2} = 2.1 \times 10^{-3} g/cm^2$, u is approximately $10^3/cm$.

Case I - Infinite half-space source

For a semi-infinite ^{151}Sm source of strength I_o (betas/cm^3·sec), the contribution to the track production rate at the surface $d\beta$ of a volume element dv (located at a polar angle θ with respect to the surface) is given by

$$d\beta = I(r) \cos\theta\, dv/(4\pi r^2) = I_o\, e^{-ur} \cos\theta\, dv/(4\pi r^2)$$

integrating over all volume yields $\beta = I_o/4u$.

Case II - Hemispherical source, radius R

This case is very similar to the infinite half-space but with different limits of integration. Therefore, at the center of the hemisphere

$$\beta = I_o\, (1 - e^{-uR})/4u$$

Case III. - Infinite thin source

For a thin plate of thickness t, the solution consists of two parts: r(distance from source volume dv to surface) $\leq$ t and (2) r>t. For r $\leq$ t,

$$\beta_1 = I_o\ (1 - e^{-ut})/4u$$

as in the case of the hemispherical grain. For r>t

$$\beta_2 = I_o \int_t^\infty (t^2/r^2)\ e^{-ur}\ dr/4$$

and $$\beta = \beta_1 + \beta_2 = I_o/4u\ [1 - e^{-ut} + \int_t^\infty (ut^2/r^2)\ e^{-ur}\ dr]$$

Case IV. - Long cylindrical source, radius R.

The axial track production rate β is given by

$$\beta = I_o/4u\ [1 - e^{-uR} + u \int_R^\infty f(R/r)\ e^{-ur}\ dr]$$

where $$f(R/r) = \sin^{-1}(R/r) - (R/r)(1 - (R/r)^2)^{1/2}\ .$$

Case V. - Edge of a thick source

On the surface of a large, thick source (infinite quarter-space) at a distance Z from the edge (source boundary normal to the surface containing Z), β is given by

$$\beta = I_o/4u\ [1/2 + 1/2(1 - e^{-uZ}) + 1/\pi \int_Z^\infty u\ e^{-ur}\ g(Z/r)\ dr]$$

where $g(Z/r) = \sin^{-1}(Z/r) + (Z/r)(1 - (Z/r)^2)^{1/2}$.

As examples these cases will be tabulated and compared to the semi-infinite slab (Case I), to show how β is affected by grain size. All calculations assume the "grain" to be surrounded by inert material.

For Case II, the hemispherical grain, radius R

R	βcenter/βcase I
10μ	0.63
20μ	0.86
30μ	0.95
50μ	0.99

For Case III, thin grain of thickness t

t	βIII/βI
10μ	0.75
20μ	0.94
30μ	0.98

For Case IV, long, cylindrical source, radius R

R	βIV/βI
10μ	0.73
20μ	0.92
30μ	0.98

For Case V, a distance Z from the edge of a thick source

Z	βV/βI
10μ	0.92
20μ	0.97

Based on these calculations, large crystals analyzed > 20μ from glass-crystal interfaces should yield satisfactory results.